NORM FASTENERS
AR-GE MERKEZİ YAYINLARI

R&D CENTER PUBLICATIONS

2021

VOLUME 7

NORM
FASTENERS

NORM FASTENERS

AR-GE MERKEZİ YAYINLARI

R&D CENTER PUBLICATIONS

ÖN SÖZ

Umut İnce
Norm Fasteners Ar-Ge ve Mühendislik Direktörü

Değerli İş Ortaklarımız;

Norm Holding olarak benimsediğimiz "geleceğe değer" vizyonumuzla sürdürülebilir bir dünya ve gelecek hedefimizden güç alarak sizinle birlikte ortak bir amaç çerçevesinde Ar-Ge çalışmalarımızı yönlendirmekteyiz.

Akademik temeli olan, uygulama becerisi yüksek, alanında uzman Ar-Ge ekibimizin her geçen gün artan motivasyonu ve azmi ile hedeflerimize doğru emin adımlarla yol alıyoruz. Gerçekleştirdiğimiz çalışmalarımız ve güçlü işbirliklerimiz sayesinde sadece sektöre yön ve ilham veren katma değeri yüksek ürün ve çözümler üretmiyor, aynı zamanda ulusal ve uluslararası alanda sektörümüze özgü bilimsel bilgi kütüphanesine katkıda bulunmayı da kendimize bir görev addediyoruz. 2021 yılı içinde yaptığımız çalışmalardan ortaya çıkan makale ve bildirilerimizi bu kitapçıkta birleştirerek siz değerli iş ortaklarımızla paylaşmaktan gurur ve mutluluk duyuyoruz.

ÖN SÖZ

Dr. Muhammed Burak Toparlı
Norm Fasteners Ar-Ge Müdürü

Değerli İş Ortaklarımız;

Norm Fasteners Ar-Ge Merkezi olarak kurulduğumuz günden itibaren yürüttüğümüz projelerimiz ve gerçekleştirdiğimiz özgün çalışmalarımız, ulusal ve uluslararası saygın konferans, kongre, sempozyum ve dergilerde, makale ve bildiriler olarak kabul edilip yayınlanmaktadır. Yayınlanan çalışmalarımız ile sektöre ve teknolojik gelişmelere katkıda bulunmaktan her zaman gurur duymaktayız.

2014 yılından itibaren her yıl, o yıl içerisinde yayınlanan makale ve bildirilerimizi kitapçık haline getirerek birlikte yol aldığımız, sektörde emin adımlarla daha da güçlenerek ilerlememize katkıda bulunan yurt içi ve yurt dışındaki iş ortaklarımızla paylaşmaktayız. Böylelikle bağlantı elemanları sektöründe gerçekleştirilen araştırma ve geliştirme çalışmalarında yol gösterici olmanın yanı sıra paydaşlarımızın Ar-Ge Merkezimizde gerçekleştirdiğimiz çalışmalar ve odaklandığımız teknik alanlar hakkında bilgi sahibi olmasını da sağlıyoruz. Bu doğrultuda iş birliklerimizi daha geniş bir kapsamda ve çok yönlü olarak sürdürmeyi hedeflemekteyiz. 2021 yılı makale kitapçığımızda yıl içerisinde yayınlanan ve cıvatalı bağlantıların gevşemesi, korozyonun yorulma davranışına etkisi, soğuk dövme proses operasyonu optimizasyonu, yapay sinir ağı modelleri kullanarak malzeme modeli tahmini, hasar analizleri, kaplama tiplerinin kalıp ömrüne etkisi ve ağırlığı azaltılmış bağlantı elemanı tasarımı gibi konulara yer verdiğimiz makale ve bildirilerimizi siz değerli iş ortaklarımız ile paylaşmaktan mutluluk duyuyoruz.

Güçlü Ar-Ge altyapımız ve alanında uzman çalışma arkadaşlarımız ile inovatif, akıllı, çevreci ve hayatı kolaylaştıran çözümler üreten, geleceğin teknolojilerini üretimin merkezine taşıyan ve fark yaratan yenilikçi ürünlerimizle sektöre ilham vermeye devam edeceğiz.

OPTIMIZATION OF TRIMMING PROCESS IN COLD FORGING OF STEEL BOLTS BY TAGUCHI METHOD

Fatih KOCATÜRK
Barış TANRIKULU
Sarper DOĞAN
Cenk KILIÇASLAN
Sezgin YURTDAŞ
Umut İNCE

International Journal of Pressure Vessels and Piping Volume 194, Part A, 1 December 2021, 104503

OPTIMIZATION OF TRIMMING PROCESS IN COLD FORGING OF STEEL BOLTS BY TAGUCHI METHOD

Fatih Kocatürk[a]*, Barış Tanrıkulu[a], Sarper Doğan[a], Cenk Kılıçaslan[a], Sezgin Yurtdaş[a], Umut İnce[a]

[a]R&D Center, Norm Cıvata San. ve Tic. A.Ş., AOSB, Çiğli, İzmir, Türkiye

*Corresponding author: Fatih Kocatürk. E-mail: fatih.kocaturk@norm-fasteners.com.tr

Abstract

In this study, die-service life analysis of hexagonal trimming dies with different edge radius and cutting width was performed. The trimming dies were prepared by grinding the front face of the die due to desired cutting width and edge radius. Prepared dies were used in cold forging of steel M6x25 hexagonal bolts and service life of each die were determined in terms of number of bolts that they can produce until they experience fracture. Numerical models of trimming operation with varying cutting width were also prepared in finite element software simufact.forming to conduct stress analysis. Production trials and finite element analysis showed that service life of trimming die was significantly affected by cutting width. It was seen that die-service life increases linearly with increasing cutting width within an optimum range of 0.8 and 1.2 mm. Similarly, the die-service life improved with increasing edge radius values. Moreover, the trimming operation carried out by using hexagonal trimming die was optimized with Taguchi method by defining 5 design parameters and 3 levels for each parameter. Minimizing the peak trimming load and maximizing the peak damage value were determined as the objective functions to find the most effective design parameters. According to the Taguchi results, the cutting width and stopping distance were seen to have significant impact on peak trimming load while the edge radius was determined to be effective on the peak damage value.

Keywords: Trimming die; bolt forming; finite element analysis, taguchi method; optimization.

1. Introduction

Shearing process to obtain a final shape of a product by removing scrap parts from the edge of a forged product is called as trimming. Trimming is used in forming industry to form various geometries on sheet and bulk parts. Maintaining the cutting surface quality and reducing the stresses on the trimming die are the essentials in the trimming process. Any improvements in trimming process can significantly increase die life and productivity. Edge radius (blade radius), cutting width and stopping distance between trimming and bottom dies are the parameters that affect trimming process. The most common problem during production for the trimming process is the fatigue fractures on the edge radius region.

In the literature, studies are mainly focused on shearing process of metal sheets. However, there are limited number of publications that are dealing with cutting of bulk metals, especially in cold bolt forging. One of the important studies was conducted by McCormack and Monaghan [1]. In their study, trimming die-service life analysis of M6 bolt was examined by considering process parameters like stopping distance and knockout (K.O.) pin load. In addition, the effect of the critical damage value on the surface quality was investigated. As a result, increasing the stopping distance caused an increase in K.O. pin load and reduced the level of induced effective stresses of the trimming die about 17.7%. In order to improve the trimming die life used for bolt production, different cutting die designs were examined using numerical simulations in reference [2]. Edge radius, cutting width, rake angle and petal angle parameters were examined for trimming die design. The highest stress concentration occurred within the body of the tool not along the contact surfaces as predicted in finite element (FE) analysis. Moreover, variation in tool stress was presented as a function of changes in trimming die cutting edge corner geometry. For the trimming process of Al6061 alloy bolt head, the surface quality and shear load were optimized using the Taguchi method and numerical simulations using the blade radius, land width of the bottom die and stopping distance parameters in reference [3]. Blade radius had the most significant effect on both the surface quality and shear load as a result of Taguchi optimization. The production trial was carried out with the best parameter set found by FE analysis and Taguchi method, and similar results were obtained. In the following study carried out as a continuation of this study, thread-rolling process optimization in the production of Al6061 alloy bolts was carried out by Taguchi method and FE analysis [4]. It was observed that the most important parameter for the trimming process that affects the surface quality and the trimming load was found to be blade radius, and the most effective parameter for threading was determined to be penetration depth. Prediction of tool life of heavily loaded cold forging dies was investigated in reference [5]. FE analysis under the condition of low-cycle fatigue and fatigue crack growth testing on tool materials were carried out to predict tool life. Tool life corresponding to low-cycle fatigue tests was predicted as 782 cycles, and additional cycles of 82 were predicted by using dynamic fracture mechanics. In comparison, the experimental tool life before the occurrence of surface cracks was found to be 1,000 cycles. Fatigue life of cold forging dies with respect to hardness was investigated in reference [6]. To obtain various values of hardness, four kinds of die materials, SK4, SKS3, SKD11 and SKH9 were examined. A theoretical model using die hardness and fatigue total strain was also proposed as parameters to predict the die fatigue life. WC-5TiC-10Co ultrafine cemented carbides and conventional cemented carbide with same composition and medium grain size were prepared and used as cutting tool for AISI H13 hardened steel in reference [7]. The effects of cutting parameters on tool life and tool wear mechanism was analysed and the results showed that hardness and transverse rupture strength of WC-5TiC-10Co ultrafine cemented carbides were higher, and the cutting performance of ultrafine cemented carbides were better than conventional insert with the same cutting condition. An extended Taylor's tool life equation was used to analyse tool life and the results showed that cutting speed played a significant role on the tool life and wear behaviour of both cutting inserts. Rod cutting and bolt head trimming operation were analysed with FE analysis by using seven calibrated ductile fracture criteria in reference [8]. The cutting operation was carried out by deleting the elements of which damage value reached the fracture limit with respect to appropriate fracture criteria. The fracture formation was predicted correctly by Cockroft-Latham-Oh criterion.

By using a special designed die in a mechanical press, trimming experiments were carried out on sheet metals including two drawing steels, an aluminium alloy and a magnesium alloy in reference [9]. The rollover and burr height formed on the trimmed surface were analysed as a function of punch-die clearance. Crack initiation, generation of the fracture surface profile and burr formation mechanism were examined by partially trimming samples. As a result of experiments, burr height and rollover depth generally increased with increasing clearance for all material types. However, there were differences in the fracture surface profile shape, the burr shape, and burr formation mechanism between steel and non-ferrous alloys. Crack propagation rate through sheet material was observed as the major cause of these differences. A FE model of trimming process and hardness contours of partially deformed samples were used to investigate the shearing behaviour of a drawing-steel and aluminium alloy in reference [10]. It is shown that the stress and strain distributions within the work-piece were more strongly dependent on the punch penetration compared to material properties of work-piece. A very common test to estimate formability of a sheared edge is the Hole Expansion Test (HET) in accordance to ISO16630 (HET-ISO) [11]. The relative cutting clearance c for the piercing process is evaluated with respect to the common Equation 1 [11];

$$c[\%] = \frac{d_d - d_p}{2 * t} \times 100 \tag{1}$$

where d_d is diameter of die, d_p is diameter of punch and t is sheet thickness. Experimental techniques were developed in reference [12] for aluminium alloy 6111-T4 and ultra-high strength steels (UHSS) which are sensitive to sheared edge cracking. Sheared edge stretchability and burr height were found to have strong dependency upon the cutting clearance for aluminium sheet 6111-T4, i.e. increasing the cutting clearance to 40% leads to substantial burrs and lower formability. No burrs occurred in the range of cutting clearance up to 40% for DP980 steel and the best stretchability could be achieved for the cutting clearances 10-15% according to sheared edge stretchability measured in diffuse necking area and in HET. A new approach was introduced in reference [13] which can be used as an alternative to HET given in ISO 16630 [11] to determine formability of a steel sheet sheared edge by HET that uses a forming limit curve (FLC) tool set. Additional information about the forming and failure behaviour of the material was also provided by the proposed approach. The trimming process of AA6111-T4 aluminium sheet with 0.93 mm thickness was modified to eliminate slivers and burrs from trimmed surface in the reference [14]. The mechanisms of sliver generation were studied to formulate the root cause of their production. To this end, a new robust trimming process was suggested to eliminate the main cause of slivers and burrs generation, and to lower the requirements to the accuracy of trim dies alignment. This new robust trimming process using an elastic pad under the upper trimming die avoids bending of the blank and eliminates the separation of potential slivers by horizontal forces. Desirable robustness of the trimming process for gaps in the range between 2% and 107% of the sheet thickness was achieved by the combination of the mechanical support and the preferential fracture development on the lower-shearing edge achieved by dulling the upper-shearing edge. The mechanisms of burr generation and the impact on advanced-high strength steels (AHSS) formability in stretch flanging were analysed in [15] by using robust trimming process and convenient trimming process. A numerical model which simulates deformation of the dual phase steel DP500 blank in trimming processes and predicts the corresponding initiation of fracture was developed and validated in [16]. It is observed that better quality of trimmed surface could be obtained if fracture initiates from the lower shearing edge and propagates in the opposite direction to the material flow. The quality of trimmed edge of DP980 steel was analysed by considering the effect of trimming clearance and tool wear in the reference [17]. The effect of sheet material type on the burr height and shear edge quality was also examined based on the experimental studies. The results for DP980 showed that the burr height increases as the clearance between the upper and lower trimming tool increases and that there is almost no measurable burr at trimming clearances below 17% of the material thickness. Die wear for trimming operations of UHSS components was analysed and some examples of tool wear analysis were conducted with 1.5 mm thick DP980 steel sheets in [18]. It is observed that sheared edge quality was affected by tool wear which causes increasing in both burr height and burnished area depth. An evaluation of the correction and treatment methodologies that can precisely adjust the mesh to the trimming surface for trimming solid finite element meshes were presented in [19]. It was observed that the error in the equivalent plastic strain distribution, related with the rotation angle, is less than 3 % and the increase of this error, for each trimmed mesh, results from the presence of distorted and degenerated elements. It was therefore recommended, when selecting the mesh correction strategy, to try to minimize the misalignment with the inner finite elements, but also to consider the loading direction. A comprehensive algorithm, with which trimming induced residual stresses can easily be included in the subsequent simulation steps, was developed to simulate the trimming process as part of the overall forging process in reference [20]. The elimination of discarded elements, the mapping of state variables and the 3D FE simulation using the DEFORM 3D software were embedded into a C++ coded software system. The trimmed edge stretchability under different trimming clearances for AA6111-T4 sheets was predicted with a developed integrated computational manufacturing process simulation framework in the reference [21]. The influence of the trimming die clearances on the predicted tensile stretchability was quantitatively compared with experimental measurements, and it was observed that stretchability decreases with increasing cutting clearances.

In this study, the die-service life analysis of the hexagonal trimming dies with different edge radius and cutting width values was investigated both experimentally and numerically. Experimental studies were conducted in a forging press with a capacity of 2.94 MN. All forging experiments were carried out in serial production in which steady-state forming conditions were achieved. Trimming operation was also coupled with numerical models using simufact.forming finite element software for stress analysis. After determining effects of cutting width and edge radius on die-service life of trimming dies, further analysis was performed to analyse the effect of design parameters on the trimming operation by using Taguchi method. For this purpose, 5 design parameters and 3 levels at each were determined in order to examine significance of the parameters with respect to peak load and damage value in trimming operation. Experimental set constructed by Taguchi method was conducted with numerical simulations by defining relative parameter settings.

2. Materials and Methods

In this study, a medium carbon steel 23MnB4 was chosen as a bolt material and chemical composition was given in Table 1. Surface cleaning, phosphate coating, annealing and wire drawing processes were applied on the raw material before cold forging. Phosphate coating operation increases the performance of forming process by decreasing friction coefficient. Mechanical properties of annealed 23MnB4 was given in Table 2. Within the scope of this study, a M6x25 hexagonal bolt produced in our company was taken as a reference in order to perform die-service life analysis of the SW10 cutting die and to carry out simulation studies. Numerical simulation studies were performed by applying

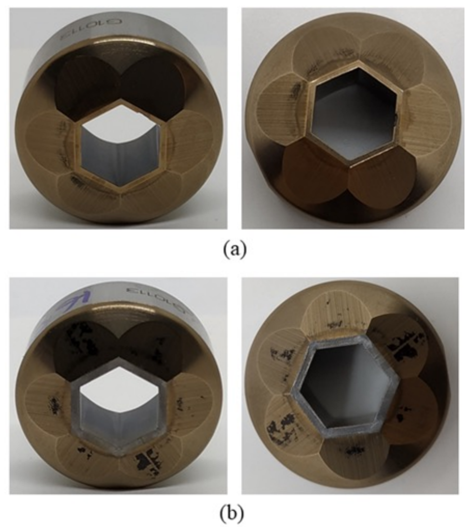

Fig. 1. Examples of hexagonal trimming dies before and after grinding operation: a) Before; b) After.

the four-stage forming design which is also used to produce M6x25 hexagonal bolt in production. The strains and stresses on the work-piece were transferred from the first stage to the next stages accordingly, and the trimming load and damage value were determined by utilising cumulative strain and stress at the last stage where the cutting

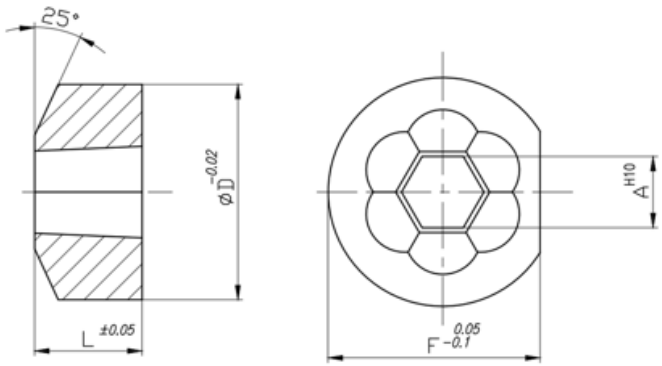

Fig. 2. Technical drawing of trimming die.

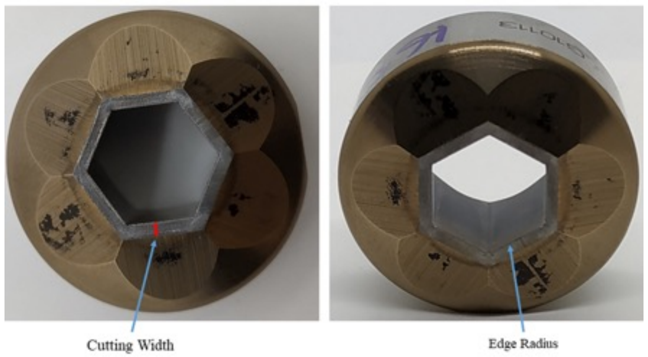

Fig. 3. The cutting width and edge radius measurements on the trimming die.

process was performed. In order to reach the final M6x25 hexagonal bolt form, the dimensions of the billet were chosen as 5.70 mm in diameter and 35.12 mm in length.

In order to analyse the effect of cutting width and edge radius on die-service life of trimming dies used in the production of the reference M6x25 hexagonal bolt, a representative hexagonal SW10 die with cutting width of 0.7-0.75 mm and edge radius of 0.04-0.055 mm was chosen to carry out production trials. The selected trimming die used in the scope of this study was made of tool steel, M2 1.3343, having hardness of 65 HRC and compressive yield stress of 3,250 MPa, Poisson's ratio of 0.27-0.30 and elastic modulus of 190-210 GPa. Chemical composition of M2 tool steel was given in Table 3.

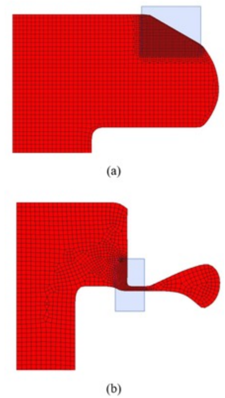

Fig. 4. Mesh distributions in (a) compressing, (b) trimming steps.

The hexagonal trimming dies were produced by grinding the front surface to obtain various cutting width and edge radius. For each grinding operation, the surface was machined approximately 0.1 mm. Grinding operation leads to vanish TiN coating which causes excessive wear during forging. To eliminate that, dies were coated again with TiN after grinding operation. Examples of hexagonal trimming dies before and after grinding operation were given in Fig. 1. The technical drawing of the trimming die was given in Fig. 2. In this figure, A = 9.81mm, D = 27.05mm, L = 16mm, F = 26.60mm.

Cutting width and edge radius on trimming dies were shown in Fig. 3. Cutting width and edge radius measurements were taken for all six edges of the hexagonal and average of six measurements was taken.

3. Finite Element Model

Forming and trimming processes were simulated with simufact.forming software. Simulation model was selected as 2D–axisymmetric for simplification, since trimming die has a hexagon shape which is axisymmetric. In the stage where the trimming operation was performed, the trimming diameter of the work-piece was determined as 9.85 mm, and the shaft diameter as 5.21 mm in order to obtain the reference M6x25 hexagonal bolt. During the simulation, all parameters were modelled to simulate real forging conditions. In this context, the coefficient of friction used during forging was carried out with reference to the friction model, which changes depending on the temperature. While the coefficient of friction at room temperature is 0.09, it drops to 0.04 when it reaches 200 °C. Crank press was used as forging press and the rotation speed of the press was set to 70 Rpm, the radius of the crank was 100 mm and the rod length was 425 mm. Finally, mesh type was set as quadtree and 6.000 elements was used in the model. Trimming operation completed with two steps: compressing and trimming. First, punch compressed the work-piece until the stopping distance and then trimming was carried out with knockout pin by removing the scrap from the work-piece. In order to simulate the trimming process, the 'element removal' method was used. Cockcroft-Latham fracture criteria was used to simulate the damage behaviour of steel in reference [3] and critical damage value of 23MnB4 was selected as 0.70 as a result of the conducted compression tests. In case the damage value exceeds the critical limit value in the simulation model, the trimming process is simulated by performing mesh removal. Moreover, trimming operation results are sensitive to the number of mesh elements. Therefore, compressing and trimming region had more element compared to the other regions as depicted in Fig. 4. These regions had two times more element concentration.

4. Design Parameters and Taguchi Orthogonal Array Table

Trimming process of 23MnB4 steel bolt head was optimized with respect to different design parameters by using Taguchi design of experiment method. Performance of trimming operation is affected by several design parameters such as cutting width (CW), edge radius (ER), petal angle (PA), bottom angle (BA) of stationary die and stopping distance (SD) between trimming die and the stationary die depicted as Fig. 5. Three levels were determined for each design parameter and given in Table 4. In Taguchi method, the orthogonal array table was generated according to the number of parameters (operators) and the number of levels of each parameter. In this study, 5 parameters and 3 levels for each parameter were selected to examine the effect of the parameters for the selected objective functions. While, L_{18} (2^1x3^7) orthogonal array design consists of one parameter at 2 levels and up to 7 parameters at 3 levels each, L_{27} (3^{22}) design consists of up to 22 parameters at 3 levels each. Since, there is no parameter at 2 levels, L_{27} orthogonal array design, including 27 rows/experiments, was selected to carry out the finite element analysis experiments. L_{27} (3^5) orthogonal array table created for using the Taguchi method was presented in Table 5.

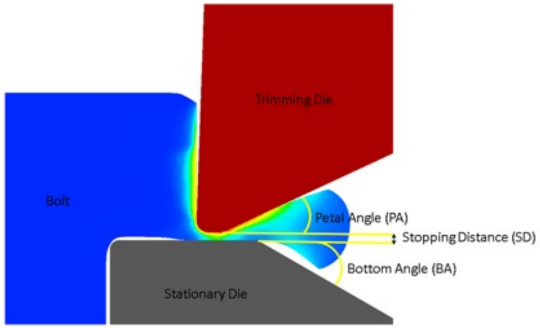

Fig. 5. Design parameters of trimming process.

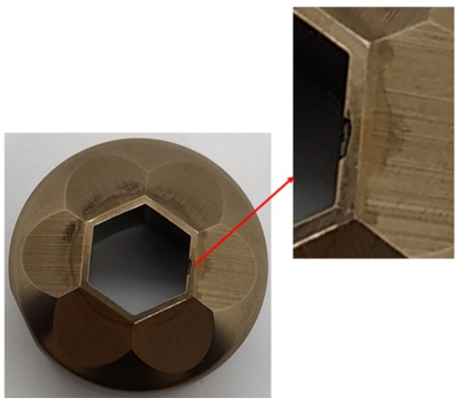

Fig. 6. Chips occurrence on the reference trimming die.

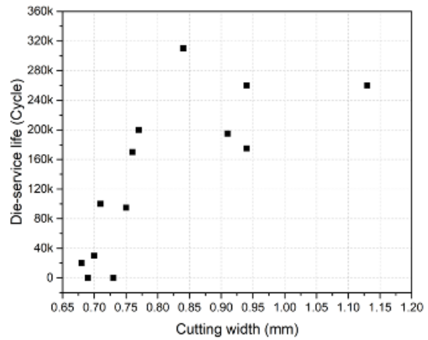

Fig. 7. Graph of cutting width versus die-service life.

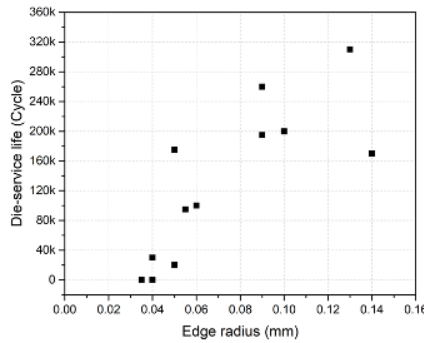

Fig. 8. Graph of edge radius versus die-service life.

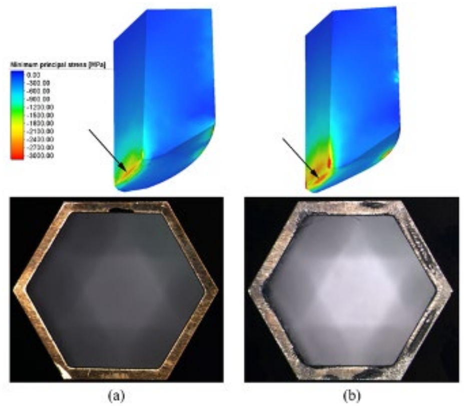

Fig. 9. Minimum principal stresses occurred on the edge radius and cutting width part: a) Cutting Width: 0.7 mm; b) Cutting Width: 1.1 mm.

5. Results and Discussions

5.1 Experiments in The Production

In forging shop, it was seen that analysed trimming die experienced sudden fracture after forging of 20,000 bolts. Failed die surface was shown in Fig. 6. As seen in the figure, fracture started from the edge radius and chipping was formed on the edge. In order to analyse the effect of cutting width and edge radius parameters on the die-service life of trimming dies, production trials were carried out for 13 cutting dies with various cutting width and edge radius measurements obtained by grinding front surface. In Fig. 7 and Fig. 8, the effect of cutting width and edge radius on the

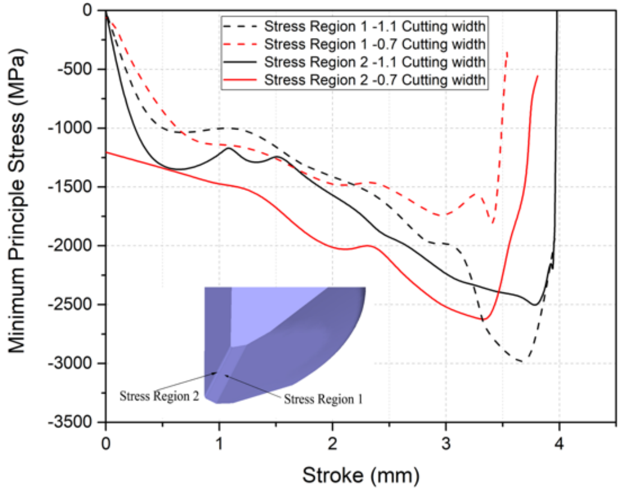

Fig. 10. Graph of maximum principal stress - stroke occurred on the edge radius and cutting width regions for cutting width of 0.7 mm and 1.1 mm.

die-service life in production trials were shown, respectively. Cutting width values of dies vary between 0.68-1.13 mm. According to Fig. 7, it was seen that the die-service life increases as the cutting width increases. Die-service life versus edge radius graph was shown in Fig. 8. As seen in the figure, die life is significantly low at smaller edge radius values. When edge radius increases, die life increases up to 3 times. Best die life is obtained when the edge radius is

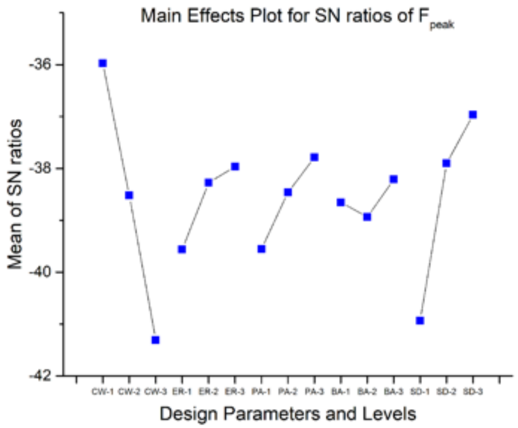

Fig. 11. Main effect plot for the peak trimming load objective function.

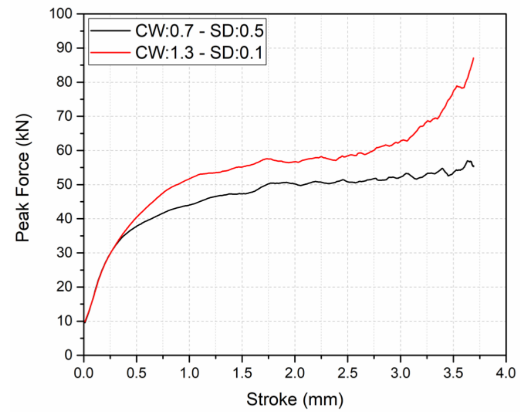

Fig. 12. Trimming force - stroke for the best and worst levels of CW and SD parameters.

between 0.12 and 0.14 mm. The edge radius of the trimming dies wears out over time during the trimming process. Although edge radius size and other tribological properties affect the wear behaviour seriously, the minimum principal stress at the surface and trimming load values were taken as reference, which are the most important parameters for die-service life and wear.

5.2 FEA Verification of Experimental Studies

Trimming die failure is caused by two different stress types, maximum and minimum principal stresses. Within the scope of this study, the maximum and minimum principal stresses on the trimming die were also examined, but the maximum principal stress value was obtained as 324 MPa, well below the critical value. Therefore, minimum principal stress distributions formed on trimming dies with cutting width values of 0.7 mm and 1.1 mm were compared to numerical findings. According to numerical simulation results, it was found that the stress accumulation occurs on the edge radius for the model with the cutting width of 0.7 mm similar to the chips occurrence problem of the reference die (the point indicated by the arrow in Fig. 9 (a)). Here, it is observed that the minimum principal stress accumulates exactly on the corner. In trimming die with cutting width of 1.1 mm, it was observed that the stress accumulation occurred on the land part and did not accumulate on the edge radius. When the damage occurred in the tested trimming dies was analysed, a collapse/dent like damage in the land part was observed for the samples with high cutting width values. The point at which the collapse/dent occurs was similar to the stress density formed in the numerical simulation (Fig. 9 (b)).

As a result of FEA, the minimum principal stresses occurred on the trimming die were examined. Accordingly, the variation of the minimum principal stress value was obtained on the trimming die surface depending on the different regions and CW parameter values. As it can be seen from the graph in Fig. 10, stroke-based stress changes were obtained from two different regions. While the stress region 1 refers to the middle of land part, the stress region 2 refers to edge radius region. According to the results, the minimum principal stress values increased from -1750

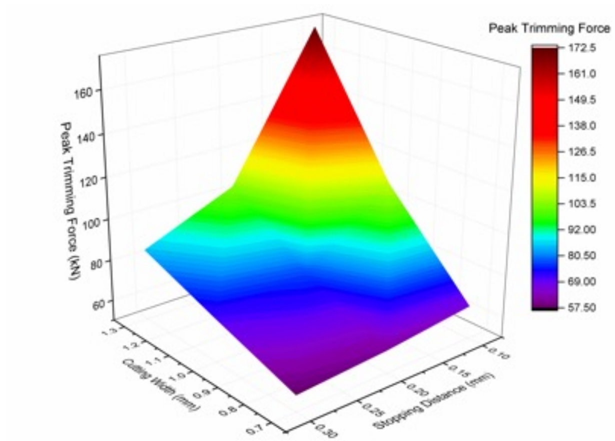

Fig. 13. The relationship between peak trimming load values and CW - SD parameter levels.

MPa to -3000 MPa with the increase of CW value in the stress region 1. In the stress region 2, increasing the CW value caused a decrease in the stress values. Therefore, it was observed that CW parameter has different effects on different parts of the trimming die.

5.3 Taguchi Analysis

Peak trimming load (F_{peak}) and peak damage value (D_{peak}) were set as objective functions to analyse the effects of design parameters defined in Section 4 on the performance of trimming process. In order to improve the die-service life of trimming dies, it is favourable to have smaller peak trimming load and larger peak damage value. Moreover, maximizing the peak damage value is desired to obtain smoother surface at the end of trimming operation. Therefore, the signal-to-noise (*SN*) ratio was evaluated by applying the loss function of the smaller-better characteristics in Equation (2) for the peak trimming load and by applying the loss function of the larger-better characteristics in Equation (3) for the peak damage value:

$$SN = -10\log\left(\frac{1}{n}\sum_{i=1}^{n} y_i^{2}\right) \tag{2}$$

$$SN = -10\log\left(\frac{1}{n}\sum_{i=1}^{n} \frac{1}{y_i^{2}}\right) \tag{3}$$

where y_i is the i^{th} measured value and n is the number of measurements in the related experiment. *SN* ratio is calculated for each experiment in the experiment set generated by Taguchi method.

FE analysis results for F_{peak}, D_{peak} and the *SN* ratios obtained by Taguchi method were presented in Table 6. The main effect plot of each design parameter for the peak trimming load objective function was also given in Fig. 11. Peak

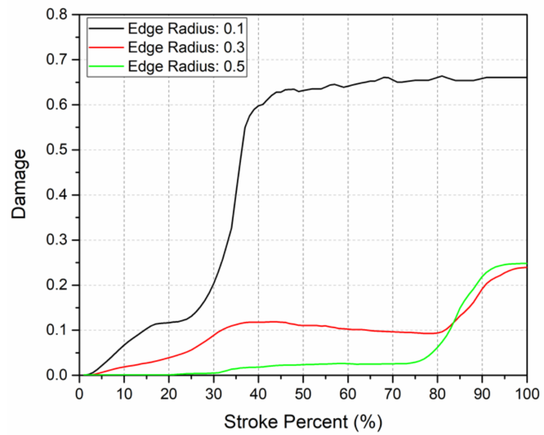

Fig. 14. Damage – stroke graph for all levels of ER parameter.

trimming load was affected significantly by the cutting width (CW) design parameter at the first level. Peak trimming load was also affected significantly by stopping distance (SD) parameter at level 3. Edge radius and petal angle parameters had similar impact on the results, and the bottom angle was insignificant for peak trimming load. The process conditions that resulted the highest *SN* ratio were 0.7 mm cutting width, 0.5 mm edge radius, 35° petal angle, 30° bottom angle and 0.3 mm stopping distance.

The effect of the efficient design parameters (CW, SD) on the peak trimming load was examined by comparing the peak trimming load change for the best and worst levels of CW and SD parameters with respect to *SN* ratios, and taking the nominal values for the other parameters as level 2. As can be seen in Fig. 12, for the worst levels of CW and SD, when CW is 1.3 mm and SD is 0.1 mm, trimming load reached to 85 kN and for the best levels, when CW is 0.7 mm and SD

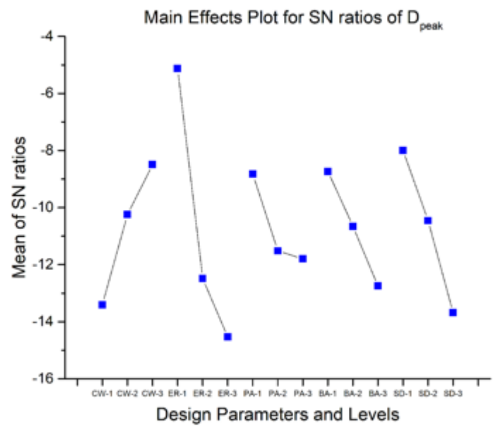

Fig. 15. Main effect plot for the peak damage value objective function.

is 0.5 mm, trimming load reached to 58 kN. As expected, lower trimming loads were obtained for the best levels of significant design parameters to minimize the peak trimming load. The mapping was created by taking into account the CW and SD parameter values of the two most efficient parameters affecting the trimming load. By means of the mapping, the effects of the parameters on the trimming load can be seen more clearly in Fig. 13.

In order to see the effect of the significant design parameter, edge radius (ER), on damage value, analyses were carried out for all levels of ER parameter and taking the nominal values for the other parameters as level 2. It is observed that ER directly affects the damage value as can be seen in Fig. 14. As the ER value decreases, the damage values on the material cutting surface increase, which confirms the results of Taguchi analysis. Moreover, the damage value increased very rapidly with the decrease of the ER parameter. For ER values of 0.3 mm and 0.5 mm, an increase of the damage vale occurred later on material surface due to the stroke progress.

The main effect plot of each design parameter for peak damage value objective function was given in Fig. 15. Peak damage value was affected significantly by edge radius parameter at level 1. Stopping distance, cutting width and bottom angle had similar impacts on peak damage value in decreasing order. Petal angle parameter was found to be insignificant for peak damage value. The process conditions that resulted the highest SN ratio were 1.3 mm cutting width, 0.1 mm edge radius, 15° petal angle, 20° bottom angle and 0.1 mm stopping distance.

The optimum levels for cutting width, stopping distance and petal angle design parameters were selected based on the peak trimming load that performed relatively high sensitivity. Since edge radius parameter had the most significant effect on peak damage value, the first level was selected as optimum with respect to maximum *SN* ratio value for D_{peak}. The bottom angle parameter had greater impact on peak damage value than peak trimming load. Therefore, the optimum level for the bottom angle was selected based on peak damage value. To sum up, the optimum process conditions in the trimming process obtained by the results of FEA with the Taguchi method were 0.7 mm cutting width, 0.3 mm stopping distance, 35° petal angle, 0.1 mm edge radius and 20° bottom angle.

5.4 FEA Confirmation for The Optimum Process Conditions of Taguchi Method

Numerical simulation was performed at optimum process conditions in order to confirm the trustworthiness of Taguchi's experimental results. As a result of numerical simulation, the peak trimming load was recorded as 46.593 kN and 7.76% lower than the lowest peak trimming load obtained as a result of experiments. Since 3 of the optimum process parameters were determined according to the peak trimming load and 2 of them were determined according to the peak damage value, the damage value was recorded as 0.6347 and 17.56% lower than the maximum damage value obtained as a result of the experiments. The results confirmed the reliability of the Taguchi parameter analysis.

6. Conclusions

In this study, trimming operation design parameters are optimized by using Taguchi method. In order to determine the effect of cutting width and edge radius parameters on the die-service life, production trials were carried out for the hexagonal trimming die. Trimming operation was also modelled numerically. Taguchi design of experiment was created by defining 5 design parameters and 3 different levels for each parameter in order to analyse and improve the trimming operation performed in the production of hexagonal steel bolts. Minimization of peak trimming load and maximization of peak damage value were determined as objective functions. According to results, below listed conclusions can be drawn;

• According to the results of the Taguchi method, the cutting width and stopping distance parameters were the most effective parameters according to the peak trimming load, the edge radius parameter was the most effective parameter according to the peak damage value.

• Cutting width of 0.7 mm, stopping distance of 0.3 mm, petal angle of 35° were the best parameter levels for the peak trimming load, and edge radius of 0.1 mm, bottom angle of 20° were the best parameter levels for the peak damage value with respect to the conducted Taguchi analysis results.

7. References

[1] C. McCormack, J. Monaghan, Failure analysis of cold forging dies using FEA, J. Mater. Process. Technol. 117 (2001) 209– 215. doi:10.1016/S0924-0136(01)01139-6.

[2] C. McCormack, J. Monaghan, A finite element analysis of cold-forging dies using two- and three-dimensional models, J. Mater. Process. Technol. 118 (2001) 286–292. doi:10.1016/S0924-0136(01)00960-8.

[3] S.-C. Park, K.-H. Lee, Design of the trimming process of an Al6061 alloy bolt head using finite element analysis and the taguchi method, J. Korean Soc. Mar. Eng. 42 (2018) 800–806. doi:10.5916/jkosme.2018.42.10.800.

[4] S.-C. Park, D.-H. Lee, D.-C. Ko, B.-M. Kim, M.-H. Kim, K.-H. Lee, Integrated process design of Al6061 alloy bolts for fastening offshore platforms, J. Mech. Sci. Technol. 33 (2019) 3695–3707. doi:10.1007/s12206-019-0711-5.

[5] P. Skov-Hansen, N. Bay, J. Grønbæk, P. Brøndsted, Fatigue in cold-forging dies: tool life analysis, J. Mater. Process. Technol. 95 (1999) 40–48. doi:10.1016/S0924-0136(99)00319-2.

[6] Y.C. Lee, F.K. Chen, Fatigue life of cold-forging dies with various values of hardness, in: J. Mater. Process. Technol., 2001: pp. 539–543. doi:10.1016/S0924-0136(01)00720-8.

[7] J. Xiong, Z. Guo, M. Yang, W. Wan, G. Dong, Tool life and wear of WC–TiC–Co ultrafine cemented carbide during dry cutting of AISI H13 steel, Ceram. Int. 39 (2013) 337–346. doi:10.1016/j.ceramint.2012.06.031.

[8] J.Petruška,J.Borkovec,J.Hulka,R.Foret,ApplicationofDuctileFractureCriteriatoIndustrialCuttingProcesses,Adv. Mater. Res. 264–265 (2011) 913–918. doi:10.4028/www.scientific.net/AMR.264-265.913.

[9] T.B.Hilditch,P.D.Hodgson,Developmentoftheshearededgeinthetrimmingofsteelandlightmetalsheet Part1:Experimental observations, J. Mater. Process. Technol. 169 (2005) 184–191. doi:10.1016/j.jmatprotec.2005.02.266.

[10] T.B. Hilditch, P.D. Hodgson, Development of the sheared edge in the trimming of steel and light metal sheet Part 2: Mechanisms and modeling, J. Mater. Process. Technol. 169 (2005) 192–198. doi:10.1016/j.jmatprotec.2005.02.267.

[11] ISO 16630-Metallic materials-Method of hole expanding test. Standard, Genf, Switzerland, 2009.

[12] S. Golovashchenko, W. Zhou, S. Nasheralahkami, N. Wang, Trimming and Sheared Edge Stretchability of Light Weight Sheet Metal Blanks, Procedia Eng. 207 (2017) 1552–1557. doi:10.1016/j.proeng.2017.10.1077.

[13] M. Schneider, I. Peshekhodov, A. Bouguecha, B.-A. Behrens, A new approach for user-independent determination of formability of a steel sheet sheared edge, Prod. Eng. 10 (2016) 241–252. doi:10.1007/s11740-016-0677-4.

[14] S.F. Golovashchenko, A study on trimming of aluminum autobody sheet and development of a new robust process eliminating burrs and slivers, Int. J. Mech. Sci. 48 (2006) 1384–1400. doi:10.1016/j.ijmecsci.2006.07.007.

[15] S.F. Golovashchenko, A.M. Ilinich, Trimming of advanced high strength steels, in: ASME Int. Mech. Eng. Congr. Expo., Orlando, Florida USA, 2005: pp. 1–9.

[16] S.F. Golovashchenko, A.M. Ilinich, N.M. Bessonov, L.M. Smith, Analysis of Trimming Processes for Advanced High Strength Steels, SAE Int. J. Mater. Manuf. 2 (2009) 487–493.

[17] S. Nasheralahkami, S. Golovashchenko, K. Pan, L. Brown, B. Gugnani, Characterization of Trimmed Edge of Advanced High Strength Steel, in: SAE Tech. Pap., 2016. doi:10.4271/2016-01-0358.

[18] S. Nasheralahkami, S. Golovashchenko, S. Dawson, R. Sohmshetty, Analysis of Tool Wear for Trimming of DP980 Sheet Metal Blanks, SAE Int. J. Engines. 10 (2017) 2017-01-0302. doi:10.4271/2017-01-0302.

[19] P.D. Barros, A.J. Baptista, J.L. Alves, M.C. Oliveira, D.M. Rodrigues, L.F. Menezes, Trimming of 3D solid finite element meshes: sheet metal forming tests and applications, Eng. Comput. 31 (2015) 237–257. doi:10.1007/s00366-013-0344-8.

[20] B. Lu, H. Ou, An efficient approach for trimming simulation of 3D forged components, Int. J. Mech. Sci. 55 (2012) 30–41. doi:10.1016/j.ijmecsci.2011.11.013.

[21] X.H. Hu, X. Sun, S.F. Golovashchenko, Predicting tensile stretchability of trimmed AA6111-T4 sheets, Comput. Mater. Sci. 85 (2014) 409–419. doi:10.1016/j.commatsci.2014.01.015.

[22] EN ISO 10263-4 Steel rod, bars and wire for cold heading and cold extrusion - Part 4: Technical delivery conditions for steels for quenching and tempering, 2002.

[23] EN ISO 4957-Tool steels, 2018.

Table 1. Chemical composition (in %) of 23MnB4 (EN10263-4:2002)[22].

Fe	C	P	S	Mn	Cr	Si	B	Cu
97.65-98.9	0.2-0.25	0-0.025	0-0.025	0.9-1.2	0-0.3	0-0.3	0.0008-0.005	0-0.25

Table 2. Mechanical properties of annealed 23MnB4.

Property	Value
Ultimate Tensile Strength (UTS) [MPa]	520
Yield Strength [MPa]	359
Poisson's Ratio	0.29
Elastic Modulus [GPa]	210
Hardness (HV)	120
Reduction in Area (%)	67

Table 3. Chemical composition (in %) of M2 1.3343 tool steel (EN ISO 4957:2018)[23].

Fe	C	Mn	P	S	Si	Cr	V	Mo	W
79.65-83.04	0.86-0.94	0-0.40	0-0.03	0-0.03	0-0.45	3.80-4.50	1.70-2.10	4.70-5.20	5.90-6.70

Table 4. Design parameters and their values at each level.

Parameters	Level 1	Level 2	Level 3
Cutting Width (CW) [mm]	0.7	1.0	1.3
Edge Radius (ER) [mm]	0.1	0.3	0.5
Petal Angle (PA) [°]	15	25	35
Bottom Angle (BA) [°]	20	30	45
Stopping Distance (SD) [mm]	0.1	0.2	0.3

Table 5. L_{27} (3^5) orthogonal array table.

Simulation #	CW	ER	PA	BA	SD
1	0.7	0.1	15	20	0.1
2	0.7	0.1	15	20	0.2
3	0.7	0.1	15	20	0.3
4	0.7	0.3	25	30	0.1
5	0.7	0.3	25	30	0.2
6	0.7	0.3	25	30	0.3
7	0.7	0.5	35	45	0.1
8	0.7	0.5	35	45	0.2
9	0.7	0.5	35	45	0.3
10	1.0	0.1	25	45	0.1
11	1.0	0.1	25	45	0.2
12	1.0	0.1	25	45	0.3
13	1.0	0.3	35	20	0.1
14	1.0	0.3	35	20	0.2
15	1.0	0.3	35	20	0.3
16	1.0	0.5	15	30	0.1
17	1.0	0.5	15	30	0.2
18	1.0	0.5	15	30	0.3
19	1.3	0.1	35	30	0.1
20	1.3	0.1	35	30	0.2
21	1.3	0.1	35	30	0.3
22	1.3	0.3	15	45	0.1
23	1.3	0.3	15	45	0.2
24	1.3	0.3	15	45	0.3
25	1.3	0.5	25	20	0.1
26	1.3	0.5	25	20	0.2
27	1.3	0.5	25	20	0.3

Table 6. Finite element analysis results for F_{peak}, D_{peak} and their respective *SN* ratios.

Simulation #	F_{peak} (kN)	*SN* ratio (F_{peak})	D_{peak}	*SN* ratio (D_{peak})
1	92.937	-39.3638	0.6189	-4.1676
2	75.373	-37.5443	0.7699	-2.2713
3	70.001	-36.9021	0.5359	-5.4183
4	68.073	-36.6595	0.3031	-10.3683
5	60.816	-35.6804	0.1265	-17.9582
6	57.526	-35.1973	0.1067	-19.4367
7	50.797	-34.1168	0.2251	-12.9525
8	51.393	-34.2181	0.1065	-19.4530
9	50.510	-34.0675	0.0372	-28.5891
10	120.829	-41.6434	0.5293	-5.5260
11	82.644	-38.3442	0.4268	-7.3955
12	69.743	-36.8700	0.3324	-9.5668
13	99.234	-39.9332	0.3900	-8.1787
14	66.743	-36.4881	0.3189	-9.9269
15	62.341	-35.8955	0.1731	-15.2341
16	116.174	-41.3022	0.2921	-10.6894
17	83.170	-38.3993	0.2420	-12.3237
18	77.768	-37.8160	0.2150	-13.3512
19	202.416	-46.1249	0.6718	-3.4552
20	106.501	-40.5471	0.6815	-3.3307
21	85.983	-38.6883	0.5610	-5.0207
22	179.411	-45.0770	0.4922	-6.1572
23	106.312	-40.5316	0.2960	-10.5742
24	89.373	-39.0241	0.1881	-14.5122
25	162.008	-44.1907	0.2990	-10.4866
26	93.030	-39.3725	0.2865	-10.8575
27	81.264	-38.1980	0.2504	-12.0273

RESIDUAL STRESS MEASUREMENTS OF COLD-FORGED BALL STUDS BY THE CONTOUR METHOD

M. Burak TOPARLI
N. Emrah KILINÇDEMİR
Sezgin YURTDAŞ
Barış TANRIKULU
Umut İNCE

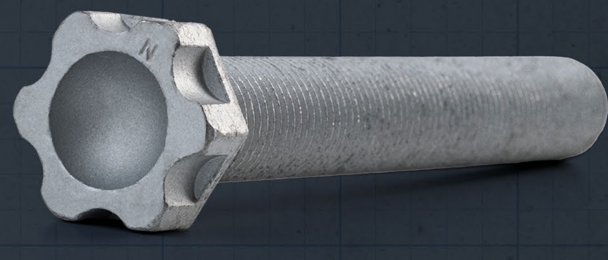

Experimental Techniques, 2021

RESIDUAL STRESS MEASUREMENTS OF COLD-FORGED BALL STUDS BY THE CONTOUR METHOD

M. Burak Toparli[1*], N. Emrah Kılınçdemir[2], Sezgin Yurtdaş[1,3], Barış Tanrıkulu[1,4], Umut İnce[1]

[1]R&D Center, Norm Cıvata, IAOSB, Cigli, Izmir, 35620 Türkiye
[2]Norm Fasteners Co., 735 East Hazel Street, Lansing, Michigan, 48912, USA
[3]Mechanical Engineering Department, Izmir Katip Çelebi University, Cigli, Izmir, 35620, Türkiye
[4]Mechanical Engineering Department, Dokuz Eylül University, Izmir, 35390, Türkiye
[*]Corresponding author: Email address: burak.toparli@norm-fasteners.com.tr

Abstract

In this study, residual stresses of cold-forged ball studs were investigated by the contour method with using widely available wire-Electro-Discharging Machine (wire-EDM) and Coordinate Measuring Machine (CMM). After the wire-EDM cutting, one of the steps of the contour method, it was revealed that the surface contour data was affected from the cutting step. Therefore, to increase the accuracy of the measured residual stresses, one of the ball studs were heat-treated to normalize residual stresses due to cold forging. The contour data of the heat-treated sample was subtracted from the as-forged surface contour to eliminate any cutting-induced artefacts. The final residual stress profiles suggested that the subtracting procedure minimized the cutting errors. In addition, a new classification approach for the cutting-induced errors for the contour method was introduced. According to final stress maps obtained by the contour method, it was revealed that high compressive residual stresses were obtained at the socket regions of the ball studs, as expected. Balancing tensile residual stresses were observed at the inner regions.

Keywords: Cold forging; residual stress; contour method; ball stud; cutting-induced artefacts

1. Introduction

Cold forging is one of the metal forming processes, preferred mainly for mass production in various industries such as automotive. Having various types and classifications, cold forging is based on plastic deformation introduced through dies and tools. Depending on the geometry, complex residual stress fields are inherently introduced due to non-homogenous plastic deformation [1]. In terms of fasteners, significant number of cold-formed products such as bolts, nuts, studs, rivets, bushings are used in as-forged conditions. Therefore, characterization of residual stresses is very important, since they play a critical role in structural integrity.

Residual stresses are locked-in and self-balanced stresses observed in the absence of external loads. Any source of misfit such as non-homogenous plastic deformation after forming processes can lead to formation of residual stresses. Being tensile or compressive, residual stresses can superimpose with applied loads and lead to premature failures. In addition to analytical and numerical methods, residual stresses can be obtained by experimental techniques. Since its introduction in 2000 [2], the contour method has been preferred as one of the destructive residual stress measurement methods. Obtaining stresses normal to free surface with 2D spatial variation, being generally insensitive to microstructural features and direct stress calculation without any approximated coefficients are the key features compared to other measurement techniques. In addition, by using widely available wire-Electro-Discharging Machine (wire-EDM) and Coordinate Measuring Machine (CMM), residual stresses can be obtained without any need of special tools or equipment. The contour method has been widely used in the literature to obtain residual stresses of various samples with different material-process combinations [3-8].

The principle of Bueckner for cracked body [9] was adopted to be used in the contour method. In practice, the method can be applied through a 4-steps procedure. Sample to be investigated is cut by wire-EDM and original residual stresses are assumed to be relaxed elastically. The surface contours after stress relaxation are measured by using a CMM or non-tactical methods such as laser profilometer. After obtaining relaxed surface contours, data analysis is required for the next step. The final surface contour after data analysis is employed as a boundary condition of the FE model and linear elastic analysis is carried out to obtain 2D residual stresses. In addition to FE modelling, a new mathematical model was developed to calculate the residual stresses directly from the measured data [10].

As discussed in the literature, cutting can be considered as the most critical step of the contour method [11]. All the subsequent steps are built on the cutting and the final accuracy of the obtained results mainly depends on the cutting step. In addition, cutting is irreversible, therefore, any cutting-related issue can have a significant effect on the residual stress results. Therefore, all precautions should be taken into account to minimize any cutting-related errors. There are well-number of studies in the literature examining the reasons and influence of cutting artefacts considering the contour method. Obtaining flat cut surfaces with low surface roughness can be considered as the main requirement expected from an ideal cutting for the contour method [12]. Flatness is very crucial in terms of the accuracy of the final residual stress profiles, since any deviation in flatness will induce incorrect surface contour data to be processed in the data analysis stage. Local artefacts due to wire breakage/stoppage and cutting instabilities lead to steps or ledges, affecting surface contour data. In addition, start/end of cutting and wire entrance/exit regions, i.e. outermost region of the sample are also more susceptible to artefacts as noted in the literature [13]. Surface waviness and surface bowing are also other cutting artefacts that can be observed during wire EDM cutting for the contour method [14]. Different cutting strategies [14] and conducting cutting trials to minimize the cutting artefacts including cutting-induced plasticity [11] were applied in the literature. Various cutting configurations [15], self-equilibrating cutting strategies [16] and employing sacrificial blocks [17] were also investigated to minimize cutting errors. In addition, stress-free reference cuttings to determine and quantify cutting errors were carried out for different material and processing combinations [15,18-20]. After obtaining cutting artefacts from reference cutting, surface contour data was subtracted from the data of samples to be investigated, which was cut with the same cutting configuration of the stress-free reference cutting.

In this work, residual stress profiles of cold-forged ball studs were obtained by the contour method. After the cutting of as-forged sample, it was revealed that there were various sources of cutting artefacts affecting the accuracy of the final residual stresses. In order to quantify the cutting artefacts, one of the samples was heat-treated to obtain a stress-free sample. Then, the heat-treated sample was cut with the same cutting configuration and the surface contour was obtained. In order to minimize the cutting errors, the surface contour data of the heat-treated sample was subtracted from the as-forged sample and final residual stress fields were obtained. As a result, residual stress maps of forged samples were obtained. In addition, based on the observed cutting-induced features, an alternative classification of the cutting-induced artefacts was introduced for the contour method.

2. Sample Preparation

In this study, ball studs used in automotive industry were produced by cold forging for residual stress measurements.

Cold forging is one of the fundamental metal shaping processes particularly suitable for mass production. The final shape of the products is obtained through a multi-stage production route by vertical or horizontal presses. Shaping is based on exerting enough forces through dies and tools so that the material is plastically deformed. The production stages of the ball studs investigated in this study were given in Fig. 1. The ball studs were cold-forged in five stages. After obtaining the shaft diameter by reduction stage, the sample was prepared for the head geometry. At the final stage, the sockets were introduced from top and bottom sides of the samples through punches. In terms of residual stress generation, due to non-homogenous plastic deformation, residual stresses were formed. Since, plastic deformation was different in each stage and the stages were sequential, residual stress distribution was built on the

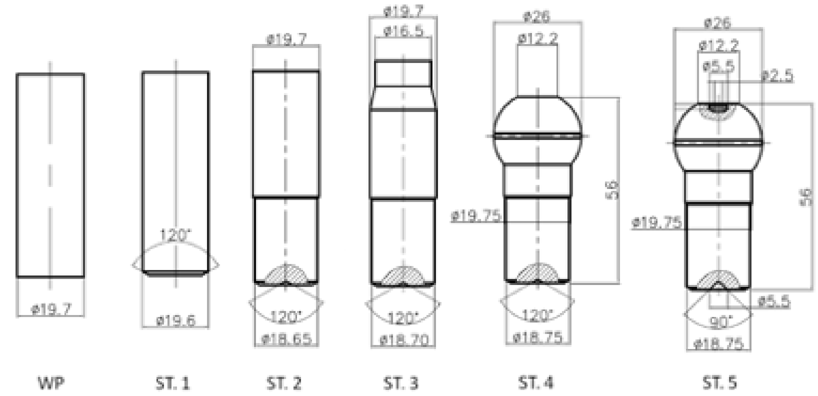

Fig. 1. Cold forging stage designs and final dimensions of ball studs.

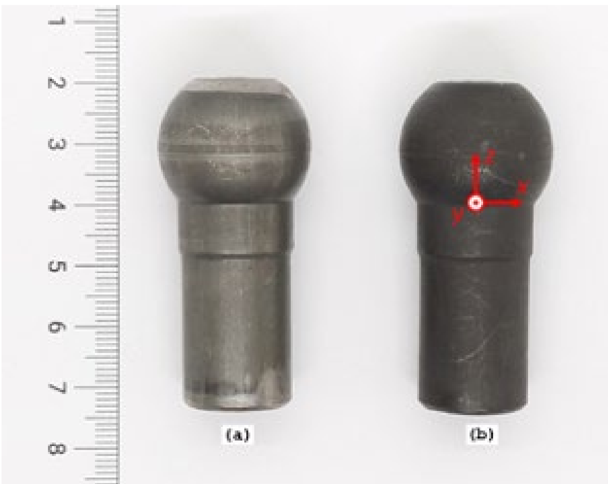

Fig. 2. (a) As-forged and (b) heat-treated ball studs used in this study. (y=0 is the mid-thickness of the ball stud)

history of previous stage and the plastic deformation obtained in the current stage. Therefore, final residual stress distribution was the superposition and redistribution of residual stresses obtained at each stage. The raw material was deformed without any prior heating. The dimensions of as-forged and heat treated samples were given in Fig. 1 (ST. 5). The ball studs used for residual stress measurements can be seen in Fig. 2.

The elemental composition and mechanical properties of the raw material, i.e. 41Cr4, was given in Tab. 1, according to EN 10263-4:2002 standard [21]. One of the ball studs was heat-treated to normalize residual stresses to obtain a stress-free sample required to quantify cutting-induced artefacts. Therefore, the sample was subjected to spheroidizing heat treatment, which is widely applied in forging industry prior to cold forging not only to decrease required forging loads by increasing the ductility but also to normalize residual stresses and grain size orientation history leading to non-isotropic material behaviour. In this study, spheroidizing was applied after cold forging to obtain a stress-free sample. Compared to stress-relief operations for steel parts defined by SAE AMS2759/11A [22], the reference sample was held for 24 hours at elevated temperatures (i.e. below eutectoid temperature, i.e. AC1 or A1) and furnace cooling (8 hours) was carried out instead of air cooling. Therefore, it was reasonable to assume that the residual stress fields were very close to stress-free after spheroidizing.

Table 1. Elemental composition and mechanical properties of 41Cr4 alloying steel according to EN 10263-4:2002 standard [21].

Material	Elemental composition							
41Cr4	C	Si	Mn	P	S	Cr	Cu	Fe
	0.38-0.45	≤0.30	0.60-0.90	≤0.025	≤0.025	0.90-1.20	≤0.25	Bal.
	Mechanical properties							
	max. Rm (tensile strength) (MPa)				*min. Z (percentage reduction of area) (%)*			
	610-650				58-60			

3. Residual Stress Measurement

3.1. Contour Method

Residual stress measurement by the contour method is based on the Bueckner's Superposition Principle revealed in 1958 [9]. The schematic 3-D representation of the contour method and Bueckner's Superposition Principle was given in Fig. 3 [23]. Step A is the initial residual stress state to be measured. In Step B, the part is cut into two parts so that residual stresses are relaxed leading to a contoured surface profile. In Step C, the deformed cut surface is forced back to its original state in Step A. Therefore, in order to obtain original residual stresses in Step A, stresses from Step B and Step C are required to be superimposed:

$$\sigma^A(x,y,z) = \sigma^B(x,y,z) + \sigma^C(x,y,z) \tag{1}$$

where σ represents the complete stress sensor and *x*, *y* and *z* are the directions shown in Fig. 3.

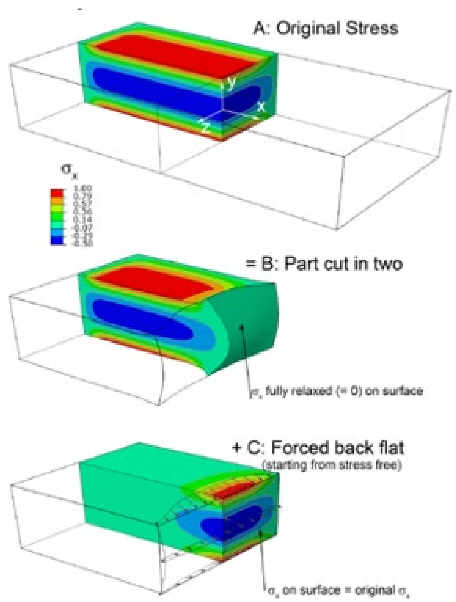

Fig. 3. Superposition Principle employed for the contour method. Only quarter of the sample is plotted [20].

Considering stresses at the cut surface in Step B, i.e. σ^B (0,*y*,*z*), σ_x, τ_{xy} and τ_{xz} are zero on the free surface due to elastic stress relaxation:

$$\sigma_x^B(0,y,z) = 0 \tag{2}$$

$$\tau_{xy}^B(0,y,z) = 0 \tag{3}$$

$$\tau_{xz}^B(0,y,z) = 0 \tag{4}$$

Therefore, to obtain original normal stresses perpendicular to cut surface in Step A, Eq. 1 can be rewritten considering the Eq. 2:

$$\sigma_x^A(0,y,z) = \sigma_x^C(0,y,z) \tag{5}$$

For the normal stresses in y- and z-directions, stresses are partially relaxed due to cutting. Therefore, in order to obtain stresses in Step A, stresses in Step B are also required:

$$\sigma_y^A(0,y,z) = \sigma_y^B(0,y,z) + \sigma_y^C(0,y,z) \tag{6}$$

$$\sigma_y^A(0,y,z) = \sigma_y^B(0,y,z) + \sigma_y^C(0,y,z) \tag{7}$$

For standard implementation of the contour method, stresses normal to cut plane can be obtained by employing Eq. 5. However, in order to obtain in-plane normal stresses, additional effort is required. Considering the effect of shear stresses (i.e. transverse displacements after cutting), averaging the surface contours after surface relaxation (i.e. displacements normal to cut plane), any anti-symmetrical transverse displacements are cancelled out [24]. Therefore, by obtaining the surface contours and averaging, normal stresses perpendicular to cut surface can be obtained by the contour method.

The contour method offers advantages compared to other residual stress measurement techniques. The ability to obtain a full 2D stress map with a single measurement process makes the contour method unique. In order to obtain a similar map by using diffraction techniques or hole drilling, repetitive measurements are required at different locations. Since measured displacement can be directly used, direct stress calculation can be carried out without any approximated coefficients as used in other destructive methods including hole drilling and slitting, i.e. displacements are measured at remote locations [25]. Owing to direct stress calculation, no calibration is required for this method. In addition, the contour method is also insensitive to large grain sizes and crystallographic texture from which diffraction techniques are highly affected [26], as long as these factors do not cause significant global change of elastic constants.

Besides its advantages, there are mainly two limitations of the contour method. The residual stresses can be determined only in one direction. However, there have been studies on methods to obtain all orthogonal stress components by employing several techniques, such as the eigenstrain approach [27,28], multiple cuts [29,6,7] and the superposition principle based on a combination of results from the contour method and other methods such as X-ray diffraction [30]. The second limitation is the measurement of residual stresses near the outer surfaces of the cut region [24]. Since these regions are highly affected due to wire-EDM cutting, extra precautions in cutting strategy and data analysis are required. Use of sacrificial blocks is one of the preferred methods to protect the outer region from cutting artefacts [17].

After its introduction in 2000, numerous comparison and validation studies were performed for the contour method. Residual stresses after various types of processes applied to different materials were obtained by the contour method and were compared with the results obtained by neutron diffraction [31,32], synchrotron X-ray diffraction [4,33], X-ray diffraction [11,34], hole drilling [11,17] and slitting [8,35]. Considering the comparison studies, most of the residual stresses were in one standard deviation [36]. Therefore, it was shown that residual stresses can be obtained by the method considering the limitations.

In this study, contour method was applied to obtain residual stresses according to Eq. 5. According to Cartesian coordinate system as shown in Fig. 2 (*y*=0 is the mid-thickness of the ball stud) two orthogonal residual stresses, i.e. σ_x and σ_y, will be the same considering the axis-symmetrical configuration of the ball studs. σ_z will be highly dependent on the location of the cut. In addition, the cutting configuration will not be symmetrical at any cutting location, which is one of the necessities of the contour method. Therefore, the cutting was performed at *y*=0, so that the cutting was symmetrical and σ_x and σ_y were obtained. Residual stress measurements via the contour method were executed in four main steps: cutting, contour measurement, data analysis and finite element modelling.

3.2. Contour Method Cutting

Heat-treated and as-forged samples were cut by employing a SPM e-Zcut EDM using Brass wires with 0.25 mm diameter. The cutting configuration of the samples can be seen in Fig. 4. Owing to geometry of the sample, both cutting and clamping were symmetric with respect to cutting plane. Cuttings were performed by employing adaptive control feature, so that cutting parameters were adjusted during cuttings.

Fig. 4. Cutting configuration employed for the contour method.

3.3. Contour Measurement

The surface contours after stress relaxation were measured by using a Zeiss Contura G2 CMM. Surface displacements of both halves of the ball studs were obtained. The measurement density was selected as 100 μm, leading to about 28000 points for both halves. The maximum peak-to-valley differences of averaged heat-treated and as-forged samples were around 25 μm and 70 μm, respectively.

3.4. Data Analysis

The measured surface contours of both halves were gridded and averaged before employing a data analysis. After averaging, the surface contour data of the heat-treated sample was subtracted from the as-forged sample to eliminate any artefacts arising from the cutting. The contour data of all the samples were used in as-measured condition. Bivariate spline smoothing, widely used data fitting method for the contour method, was employed after averaging. The optimum knot spacings required for bivariate spline smoothing, i.e. surface fitting for the contour data without under or over-fitting, were obtained for each sample according to the guidelines presented in [11]. The data analysis was carried out for heat-treated, as-forged and subtracted as-forged samples by using quadratic order bivariate splines.

3.5. Finite Element Analysis

The model representing the half of the ball stud was constructed from the surface displacements measured by CMM. The relaxed surface contours after data analysis were introduced as a displacement boundary condition to finite element model. The mesh was generated with a bias so that refined elements near surface region was obtained. Linear elastic static analysis was performed by employing C3D8R type elements. The number of total elements and nodes were 201446 and 204612, respectively. The FE model was constrained from two corners to avoid any rigid body motion. The same FE model was used for heat-treated, as-forged and subtracted as-forged contour data.

4. Results

One of the cut surfaces of as-forged sample can be seen in Fig. 5. Start and end of the cut locations, as well as wire entrance and exit regions were indicated in the Figure. Cutting-related issues such as burn marks, wire stoppage etc. affecting the final accuracy of the residual stress profiles were observed. Therefore, before obtaining the final residual stress fields by FE modelling, cutting artefacts were planned to be investigated. In order to obtain cutting artefacts and isolate those artefacts from the as-forged sample, heat treated sample having normalized residual

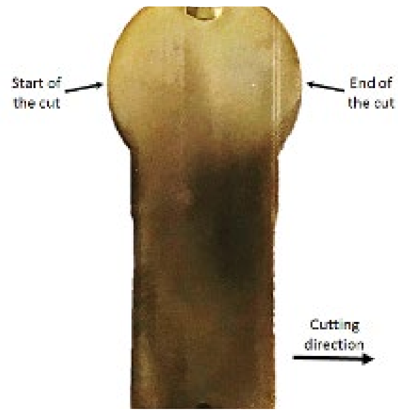

Fig. 5. One of the cut surfaces of as-forged sample. The height of the ball stud is 56 mm.

stress fields was used. One of the cut surfaces and the contour data of the heat-treated sample can be seen in Fig. 6. Owing to heat treatment, it was expected that residual stresses were normalised leading to theoretically no surface contour data. However, there were significant artefacts observed for the contour profiles of heat-treated sample. Therefore, any surface contours after heat treatment were associated with the cutting step (Fig. 6a). Clear representations of the cutting induced artefacts and corresponding locations were shown in Fig. 6b. As noted from the measured contour data, wire entrance edges were disturbed particularly for the regions where the geometry of the sample was changing. A very local cutting artefact was observed inside the top socket edge region close to the wire entrance, which was associated with geometry change and edge effect. However, due to cutting configuration, i.e. samples were fixed on the machine table, the wire exit region was preserved from the cutting artefacts, compared

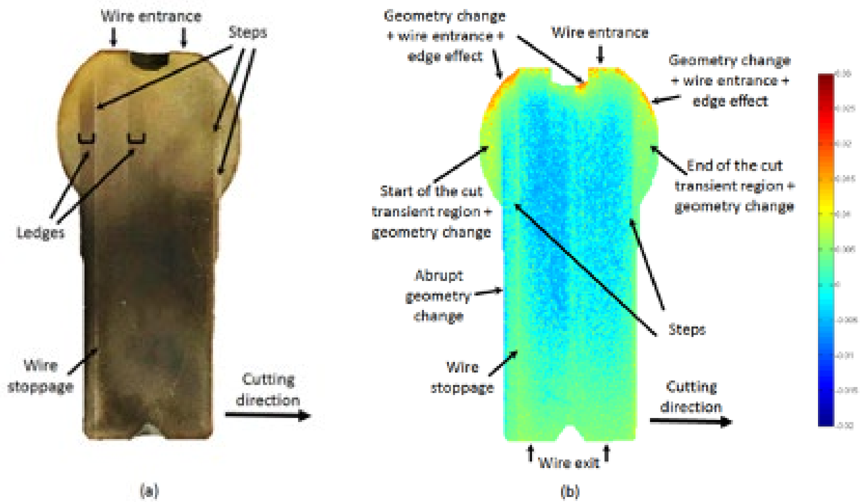

Fig. 6. (a) One of the cut surfaces and (b) averaged and gridded contour data of heat-treated sample. The contour plot is in mm.

to the wire entrance region. This can be incorporated with the machine table acting as a sacrificial block, as used in the literature for edge protection [17]. In addition, the start and end of the cut regions were also affected due to not only EDM cutting-originated artefacts but also geometric variations at these regions. There were very distinct contour variations for the start and end of the cut regions. Furthermore, there were clear steps, i.e. abrupt colour and contour variations observed for the cut surface and measured contour data. One of the steps was observed due to wire stoppage, observed while monitoring the cutting process. Another cutting artefact known as "ledge" was also observed for the cut surface. A very clear cutting-induced error was also seen for the measured contour data when the geometry was changing abruptly. The cutting artefacts mentioned in Fig. 6 led to surface contour variations, which would cause superficial residual stresses. Burn marks were also noted on the cut surfaces. However, there was no significant contour variation in the surface data due to burn marks.

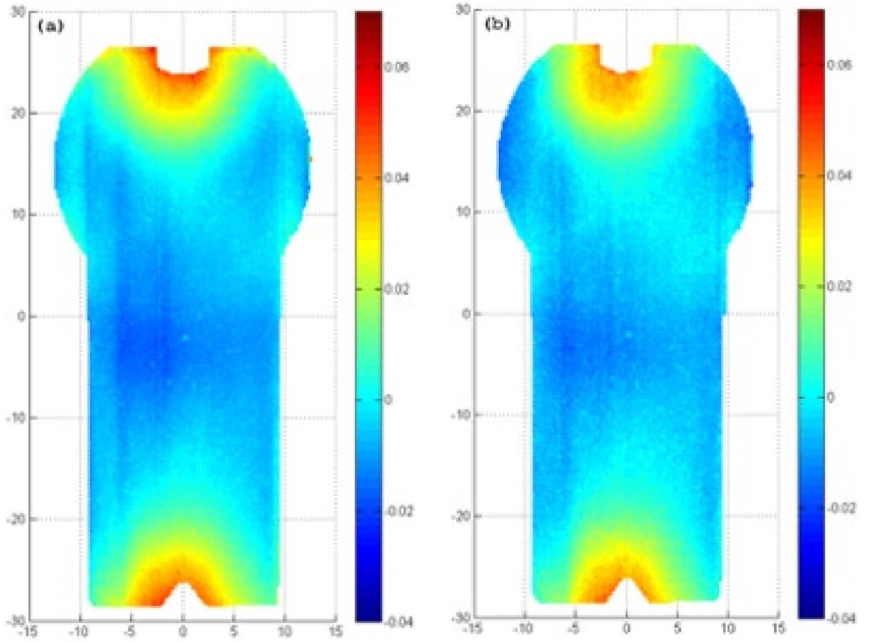

Fig. 7. One of the averaged and gridded contour data of (a) as-forged and (b) subtracted as-forged sample. The axes and the contour plots are in mm.

One of the averaged and gridded surface contours of the forged sample (as-forged and subtracted as-forged) can be seen in Fig. 7. As can be seen from the cut surface (Fig. 5), there were very similar cutting-induced artefacts compared to the heat-treated sample, as shown in Fig. 6. Considering the surface contour map of as-forged sample (Fig. 7a), there were clear contour features which was associated with the steps observed during the cutting. In addition, the cutting artefacts were visible at the start and end of the cut transient regions. Compared to as-forged sample, the effects of cutting were less for the subtracted as-forged sample particularly for the outermost regions (Fig. 7b). The near-edge region of wire entrance was changed significantly after subtracting the contour data of heat-treated data from the as-forged sample. The start and end of the cut regions were also modified substantially. According to Fig. 7a and Fig. 7b, subtracting the contour data of heat-treated surface contours from the as-forged sample minimized the cutting artefacts, however, the process was insufficient to eliminate all the cutting-induced artefacts.

2D residual stress maps of heat-treated and forged sample (as-forged and subtracted as-forged) can be seen in Fig. 8. Considering the heat-treated sample, significant residual stress fields at various locations were observed (Fig. 8a). Up to −640 MPa residual stresses were obtained at the wire entrance region, i.e. the most highly disturbed region considering the magnitude of the residual stresses. A very local cutting artefact was observed inside the top socket edge region close to the wire entrance, which can be associated with both geometry change and edge effect. The wire exit region, mechanically in contact with EDM machine table, was preserved from cutting artefacts compared to the wire entrance region. The start of the cut area was highly stressed, as expected since this region is highly susceptible to cutting artefacts. The end of the cut region was also affected from the EDM cutting, but more localized compared to the start of the cut region. In addition, there is a significant tensile residual stress field due to abrupt geometry change close to the start of the cut. As discussed in the literature, edges of the samples are prone to EDM cutting artefacts, therefore, it is suggested to not be included in the results, if particular attention was not spent [13]. Therefore,

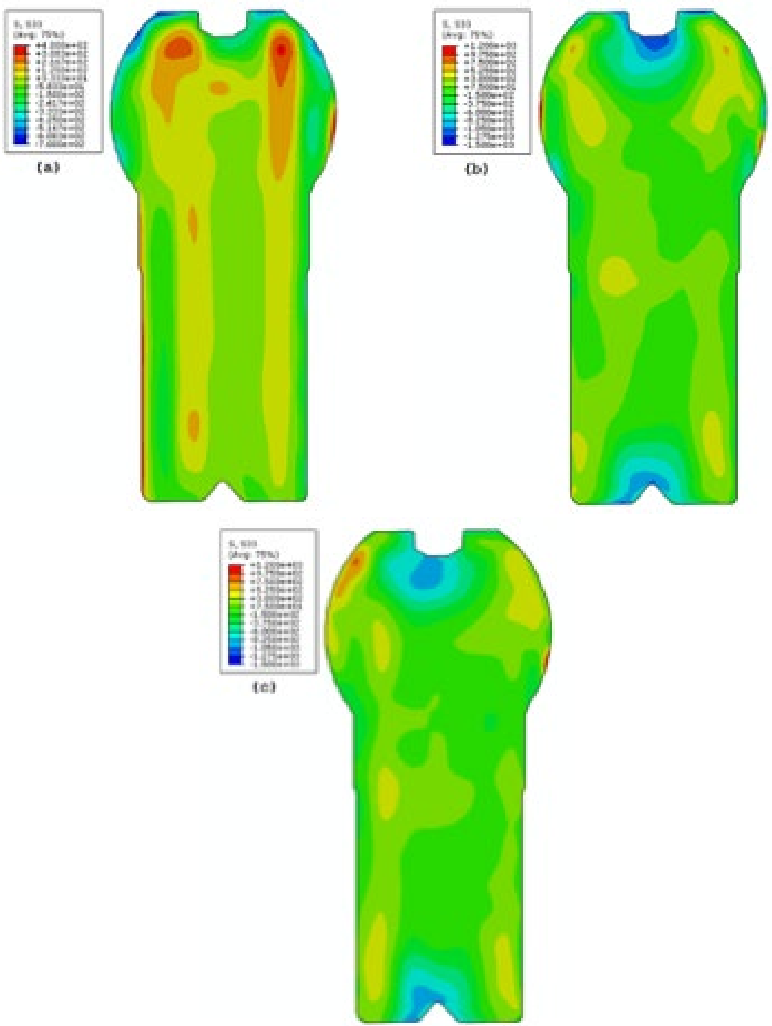

Fig. 8. 2D residual stress maps of (a) heat-treated, (b) as-forged and (c) subtracted as-forged samples. Scale for residual stresses given in (a) is different than (b) and (c). Scales are the same for (b) and (c).

residual stress fields near the edges of the heat-treated sample were more susceptible to cutting-induced errors except the wire exit region, where machine table acted as a sacrificial block. The head of the sample with geometric variation close to start and end of the cut regions, were also affected significantly. Furthermore, residual stress fields were also altered due to wire feed stoppage. Due to very high compressive stresses at the wire entrance region, cutting artefacts which can be correlated with the measured surface contours and the geometry of the sample, two balancing tensile residual stress islands were observed at the head of the sample extending until the wire exit edge. Considering the forged sample in as-forged and subtracted conditions (Fig. 8b and Fig. 8c), the residual stresses at the top and bottom socket region were compressive due to high plastic deformation introduced by punches used during cold forging. The general trends were observed similar for both cases except the wire entrance, start and end of the cut regions i.e. outer most regions except wire exit region, preserved by machine table, acting as a sacrificial block as used in the literature.

Line profiles of the heat-treated and as-forged samples can be seen in Fig. 9. For the heat-treated sample, significant residual stresses were observed for the head region of the sample, i.e. the first 10 mm of the line plots. The wire entrance effect can be regarded as one of the main reason for the observed cutting artefacts, as discussed previously.

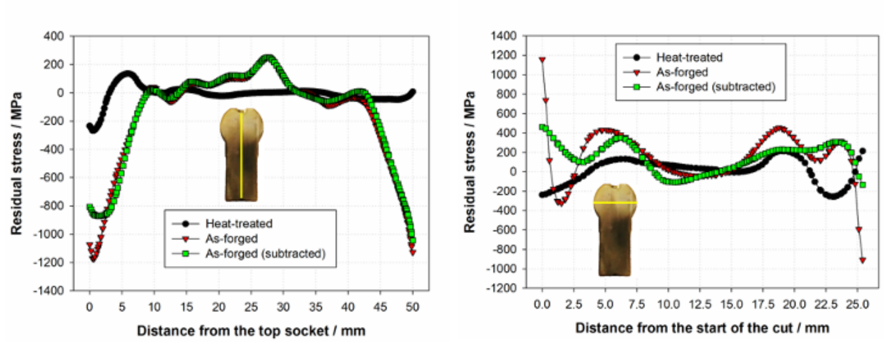

Fig. 9. Line profiles of heat-treated and forged samples. Location of the residual stresses was shown in the figure.

Considering the wire exit region, in contact with machine table as shown in Fig. 4, the as-forged and subtracted as-forged results were very close to each other. The RMS of the residual stresses obtained from the initial 5.0 mm of the wire entrance and exit regions of the subtracted as-forged sample with respect to as-forged were 131 and 39 MPa, respectively. For the inner region of the sample, influence of cutting artefacts were less, suggesting very close profiles for as-forged and subtracted as-forged results. The RMS of the residual stresses of the inner region was obtained as 19 MPa.

As the head region of the heat-treated sample was highly affected region from the cutting, line profiles across this region was obtained for further investigation (Fig. 10). The disturbed start and end of the cut regions were very clear. The RMS of the residual stresses obtained from the initial 5.0 mm of the start and end of the cut regions of the subtracted as-forged sample were 255 and 150 MPa, respectively. The cutting configuration of these regions were very challenging, since various sources of cutting artefacts were present simultaneously, as shown in Fig. 6b. In addition to start and end of the cut artefacts, geometric variations were also contributed to observed artefacts.

5. Discussion

Considering the as-forged sample, high compressive residual stress regions were observed around the socket regions, as expected. The top and bottom socket features were introduced through punches in cold-forging, introducing significant and local plastic deformation leading to residual stress generation. Superficially high residual stresses were observed for the as-forged sample, which was corrected after subtracting procedure. The peak compressive residual stresses of the subtracted as-forged sample were around −870 and −1040 MPa for the top and bottom socket regions, respectively. Compared to yield point of the material as given in Tab. 1, higher stress values were observed at the socket regions. As cold forging depends on material forming via plastic deformation, significant strain hardening can be expected. Therefore, higher stresses at the socket regions can be incorporated with strain hardening as a result of cold forging. In addition, plasticity during the cutting might also contributed to these values, particularly for the outermost edge regions [37].

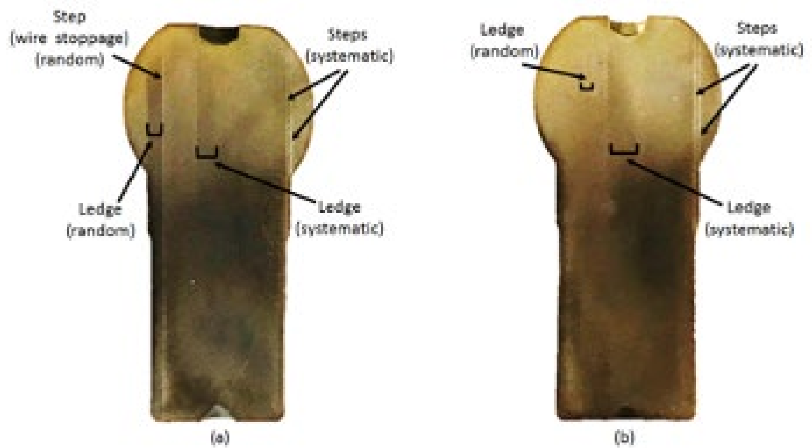

Fig. 11. Systematic and random cutting-induced artefacts for (a) heat-treated and (b) as-forged sample.

In the literature, the cutting errors or artefacts for the contour method were categorized as symmetric and anti-symmetric errors with respect to the cut plane [13]. It was noted that the symmetric errors should be taken into account and have to be minimized. It was stated that the effect of shear stress and any anti-symmetric errors were removed after averaging the contour data of the both halves. Considering the cutting-induced artefacts observed for heat-treated and as-forged samples in this study, a new classification of the cutting errors was proposed. For a particular geometry and cutting with wire-EDM used with the same process parameters, cutting artefacts can be divided into two groups: systematic and random artefacts. As observed in this study, there were cutting artefacts called "steps" which can be categorized as systematic errors, i.e. they were obtained for both heat-treated and as-forged samples at the same location (Fig. 11). However, there was a "ledge" type of artefact due to wire stoppage, observed for the heat-treated sample only. In addition, there were also "steps" type artefacts, for heat-treated and as-forged samples observed at different locations.

In this study, different and significant cutting artefacts were observed and their contributions to final residual stress fields were investigated. Considering the systematic cutting artefacts, they can be minimized by subtracting the contour data of the stress-free sample from the as-forged sample [38]. As shown in Fig. 7b and 7c, the artefacts observed at wire entrance region were modified by employing the subtracting procedure. In addition, the start and end of the cut transient regions were also altered after subtracting the contour data of the heat-treated sample. Therefore, despite significant cutting artefacts, the effects of systematic cutting can be minimized by the subtracting procedure. However, random artefacts can be minimized by only choosing optimum EDM cutting parameters leading to stable cutting.

As observed in this study, both abrupt and transient geometry changes affect the cut quality and lead to various cutting artefacts. Therefore, to obtain more reliable results, cutting configuration has to be chosen to minimize any abrupt geometric variation. In addition, accurate near-surface residual stresses measurement is known to be very challenging by the contour method [24,39]. As shown by the RMS study, near-surface regions are more susceptible to cutting-induced errors. As a result, particular attention has to be given, if the region of interest is near the outer surface of the investigated sample.

6. Conclusions

Based on this study, the following conclusions can be drawn:

1. Significant residual stresses were introduced due to cold forging, as expected. Owing to geometry and production route of the investigated samples, compressive residual stresses were observed at the top and bottom socket regions. Balancing tensile residual stresses were distributed at the head and shaft region of the investigated ball studs.

2. The cutting-induced artefacts considering the contour method can be classified as systematic and random. Systematic errors can be minimized by employing a stress-free sample cutting and subtracting the surface contour data from the actual sample. However, due to nature of occurring, random artefacts can be also observed. Therefore, it can be concluded that subtracting the surface data of the stress-free sample from the actual contour will increase the accuracy, however, it may not be adequate to remove all the cutting-induced errors.

3. Cutting trials before the actual cut will decrease the possibility of both systematic and random artefacts for the contour method. By choosing better cutting technique (cutting parameters, cutting configurations etc.), the need for a correction can be reduced. However, for the most accurate results, both cutting trials and a stress-free sample cutting are suggested to be employed to increase the accuracy of the final results.

4. The geometric variations greatly contribute to observed cutting artefacts for the contour method. Therefore, the cutting strategy should be determined considering the geometric variation of the sample. Any abrupt geometric variations should be minimized during the cutting step to obtain less-cutting-affected regions and more accurate final residual stress results.

Acknowledgement
The authors would like to thank to CMS R&D Center, Türkiye for their cooperation.

Conflict of Interest
On behalf of all authors, the corresponding author states that there is no conflict of interest.

References

1. Yurtdaş S, Toparli MB, Damla T, Tanrıkulu B, Kılınçdemir E, İnce U, Aydın L (2018) A Comparative Study of Metal Shaping Processes Between Forging and Machining. In: Arapgirlioglu H, Atik A, Hizirolu S, Elliott R, Atik D (eds) The Most Recent Studies in Science and Art, vol 2. Gece Publishing, Ankara, Türkiye, pp 1462-1471.

2. Prime MB, Gonzales AR The contour method: Simple 2-D mapping of residual stresses. In: Webster GA (ed) Sixth International Conference on Residual Stresses, Oxford, UK, 2000. Maney Publishing, pp 617-624.

3. Kartal ME, Turski M, Johnson G, Fitzpatrick ME, Gungor S, Withers PJ, Edwards L (2006) Residual Stress Measurements in Single and Multi-Pass Groove Weld Specimens Using Neutron Diffraction and the Contour Method. Materials Science Forum 524-525:671-676.

4. Evans A, Johnson G, King A, Withers PJ (2007) Characterization of laser peening residual stresses in Al 7075 by synchrotron diffraction and the contour method. Journal of Neutron Research 15 (2):147 - 154.

5. Zhang Y, Ganguly S, Edwards L, Fitzpatrick ME (2004) Cross-sectional mapping of residual stresses in a VPPA weld using the contour method. Acta Materialia 52 (17):5225-5232.

6. Pagliaro P, Prime M, Swenson H, Zuccarello B (2010) Measuring Multiple Residual-Stress Components using the Contour Method and Multiple Cuts. Experimental Mechanics 50 (2):187-194. doi:10.1007/s11340-009-9280-3.

7. Toparli MB, Fitzpatrick ME, Gungor S (2015) Determination of Multiple Near-Surface Residual Stress Components in Laser Peened Aluminum Alloy via the Contour Method. Metallurgical and Materials Transactions A 46 (9): 4268-4275. doi:10.1007/s11661-015-3026-x.

8. Hosseinzadeh F, Toparli MB, Bouchard PJ (2012) Slitting and Contour Method Residual Stress Measurements in an Edge Welded Beam. Journal of Pressure Vessel Technology 134:0114021 - 0114026.

9. Bueckner HF (1958) The Propagation of Cracks and the Energy of Elastic Deformation. Transactions of the American Society of Mechanical Engineers 80:1225-1230.

10. Kartal ME (2013) Analytical solutions for determining residual stresses in two-dimensional domains using the contour method. Proceedings of the Royal Society A: Mathematical, Physical and Engineering Sciences 469 (2159):20130367. doi:doi:10.1098/rspa.2013.0367.

11. Toparli MB, Fitzpatrick ME, Gungor S (2013) Improvement of the Contour Method for Measurement of Near-Surface Residual Stresses from Laser Peening. Experimental Mechanics 53 (9):1705-1718. doi:10.1007/s11340-013-9766-x.

12. Bouchard P, Ledgard P, Hiller S, Hosseinzadeh F (2012) Making The Cut for The Contour Method. Paper presented at the 15th International Conference on Experimental Mechanics (ICEM 2015), Porto, Portugal.

13. Prime MB, Kastengren AL (2011) The Contour Method Cutting Assumption: Error Minimization and Correction. In: Proulx T (ed) Experimental and Applied Mechanics, Volume 6. Conference Proceedings of the Society for Experimental Mechanics Series. Springer New York, pp 233-250. doi:10.1007/978-1-4419-9792-0_40.

14. Hosseinzadeh F, Kowal J, Bouchard P (2014) Towards good practice guidelines for the contour method of residual stress measurement. The Journal of Engineering 8:453-468. doi:http://dx.doi.org/10.1049/joe.2014.0134.

15. Ahmad B, Fitzpatrick ME (2016) Minimization and Mitigation of Wire EDM Cutting Errors in the Application of the Contour Method of Residual Stress Measurement. Metallurgical and Materials Transactions A 47 (1):301-313. doi:10.1007/s11661-015-3231-7.

16. Muránsky O, Hamelin CJ, Hosseinzadeh F, Prime MB (2018) Evaluation of a self-equilibrium cutting strategy for the contour method of residual stress measurement. International Journal of Pressure Vessels and Piping 164:22-31. doi:https://doi.org/10.1016/j.ijpvp.2017.04.002.

17. Toparli MB, Fitzpatrick ME (2016) Development and Application of the Contour Method to Determine the Residual Stresses in Thin Laser-Peened Aluminium Alloy Plates. Experimental Mechanics 56 (2):323-330. doi:10.1007/s11340-015-0100-7.

18. DeWald AT, Hill MR (2009) Eigenstrain-based model for prediction of laser peening residual stresses in arbitrary three-dimensional bodies Part 2: Model verification. The Journal of Strain Analysis for Engineering Design 44 (1):13-27. doi:10.1243/03093247jsa420.

19. Pagliaro P, Prime MB, Clausen B, Lovato ML, Zuccarello B (2009) Known Residual Stress Specimens Using Opposed Indentation. Journal of Engineering Materials and Technology 131 (3). doi:10.1115/1.3120386.

20. Hill MR, Olson MD Repeatability of the Contour Method for Residual Stress Measurement. In, Cham, 2014. Residual Stress, Thermomechanics & Infrared Imaging, Hybrid Techniques and Inverse Problems, Volume 8. Springer International Publishing, pp 103-111.

21. Steel rod, bars and wire for cold heading and cold extrusion - Part 4: Technical delivery conditions for steels for quenching and tempering (2002). German Institute for Standardization (DIN).

22. Stress Relief of Steel Parts AMS2759/11A (2018). SAE International.

23. The Contour Method (2013). In: Practical Residual Stress Measurement Methods. pp 109-138. doi:10.1002/9781118402832.ch5.

24. Prime MB, Kastengren AL The Contour Method Cutting Assumption: Error Minimization and Correction. In: Proulx T (ed) SEM Annual Conference & Exposition on Experimental and Applied Mechanics, Indianapolis, Indiana USA, June 7 - 9, 2010 2010. p paper # 507.

25. Schajer GS, Prime MB (2006) Use of Inverse Solutions for Residual Stress Measurements. Journal of Engineering Materials and Technology 128 (3):375-382.

26. Toparli MB, Fitzpatrick ME (2011) Residual Stresses Induced by Laser Peening of Thin Aluminium Plates. Materials Science Forum 681:504-509. doi:10.4028/www.scientific.net/MSF.681.504.

27. DeWald A, Hill M (2006) Multi-Axial Contour Method for Mapping Residual Stresses in Continuously Processed Bodies. Experimental Mechanics 46 (4):473-490.

28. Kartal ME, Liljedahl CDM, Gungor S, Edwards L, Fitzpatrick ME (2008) Determination of the profile of the complete residual stress tensor in a VPPA weld using the multi-axial contour method. Acta Materialia 56 (16):4417-4428.

29. Prime MB, Newborn MA, Balog JA (2003) Quenching and Cold-Work Residual Stresses in Aluminum Hand Forgings: Contour Method Measurement and FEM Prediction. Materials Science Forum 426-432:435-440.

30. Pagliaro P, Prime M, Robinson JS, Clausen B, Swenson H, Steinzig M, Zuccarello B (2011) Measuring Inaccessible Residual Stresses Using Multiple Methods and Superposition. Experimental Mechanics 51 (7):1123-1134. doi:10.1007/s11340-010-9424-5.

31. Ahmad B, Fitzpatrick ME (2015) Effect of Ultrasonic Peening and Accelerated Corrosion Exposure on the Residual Stress Distribution in Welded Marine Steel. Metallurgical and Materials Transactions A 46 (3):1214-1226. doi:10.1007/s11661-014-2713-3.

32. Araujo de Oliveira J, Fitzpatrick ME, Kowal J (2014) Residual Stress Measurements on a Metal Matrix Composite Using the Contour Method with Brittle Fracture. Advanced Materials Research 996:349-354. doi:10.4028/www.scientific.net/AMR.996.349.

33. Zabeen S, Preuss M, Withers PJ (2013) Residual stresses caused by head-on and 45° foreign object damage for a laser shock peened Ti-6Al-4V alloy aerofoil. Materials Science and Engineering: A 560:518-527. doi:https://doi.org/10.1016/j.msea.2012.09.097.

34. Xie P, Zhao H, Wu B, Gong S (2015) Evaluation of Residual Stresses Relaxation by Post Weld Heat Treatment Using Contour Method and X-ray Diffraction Method. Experimental Mechanics 55 (7):1329-1337. doi:10.1007/s11340-015-0040-2.

35. DeWald AT, Hill MR (2009) Eigenstrain-based model for prediction of laser peening residual stresses in arbitrary three-dimensional bodies Part 1: Model description. The Journal of Strain Analysis for Engineering Design 44 (1):1-11. doi:10.1243/03093247jsa417.

36. Olson MD, DeWald AT, Prime MB, Hill MR (2015) Estimation of Uncertainty for Contour Method Residual Stress Measurements. Experimental Mechanics 55 (3):577-585. doi:10.1007/s11340-014-9971-2.

37. Traoré Y, Hosseinzadeh F, Bouchard PJ (2014) Plasticity in the Contour Method of Residual Stress Measurement. Advanced Materials Research 996:337-342. doi:10.4028/www.scientific.net/AMR.996.337.

38. Kaiser R, Stefenelli M, Hatzenbichler T, Antretter T, Hofmann M, Keckes J, Buchmayr B (2015) Experimental characterization and modelling of triaxial residual stresses in straightened railway rails. The Journal of Strain Analysis for Engineering Design 50 (3):190-198. doi:10.1177/0309324714560040.

39. The Contour Method. In: Practical Residual Stress Measurement Methods. pp 109-138. doi:10.1002/9781118402832.ch5.

AN EXPERIMENTAL AND COMPARATIVE STUDY OF THE SELF-LOOSENING OF BOLTED-JOINTS UNDER CYCLIC TRANSVERSE LOADING

Umut İNCE
Mustafa GÜDEN

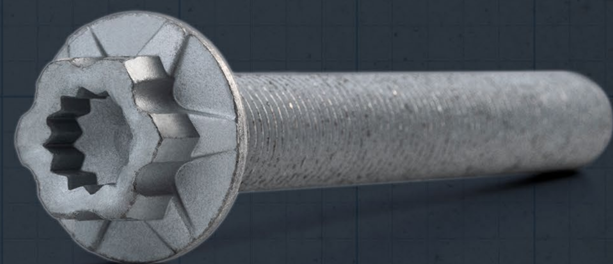

Sakarya University Journal of Science 25(2), 498-512, 2021

AN EXPERIMENTAL AND COMPARATIVE STUDY OF THE SELF-LOOSENING OF BOLTED-JOINTS UNDER CYCLIC TRANSVERSE LOADING

Umut İnce*[1], Mustafa Güden[2]

*Corresponding author: umut.ince@normcivata.com
[1]Norm Cıvata San. Ve Tic A.Ş, Atatürk Organize Sanayi Bölgesi, 10007 sokak, 35620, Çiğli, İzmir
E-Mail: umut.ince@normcivata.com
ORCID: https://orcid.org/0000-0002-3118-3060
[2]İzmir Institute of Technology, Department of Mechanical Engineering, Urla, İzmir
E-Mail: mustafaguden@iyte.edu.tr
ORCID : https://orcid.org/0000-0001-6397-8418

Abstract

The capabilities of analytic models in predicting the experimental critical displacements of the self-loosening of bolted-joints were investigated experimentally and numerically. The experimental loosening rates were determined in a Junker test bench at a constant transverse displacement amplitude (0.45 mm) and under varying initial clamp force and clamp length and controlled bearing and thread friction coefficients. The analytic critical displacements were then calculated using experimental parameters. In addition, a three-dimensional accompanying finite element (FE) model was developed in order to calculate the ratio of spring constants engaging the thread to spring. The results showed relatively low capabilities of present analytic model in the prediction of the critical displacements of the self-loosening of bolted-joints. The efforts to modify the nut reaction moment and the inclination compliance of bolt head portion in the investigated equations however resulted moderate increase in the appropriate predictions. On the other side, the use of the reaction moment determined by FE model increased the appropriate prediction from 58.3 to 73.4%. The accuracy of the equations was further increased by the use of an appropriate kw value, but the increase in this case was only ~4%.

Keywords: Bolted-joints, self-loosening, numerical simulation, Junker test, analytic model.

1. Introduction

Bolted-joints are widely used in engineering structures as they are relatively easy to implement, offer relatively low cost and generate comparatively high clamping forces. Nevertheless, they are prone to catastrophic failure, particularly at prolonged service durations, making them one of the most critical structural parts. The well-known failure mode of bolted-joints is self-loosening which is primarily caused by vibrational forces. The gradual decrease of preload with the increase of dynamic load on a bolt leads to the initiation of self-loosening. Self-loosening plays a pivotal role in the initiation of fatigue failure, causing not only material and financial losses but also fatal accidents. The crash of a Tupolev 154M type passenger jet in 1999, an example to fatal accidents, resulted in the death of 61 persons. The officially reported cause of the accident was the self-loosening of a self-locking nut connecting the pull rod and bell crank in the elevator control system [1]. A United States Air Force reconnaissance airplane caught fire in 2015 as a result of the self-loosening of a fastener, which led to damages in the aircraft control and mission-related systems. The repair cost was declared $62.4 million [2]. A high-speed train derailed in the United Kingdom in 2007, resulted from the self-loosening of a fastener according to the report published by RAIB [3]. There have been many other reports on the causalities resulted from the self-loosening of bolts. The existent analytic equations developed for the self-loosening of bolted-joints under transverse vibrational loads were reviewed in section 2. The applicability of these equations to the experimental results of the self-loosening of bolted-joints, according to authors' knowledge, has not been completely investigated so far. Hence, this study aimed at determining the capabilities of the existent self-loosening analytic models in predicting the experimental critical displacements. For that purpose, extensive transverse vibration experiments were performed under varying initial clamp force and length, controlled bearing and thread friction coefficients and a constant transverse displacement amplitude of 0.45 mm. The transverse vibration experiments were conducted in a Junker bench on the bolted-joints in conjunction with a Finite Element (FE) model. The critical transverse displacements were then calculated for each equation using the experimental parameters. Finally, the experimentally determined loosening rates were drawn as function of analytically calculated critical transverse displacements. The percentages of the correct or appropriate and wrong or inappropriate predictions of the critical displacement of self-loosening were shown in the graphs for each equation. In addition, a three-dimensional simplified accompanying FE model of the bolted-joint was used to calculate the ratio of spring constants engaging the thread to spring which was used in the equations.

2. Previous Experimental And Numeric Studies On The Self Loosening Of Bolted-Joints

Early studies on the self-loosening of bolted-joints merely focused on the effect of axial dynamic loads along fastener. Goodier and Sweeney [4] developed an equation for the loosening of nuts caused by axial vibrational forces. In the same study, the radial micro slips under axial tension, both at the bolt-nut thread interface and the bearing surface, were reported to vary with the radial contraction of bolt and the radial expansion of nut.

Sauer [5] showed that when the ratio of the amplitude of axial dynamic load to mean bolt axial tension was less than 0.7, the axial vibrational forces resulted in no loosening.

Gambrell [6] investigated the effect of fine and coarse thread size, lubrication and frequency on the loosening of fasteners under axial vibrational forces. No effect of fastener thread size and frequency was reported when the dynamic to static load ratio and frequency were less than 1 and between 3.3 and 22 Hz, respectively. When the dynamic to static load ratio was above 1, the fine threaded bolts were shown to loosen less than the coarse threaded bolts. Also, lubrication was shown to be a critical factor in the loosening of coarse threaded bolts.

Junker [7] showed experimentally that the transverse vibrational forces were much more effective than the axial vibrational forces in the self-loosening. The loosening rate expressed as the loss of clamp load per cycle (N/cycle) increased with increasing the amplitude of transverse displacement and thread pitch. An experimental testing device used in the same study, called the Junker tester, was standardized as DIN 65151 in 2002 [8]. DIN 25201 superseded DIN 65151 was published in 2010 [9].

Finkelston [10] showed that the increase of friction and preload enhanced the loosening resistance of fastener. Yamamoto and Kasei [11, 12] introduced a parameter called the critical relative slippage (S_{cr}) which determines the upper transverse displacement limit for the initiation of loosening. The schematic of threaded fastener deformation subjected to a transverse external force is shown in Figure 1(a). In the same figure, the nut bearing surface is subjected to a shear force (F_s) and a nut reaction moment (M_t). The critical relative slip proposed by Yamamoto and Kasei [11, 12] is

$$S_{cr} = 2\delta = \frac{2l_n F\mu_b(l_n^2+3k_w l_n EI)}{3EI} - \frac{3l_n M_t(l_n+2k_w EI)}{3EI} \quad (1)$$

In Eqn. 1, δ is the critical slip distance, μ_b is the friction coefficient of bearing surface, F is the clamping force, I is the moment of the inertia of the cross-sectional area of bolt, E is the longitudinal elastic modulus of bolt, k_w, is the inclination compliance of bolt head portion and ln is the length of bolt.

Based on an FE analysis, Izumi et. al. [13] refined the Yamamoto and Kasei's equation as

$$S_{cr} = 2F\left[\mu_b\left(\frac{l_g^3}{3EI_g}+\frac{l_s^3}{3EI_s}+\frac{l_g l_s l_n}{EI_g}+k_w l_n^2\right) - \frac{m}{4}\frac{\mu_t}{Cos^2\alpha}\left(\frac{l_g^2}{2EI_g}+\frac{l_s^2}{2EI_s}+\frac{l_g l_s}{EI_g}+k_w l_n\right)\right] \quad (2)$$

where, l_g and l_s are sequentially the length of bolt and bolt thread and I_g and I_s are the moment of inertia of cross-sectional area of bolt and bolt thread, respectively (Figure 1(b)). The reaction moment on the thread is given as

$$M_t = \left(\frac{m}{4}\right)\left(\frac{\mu_t F}{Cos^2\alpha}\right) \quad (3)$$

where, m is the height of nut, μ_t is the friction coefficient of threaded interface and α is the half-thread angle. Nakamura et. al [14] proposed an equation for the inclination compliance of bolt head portion (k_w) as

$$k_w = 0.168\left(\frac{1}{d}\right)^3 \left[\frac{1}{kN\ mm}\right] \quad (4)$$

where d is the bolt diameter.

Blume and Illgner [15] proposed the following equation for the critical slip distance based on a beam model fixed on both sides,

$$\delta = \frac{F\mu_b l_n^3}{12EI} \quad (5)$$

Friede and Lange [16] performed experiments on the critical slip distance of transversely loaded fasteners including M16 and M24. Comparison of test results with the Blume and Illgner's equation [15] showed conservative results. They proposed an equation for the critical slip distance as

$$\delta = F\mu_b\left(\frac{l_n^3}{12EI}+\frac{l_n^2}{2C_\varphi}\right) \quad (6)$$

where C_φ (kNm/rad) is rotational stiffness of bolt. Nassar and Housari [17-20] investigated the self-loosing of fasters and proposed a mathematical model for the loosening under cyclic transverse loads. The loosening rate was shown to be sensitive to the thread and bearing friction coefficients of fasteners. In the same study, the loosening rate of fine threaded fasteners decreased with the initiation of loosening; a larger clearance between bolt and pilot increased the loosening rate almost exponentially and the number of cycles for complete loosening was directly proportional to initial clamp force.

Yokoyama et. al [21] presented an analytic model for the bolts subjected to transverse loads. The model well agreed with the FE modelling results. In the same study M_t was proposed as

$$\Delta M_t = \frac{K_t}{K_b+K_t}\Delta F_s l_n \quad (7)$$

where K_t and K_b are the spring constant of engaged thread and the spring constant of bolt head, respectively. The spring constant of bolt head is given as

$$K_b = \frac{EI}{0.6d} \quad (8)$$

where d is the nominal thread diameter.

Although the use of numerical simulation method for the investigation of the loosening behavior of bolt-nut joints with the development of computer and allowing comprehensive analysis in a short time, the number of studies combining experimental - analytical and numerical simulation methods is quite few [22-25].

3. Experımental Study

M8x1.25 8.8 ISO 4017 [26] carbon steel bolts and M8x1.25 8 DIN 934 [27] carbon steel nuts were selected for the Junker tests. The thread forming and heat-treatment of bolts and nuts were performed sequentially according to ISO 898-1 [28] and ISO 898-2 [29]. Before testing, the bolts and nuts were coated with Delta Protekt® KL100 + VH301 GZ zinc flake by a dip-spin process in a single batch. Delta Protekt® KL100 + VH301 GZ zinc flake coating induces a friction coefficient between 0.09 and 0.14 and widely preferred by the automotive industry. Thread and bearing friction coefficients of five bolt/nut specimens were measured according to ISO 16047 [30] using SCHATZ® friction coefficient tester. Transverse vibration tests were performed in a Junker test bench shown in Figure 2(a) and Figure 2(c).

In a typical test, the test bench applies a transverse dynamic vibrational force with variable frequency and amplitude on a glider plate. The glider top plate is driven by an eccentric cam. The bolted joint being tested is clamped together the glider plate and fixed plate as shown in Figure 2(b). The clamp force is measured by means of load cells as function of time. The clamp force-cycle data are then exported for the analysis.

The parameters used in transverse vibration tests are tabulated in Table 1. The tests were performed at three different initial clamp forces, six different clamp lengths, four different bearing-thread friction coefficients and a constant transverse displacement amplitude of 0.45 mm and a frequency of 5 Hz. Total 360 vibration tests were performed for 72 test conditions and at least five tests were performed for each test condition. In order to improve the reliability of data, maximum allowable standard deviation of loosening rates was accepted as %20 of average loosening rate value of five test results. If the standard deviation is bigger than the allowed, additional tests performed until the allowable standard deviation value was reached.

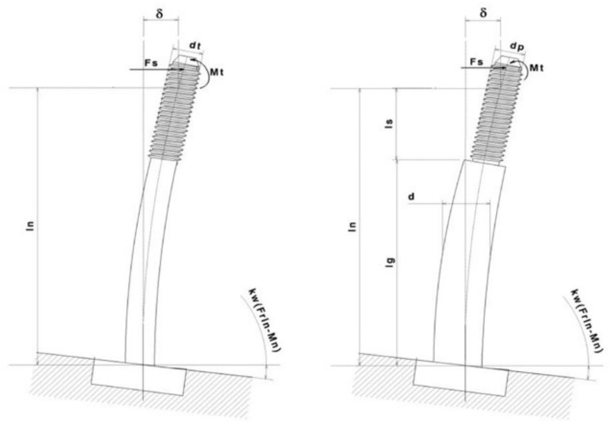

(a) (b)

Fig. 1. (a) Deflection of a bolt caused by a transverse external force and (b) deflection of multi sectioned bolt caused by transverse external force.

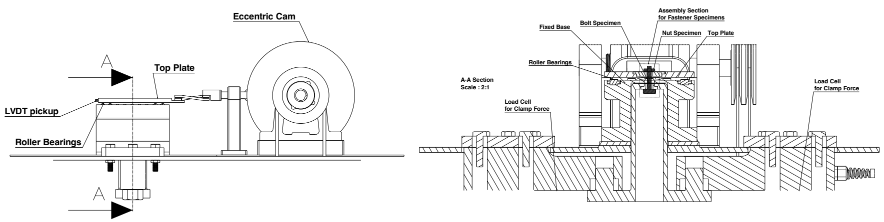

(a) **(b)**

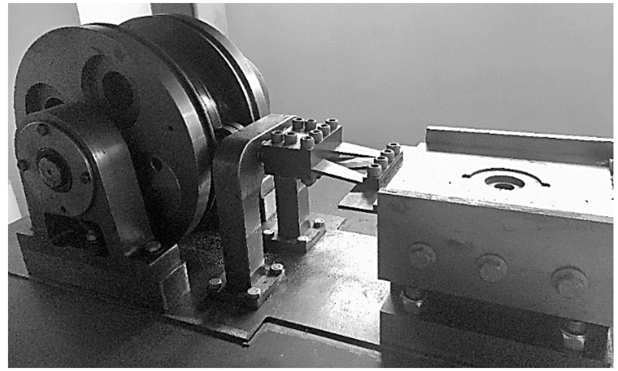

Fig. 2. (a) Transverse vibration experimental set-up and (b) cross-section view of A-A showing the fixture used in the experimental setup (c) image of Junker test bench.

An average value for loosening rate for each test condition was the calculated using 5 tests. The loosening rate (kN/cycle) was determined from the slope of a linear fit to the average clamping force-cycle curve. For the experimental test conditions resulting in self-loosening, the critical transverse displacements were then calculated using the analytic equations elaborated in section 2. These equations are also listed in Table 2 and numbered from 1 to 3 as equation sets numbers. The corresponding parameters and the equations (section 2) used to calculate the critical transverse displacements are also listed in the same table. For example, for the equation set number 1 (Eqn. Set Nr-1) of Table 2, the critical transverse displacement (δ) was calculated using Eqn.1 (Yamamoto and Kasei, 1977) and kw was calculated using Eqn. 4 (Nakamura et. al, 2001) given in section 2.

Finally, the experimentally determined loosening rates were drawn as function analytically calculated critical transverse displacements for comparison.

Table 1. Parameters used in the transverse vibration tests.

Initial Clamping Force (kN)	Clamp Length (mm)	Bearing Friction Coefficient	Thread Friction Coefficient	Transverse Displacement Amplitude (mm)	Frequency (hz)
17.6	23	0.121	0.113	0.45	5
14.3	31	0.153	0.125		
10.27	44.5	0.172	0.137		
	53	0.204	0.146		
	65				
	85				

Table 2. Equation set numbers used to calculate the critical displacement (Eqn. Set Nr-1 through Eqn. Set Nr-3).

Number	δ	M_t	K_t	k_w
1	Yamamoto and Kasei (1997)			Nakamura et. al (2001)
2	Blume and I llgner (1988)	NA		NA
3	Friede and Lange (2010)	NA		NA

4. Numerical Study

A three-dimensional simplified FE model of the bolted-joint shown in Figure 3 was used to determine the proportion of M_t to $F_s l_n$ to find the ratio of spring constant ratio in Eqn. 7. The finite element simulation was performed in commercial simulation software Simufact®. The elastic modulus and Poisson's ratio were taken 210 GPa and 0.3, respectively, for all deformable steel parts. All geometrical properties of bolt and nut joint model including helical thread (comply with DIN 13 [31]) and the tolerances given for 6h/6H, were kept the same as the experiments. The clamping force was applied by moving up "rigid nut washer" element in z-direction (Figure 3). After creating clamping force, the transverse excitation with 5 Hz frequency and 0.45 mm transverse displacement amplitude was applied to the moving "rigid nut washer" element through Y direction for 10 cycles (Figure 3). The numerical simulation was implemented with 23 mm clamp length and 17.6 kN initial clamping force. 0.121 bearing friction coefficient and 0.113 thread friction coefficient. Coulomb friction model was used and friction coefficients assigned to bearing and thread sides as 0.121 and 0.113 respectively. The numbers of tetrahedral 134 elements that are used at bolt and nut models, were 31041 and 25911 respectively. Segment to segment contact algorithm, mixed-direct iterative solver and adaptive time stepping based on automatic displacement change parameters were used.

5. Results And Discussion

The variations of experimentally measured thread and bearing friction coefficient as function of the number of tightening-loosening (1st, 3rd, 5th, and 7th tightening-loosening) are shown given in Figure 4. All thread and bearing friction coefficients were measured according to ISO 16047 Fasteners-Torque/clamp force testing. At least 5 friction coefficient measurements were taken and the values were then averaged for each tightening-loosening number. The average friction coefficients of 1st, 3rd, 5th, and 7th tightening-loosening are sequentially 0.121, 0.153, 0.172 and 0.204 for bearing friction coefficient and 0.113, 0.125, 0.137 and 0.146 for friction thread coefficient. As the tightening-loosening number increases the friction coefficients increase as seen in Figure 4. Note in the same figure that the increase of bearing friction coefficient with the tightening-loosening number is higher than that of thread friction coefficient. The increase in friction coefficients with the increase of tightening-loosening number is also noted to show nearly a linear dependence. Hence, the experimental bearing and threat friction coefficients tabulated in Table 1 were average values of these measurements and determined by applying tightening-loosening prior to the transverse vibration experiments.

The critical transverse displacement prediction was taken correct or appropriate if the calculated critical transverse displacement of the equation sets numbered from 1 to 3 in Table 2 was less than 0.45 mm in the experimentally self-loosened bolts or if the calculated critical transverse displacement was higher than 0.45 mm in the experimentally no self-loosened bolts. Otherwise, the prediction was taken wrong or inappropriate. Figures 5(a-c) show the experimentally measured loosening rates as function of calculated critical displacement of the equation sets listed in Table 2. The experimental displacement amplitude (0.45 mm) is also shown as a vertical dotted line in Figures 5(a-c). As noted in Figures 5(a) and (c), the appropriate predictions of critical displacements of the Eqn. Set Nr-1 and Eqn. Set Nr-3 of Table 2 are 50 and 36.1%, respectively. The highest appropriate predictions of critical displacements are found in the Eqn Set Nr-2 of Table 2 as seen in Figures 5(b). This equation set predicts appropriately 58.3% of the critical displacements. The value of k_w is reduced from $3.28x10^{-4}$ to $1x10^{-8}$ in order to determine its effect on the correctness of the critical displacement prediction of Eqn. Set Nr-1. Note that Eqn. Set Nr-2 and Eqn. Set Nr-3 do not use the inclination compliance of bolt head portion. The results of the calculations are shown in Figure 6 as the appropriate prediction percentage versus log k_w curve. As seen in Figure 6, the reduction of k_w is effective in increasing the appropriate prediction of the critical displacements down to $1x10^{-5}$ and further reduction is noted to have no significant effect on the appropriate prediction percentages of the equations investigated. Until this critical k_w value, $1x10^{-5}$, the appropriate prediction percentages increase to ~57% for the Eqn. Set Nr-1 (Figure 6). This critical value of k_w, $1x10^{-5}$, is noted to be much smaller than k_w values specified by Nishumira [32]. The finite element model variations of M_t and F_s with transverse displacement are shown in Figures 7(a) and (b), respectively. The ratio of spring constant ($\frac{K_t}{K_b+K_t}$) in Eqn. 7 was then calculated using numerical M_t and F_s values revealing pure bolt bending behavior during transverse loading. The ratio was determined 0.628. In order to compare the loosening rate of numerical simulation with those of experiments, the loosening rate of numerical simulation was numerically extended to higher cycles. Initially a linear fit lto the FE model clamp force-cycle curve was applied within 100 cycles; then, using the slope of this linear fitting the FE model clamp force-cycle curve was extended to 850 cycles. Figure 7(c) shows the variation of the extended FE model clamp force with the number of cycle at an initial clamp force of 17.6 kN. In the same figure, the variations of experimental clamp forces of five tests with the number of cycle at an initial clamp force of 17.6 kN are shown together with the variation of the experimental average clamp force. Note that the average experimental clamp force-cycle curve shows well agreements with the FE model clamp force-cycle curve especially at low cycles. The slope of the experimental average clamp force-cycle curve shown in Figure 7(c) yields a loosening rate of approximately 0.01256 kN/cycle. Finally, a new set of equations was developed using the FE model M_t values. This new equation is coded as Eqn. Set Nr-4 and tabulated in Table 3. Using the numerically calculated spring constant ratio and reaction moment, the critical transverse displacement amplitude was calculated for Eqn. Set Nr-4. Initially, the effect of value of k_w on the critical transverse displacement predictions of Eqn. Set Nr-4 was determined. The variation of the appropriate prediction percentage of Eqn. Set Nr-4 of Table 3 with the value of k_w is shown in Figure 8(a). The appropriate prediction percentage increases from 73.4 to 77.7% with the increase of k_w from $7.5x10^{-5}$ to $5x10^{-5}$ thereafter the appropriate percentage values saturate. Figure 8(b) shows the experimentally measured loosening rate as function of calculated critical displacement amplitudes with k_w value of $5x10^{-5}$. The use of FE model determined reaction moment increases the accuracy from 50.0 to 73.4%. The accuracy of the equations further increased with the use of appropriate kw value, while the increase is only ~4%. The total increase in the appropriate prediction percentage is 27.7%.

6. Conclusions

The capabilities of the analytic models in predicting experimental self-loosening of bolted-joints was investigated both experimentally and numerically. The experimental loosening rates were determined in a Junker test bench at a constant transverse displacement amplitude (0.45 mm) and under controlled thread and bearing friction coefficient. The experimental test parameters were then used to calculate the critical displacement for self-loosening for each equation investigated. In addition, a three-dimensional accompanying FE model of bolted-joint was developed to calculate the ratio of spring constants engaging the thread to spring. The results indicated relative low capabilities of present analytical models in the prediction of the critical displacements of bolted-joint for self-loosening. The efforts to modify the nut reaction moment and the inclination compliance of bolt head portion in the equations investigated

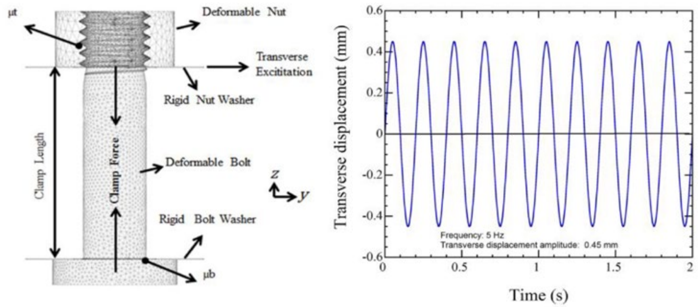

Fig. 3. Finite element model of bolted-joint and applied transverse displacement versus time curve.

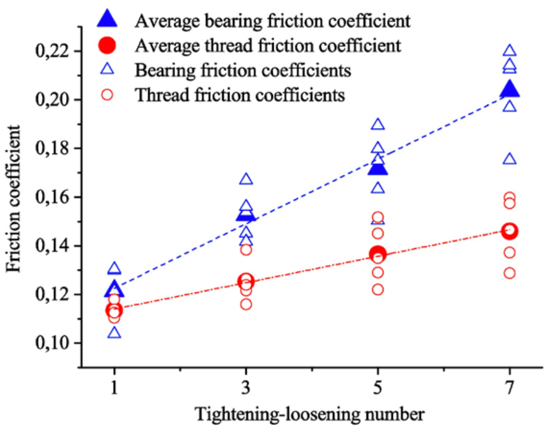

Fig. 4. The variations of the thread and bearing friction coefficients with the number of tightening-loosening.

however resulted in moderate increase in the predictions of the critical displacements for self-loosening. On the other side, the use of the reaction moment determined through the FE model was found to increase the prediction capabilities of the equations significantly.

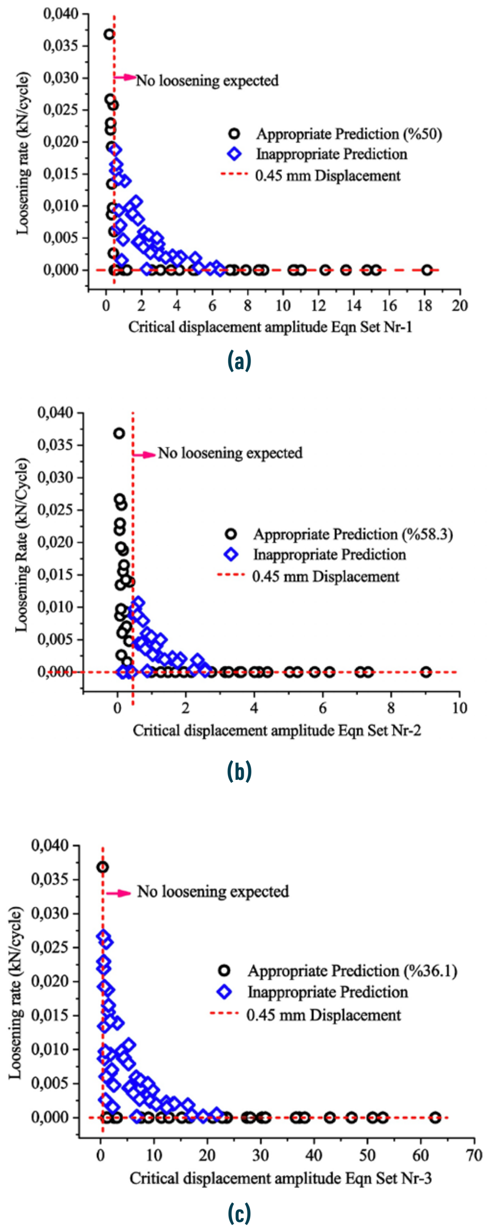

Fig. 5. Comparison of experimental and analytical results of Eqn. Set Nr (a) 1, (b) 2, (c) 3 of Table 2.

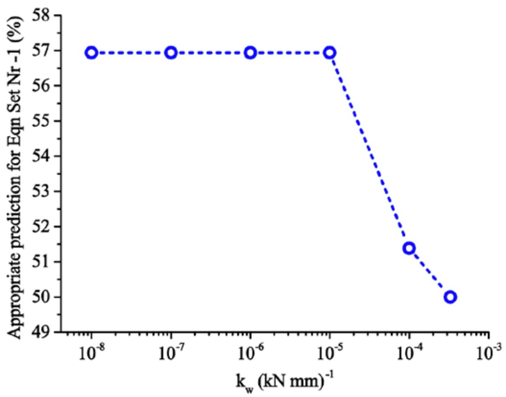

Fig. 6. Change of appropriate prediction percentage with k_w for Eqn. Set Nr-1 of Table 2.

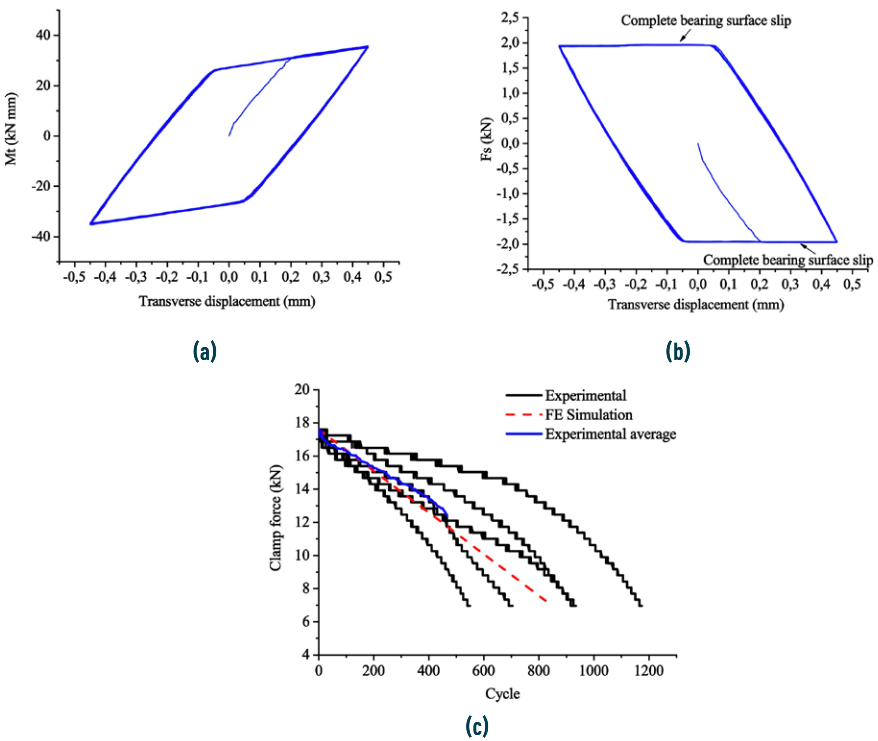

Fig. 7. The curves of numerical simulation results of (a) M_t versus transverse displacement and (b) F_s versus transverse displacement and (c) the experimental and FE model clamp force versus cycle.

Table 3. Equation set for Eqn Set Nr-4 for the critical displacement.

Number	δ	M_t	$K_t / (K_b+K_t)$	k_w
4	Yamamoto and Kasei (1997)	Yokoyama et. al (2010)	Using Yokoyama et. al (2010) equation, derived from simulation: 0.628	Various

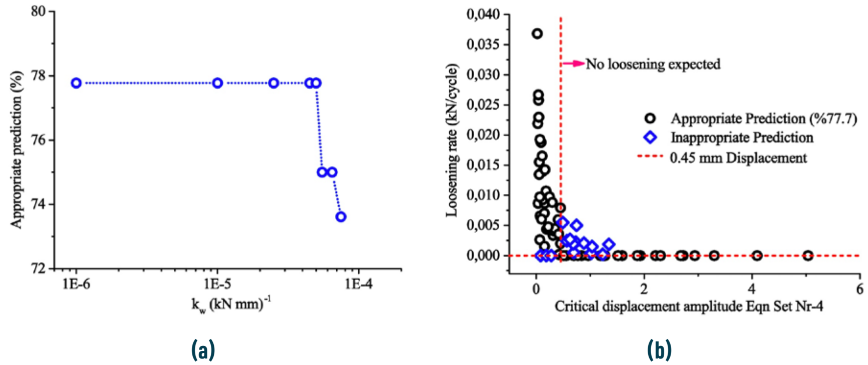

Fig. 8. (a) variation of appropriate prediction percentage with k_w and (b) comparison of experimental and analytical results of Eqn. Set Nr-4 of Table 3.

Acknowledgements

No acknowledgements has been declared by the authors.

Funding

The authors received no financial support for the research, authorship or publication of this work.

The Declaration of Conflict of Interest/ Common Interest

No conflict of interest or common interest has been declared by the authors.

Authors' Contribution

Umut İnce: Literature research, data collection, data processing, organize the execution of the study, contribution to article writing and study.
Mustafa Güden: Contribution to article writing and study, literature research

The Declaration of Ethics Committee Approval

The authors declare that this document does not require an ethics committee approval or any special permission.

The Declaration of Research and Publication Ethics

The authors of the paper declare that they comply with the scientific, ethical and quotation rules of SAUJS in all processes of the article and that they do not make any falsification on the data collected. In addition, they declare that Sakarya University Journal of Science and its editorial board have no responsibility for any ethical violations that may be encountered, and that this study has not been evaluated in any academic publication environment other than Sakarya University Journal of Science.

REFERENCES

[1] (1999, March of 3rd). Aviation Safety Network - Accident Description. Available: https://aviation-safety.net/database/record.php?id=19990224-0.

[2] W. M. Evans, "United States Air Force Aircraft Accident Investigation Board Report," 2015.

[3] R. A. I. Branch, "Rail Accident Report - Derailment at Grayrigg," 2011.

[4] J. Goodier and R. Sweeney, "Loosening by vibration of threaded fastenings," Mechanical Engineering, vol. 67, pp. 798-802, 1945.

[5] J. Sauer, D. Lemmon, and E. Lynn, "Bolts: How to prevent their loosening," Machine Design, vol. 22, pp. 133-139, 1950.

[6] S. C. Gambrell, "Why bolts loosen?," Machine Design, vol. 40, pp. 163-167, 1968.

[7] G. H. Junker, "New Criteria for Self-Loosening of Fasteners Under Vibration," SAE Transactions, vol. 78, pp. 314-335, 1969.

[8] "DIN 65151:2002-08 Aerospace series - Dynamic testing of the locking characteristics of fasteners under transverse loading conditions (vibration test)," ed. 2002-08, 2002.

[9] "DIN 25201-1:2015-12 Design guide for railway vehicles and their components " in Bolted joints - Part 4:Securing of bolted joints ed, 2015.

[10] R. J. Finkelston, "How much shake can bolted joints take," Machine Design, vol. 44, pp. 122-128, 1972.

[11] A. Yamamoto and S. Kasei, "Investigation on the self loosening of threaded fasteners under transverse vibration - A solution for self-loosening mechanism," Journal of the Japan Society of Precision Engineering, vol. 43, pp. 470-475, 1977.

[12] A. Yamamoto and S. Kasei, "A solution for self-loosening mechanism of threaded fasteners under transverse vibration," Journal of the Japan Society of Precision Engineering, vol. 18, pp. 261-266, 1984.

[13] S. Izumi, T. Yokoyama, A. Iwasaki, and S. Sakai, "Three-dimensional finite element analysis of tightening and loosening mechanism of threaded fastener," Engineering Failure Analysis, vol. 12, pp. 604-615, Aug 2005.

[14] M. Nakamura, T. Hattori, S. Tsujimoto, and T. Umeki, "Estimation of back-off loosening limit for bolted joints under trans verse cyclic loading," Transactions of the Japan Society of Mechanical Engineers, vol. 67, pp. 2976-3056, 2001.

[15] Araki.H and Pereyra.J., "Safely Secure Fasteners in Critical Applications," presented at the 2014 FAA Worldwide Airport Technology Transfer Conference, Galloway, New Jersey, USA, 2014.

[16] R. Friede and J. Lange, "Loss of Preload in Bolted Connections Due to Embedding and Self Loosening," presented at the Stability and Ductility of Steel Structures, Rio, Brazil., 2010.

[17] S. A. Nassar and B. A. Housari, "Study of the effect of hole clearance and thread fit on the self-loosening of threaded fasteners," Journal of Mechanical Design, vol. 129, pp. 586-594, Jun 2007.

[18] B. A. Housari and S. A. Nassar, "Effect of thread and bearing friction coefficients on the vibration-induced loosening of threaded fasteners," Journal of Vibration and Acoustics-Transactions of the Asme, vol. 129, pp. 484-494, Aug 2007.

[19] S. A. Nassar and B. A. Housari, "Effect of thread pitch and initial tension on the self-loosening of threaded fasteners," Journal of Pressure Vessel Technology-Transactions of the Asme, vol. 128, pp. 590-598, Nov 2006.

[20] S. A. Nassar, B. A. Housari, and Asme, Self-loosening of threaded fasteners due to cyclic transverse loads vol. 2. New York: Amer Soc Mechanical Engineers, 2005.

[21] T. Yokoyama, S. Izumi, S. Sakai, and Asme, Analytical Modeling Of The Transverse Load-Displacement Relation Of A Bolted Joint With Consideration Of The Mechanical Behavior On Contact Surfaces. New York: Amer Soc Mechanical Engineers, 2009.

[22] D. Yasui, T. Fukuoka, and M. Nomura, "Finite Element Analysis of Loosening Phenomena of Bolted Joints with Washers," The Proceedings of Conference of Kansai Branch, vol. 2018.93, p. 417, 09/25 2018.

[23] S. Borawake and S. Naik, "An Investigation of Loosening Phenomenon in Bolted Joint by Finite Element Method," SSRN Electronic Journal, 01/01 2018.

[24] M. Zhang, D. Zeng, L. Lu, Y. Zhang, and J. Xu, "Finite element modeling and experimental validation of bolt loosening due to thread wear under transverse cyclic loading," Engineering Failure Analysis, vol. 104, 05/01 2019.

[25] V. Rafik, C. Bertrand, A. Daidié, and C. Chirol, Experimental and Numerical Study of the Self-loosening of a Bolted Assembly. Advances on Mechanics, Design Engineering and Manufacturing II, 2019.

[26] "DIN EN ISO 4017 "Fasteners – Hexagon head screws – Product grades A and B", 2015/05," ed, 2015.

[27] "DIN 934 "Hexagon nuts ,with metric coarse and fine pitch thread ,product grades A and B", 1987/10.," ed, 1987.

[28] "ISO 898-1 "Mechanical properties of fasteners made of carbon steel and alloy steel Part 1:Bolts, screws and studs with specified property classes – Coarse thread and fine pitch thread", 2013/01.," ed, 2013.

[29] "ISO 898-2 "Mechanische Eigenschaften von Verbindungselementen aus Kohlenstoffstahl und legiertem Stahl – Teil 2: Muttern mit festgelegten Festigkeitsklassen – Regelgewinde und Feingewinde", 2012/08.," ed, 2012.

[30] "DIN EN ISO 16047:2013-01 Fasteners - Torque/clamp force testing ", ed, 2013.

[31] "DIN 13-1:1999-11 ISO general purpose metric screw threads - Part 1: Nominal sizes for coarse pitch threads; nominal diameter from 1 mm to 68 mm " 1999.

[32] N. Nishimura, T. Hattori, M. Yamashita, and N. Hayakawa, "Self loosening behavior of metal thread joints under transverse cyclic loading," in Engineering Plasticity and Its Applications from Nanoscale to Macroscale, Pts 1 and 2. vol. 340-341, N. Ohno and T. Uehara, Eds., ed Stafa-Zurich: Trans Tech Publications Ltd, 2007, pp. 1467-1472.

CORROSION EFFECTS ON FATIGUE BEHAVIOR OF ZN^{-}CR^{+3} AND ZN FLAKE COATED M8 DIN 933 BOLTS

Sezgin YURTDAŞ
Umut İNCE
Barış TANRIKULU
Cenk KILIÇASLAN
M. Burak TOPARLI

Sakarya University Journal of Science 25(4), 867-874, 2021

CORROSION EFFECTS ON FATIGUE BEHAVIOR OF $ZN^{-}CR^{+3}$ AND ZN FLAKE COATED M8 DIN 933 BOLTS

Sezgin YURTDAŞ, Umut İNCE, Barış TANRIKULU, Cenk KILIÇASLAN, M. Burak TOPARLI

* Corresponding author: cenk.kilicaslan@norm-fasteners.com.tr

[1] Norm Cıvata San. ve Tic. A.Ş., AOSB, Çiğli, İzmir, Türkiye.

E-mail: sezgin.yurtdas@norm-fasteners.com.tr; umut.ince@norm-fasteners.com.tr; baris.tanrikulu@normfasteners.com.tr; burak.toparli@norm-fasteners.com.tr.

ORCID: https://orcid.org/0000-0002-4120-8882; https://orcid.org/0000-0002-3118-3060; https://orcid.org/0000-0001-5441-0118; https://orcid.org/0000-0002-5787-9891; https://orcid.org/0000-0002-5203-5171.

Abstract

In this study, fatigue behavior of $Zn^{-}Cr^{+3}$ and zinc flake coated bolts was investigated experimentally by considering corrosion effects. Fatigue tests were conducted on M8x50x1.25 8.8 DIN 933 bolts at normal and corroded conditions at force amplitudes between 2.35 and 5.36 kN at test frequency of 75 Hz. A part of bolts was subjected to salt atmosphere for corrosion. According to the Wöhler curves obtained from fatigue tests before corrosion, zinc flake coated bolts showed 1.55 times higher fatigue life compared to $Zn^{-}Cr^{+3}$. After corrosion, fatigue tests showed that the fatigue life difference increased to 2.10 times for the zinc flake coating. Moreover, corrosion was found to be ineffective on crack initiation region. For both coatings and corrosion conditions, fatigue cracks were seen to initiate from the thread roots.

Keywords: Bolt; Fatigue life; Coating; Corrosion

1. Introduction

Fasteners are one of the most widely used machine elements in engineering world. They are exposed to various types of external loads and environments. Fatigue under cyclic loading can be considered as the major reason on failure of engineering components. It is estimated that 90% of the mechanical service failures are caused by fatigue [1]. Fatigue life of fasteners depends on many factors such as production method, microstructure, geometry, surface conditions, and coating type. It was shown that inadequate tension and clamping force, fasteners are highly susceptible to fatigue failures [2]. In addition to that, inter-granular cracks in the structure of material was also found to cause fatigue fracture. In another study, the fatigue behavior of the fasteners resulting from corrosion was investigated [3]. According to the experimental results, it was determined that there was a significant fatigue life loss compared to the parts that were not corroded. The previous studies showed that smooth surface conditions in the threads of fasteners and more compressive residual stresses on the surface lead to increase in fatigue strength of the parts [4]. One of the ways to achieve these conditions is to make the threading of the fasteners after the heat treatment process [5-6]. Fatigue tests revealed that fasteners which are threaded after heat treatment showed increased the fatigue life. It was also discussed that the type and angle of the thread of the bolts were very important for the fatigue life [7-8]. Specimens with 60° flank angle were found to have higher fatigue life about 20% than those with 90° flank angle. It was also found that the fatigue life of coarse threaded fasteners is higher than that of fine threaded fasteners for bolt sizes of M10 and M24. In another study, bolt length effect was evaluated on the fatigue behavior of joints [9]. Two different bolt lengths were examined and it was shown that increasing bolt length for the same tightening torque increases the joint fatigue strength. The effect of the eccentric cyclic loading on the bolt fatigue life was investigated [10]. It was found that the eccentric load reduced the fatigue life of the bolts and eccentricity did not significantly affect the shape of the cracks. However, a higher mean stress resulted in cracks with a more crescent shape. Considering the fatigue and corrosion behavior of bolts, the effects of corrosion on different threaded elements to investigate bolted joints working in a saline environment was studied [11]. FEM analysis was also carried out to evaluate the stress intensity factor and the change in applied corrosion rate. It was shown that corrosion caused a variation on the surface geometry of the threaded part, leading to a diversity of stress distribution. Corrosion fatigue performance of the high strength bolts were investigated [12]. The crack depth and fatigue life in the corrosion environment of high strength bolts were quantitatively analyzed. The fatigue life of the corroded high strength bolts was reduced by increasing material yield strength, applied tensile and stress amplitude. Stress amplitude had a crucial effect on the fatigue life. As a conclusion, it was shown that the stress amplitude should be controlled at a low level.

Despite there are many investigations on fatigue behavior of fasteners, limited studies concentrating on the corrosion effect of different coating types of fasteners are present in the literature. In this study, M8x50x1.25 8.8 DIN 933 bolts having two different coating types, $Zn_{-}Cr^{+3}$ and zinc flake, were fatigue tested. $Zn_{-}Cr^{+3}$ and Zinc flake coated bolts were subjected to salt spray test for 144 and 600 hours respectively until the red corrosion was seen, according to ISO 9227. Then, the effect of coating and corrosion to fatigue life were studied in details.

2. Materıals And Methods

M8x50x1.25 8.8 DIN 933 bolts used in this study were cold-forged in NORM Cıvata, Türkiye. The chemical composition of the bolt material, 23MnB4, was given in Table 1. After cold forging, bolts were threaded using flat rolling process. Heat treatment process according to ISO 898-1 "Mechanical properties of fasteners made of carbon steel and alloy steel - Part 1: Bolts, screws and studs with specified property classes - Coarse thread and fine pitch thread" was carried out to obtain 8.8 grade.

The bolts, obtained from the same batch, are randomly divided into two groups and coated with two different types of

Table 1. 23MnB4 Chemical Analysis (%Weight).

C	Mn	Si	P	S	Cr	Ni	Mo	Cu	Sn	Al	B	Ti
0.224	0.941	0.095	0.003	0.011	0.24	0.043	0.006	0.039	0.007	0.029	0.003	0.034

(a) (b)

Fig. 1. Specimens; a) $Zn_{-}Cr^{+3}$ b) Zinc flake.

coating as Zn_Cr^{+3} and Zinc flake. Electrolytic zinc plating is one of the most traditional and low-cost coating type for the protection of steel and ferrous metals against corrosion; a thin film layer is formed on the base metal by electrolysis to protect the base metal from corrosion. On the other hand, Zinc flake coatings are cured at comparatively low temperatures, and this type of coating does not contain Cr^{+6} and therefore, it does not cause hydrogen embrittlement. Contrary to Zn_Cr^{+3} coating, zinc flake coating process takes place with a binder system. This chemical process requires a firing process. For this reason, the strength of the salt spray test in Zinc flake coating is higher than the zinc coating in the same thickness, according to ISO 9227. Zn_Cr^{+3} and Zinc flake coated specimens are shown in Figure 1.

Fatigue tests were performed according to ISO 3800 "Threaded fasteners-Axial load fatigue testing-Test methods and evaluation of results" standard using Zwick/Roell high frequency fatigue tester. Testing equipment is shown in Figure

(a) (b)

Fig. 2. Test equipments; (a) Axial load fatigue and (b) salt spray testing chamber.

2(a). In order to determine the mean force to be applied, 75% of the proof load specified in ISO 898-1 (Mechanical properties of fasteners) was taken as 21.1 kN. Test frequency in all fatigue test, 75 Hz was kept constant. The Wöhler curves for each coating type were determined by means of 36 tests with 6 different applied stress amplitudes. Salt spray test system is shown in Figure 2(b). In this tests, bolts are placed in chamber. NaCl solution is sprayed constantly in the chamber and the atmosphere is controlled by pressured air cycle. The salt spray tests were conducted according to ISO 9227 "Corrosion tests in artificial atmospheres - Salt spray tests" standard.
The macro optical investigations were carried out by employing Zeiss Stemi 508 Streezoom microscope. Images were obtained focusing on the thread root morphology of the bolts to reveal differences between Zn_Cr^{+3} and Zinc flake coatings. In addition, SEM images were taken by using Carl Zeiss 300 VP to examine fracture surfaces of the bolts after fatigue testing.

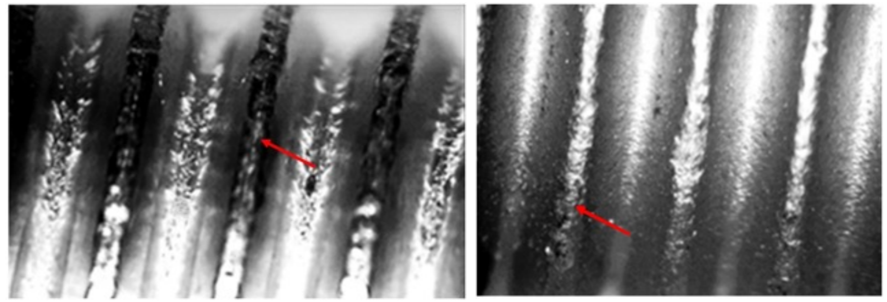

(a) (b)

Fig. 3. Pictures of thread roots; a) Zn_Cr^{+3}, b) Zinc flake [13].

3. Results and Discussions

After coating operations, bolt threads were examined under microscope since these regions were the most susceptible crack initiation locations. Figure 3(a) and (b) shows Zn_Cr^{+3} and Zinc flake coated threads, respectively [13]. As seen in the figure, thread roots (depicted with red arrow in the figure) were more homogenously coated in Zinc flake while Zn_Cr^{+3} coating was seen to have rougher surface.

(a) (b)

Fig. 4. Bolts after salt spray test; a) Zn_Cr^{+3} b) Zinc flake. The length of the bolts is 50 mm.

Bolts subjected to salt spray test are shown in Figure 4. As seen in the figure, red corrosion occurred on the bolt surface. Bolt head region was seen to be heavily corroded for Zn_Cr^{+3} coating while level of red corrosion was more less and uniformly distributed to the shaft region for Zinc flake coating.

Fatigue tests were carried out before and after salt spray test for both coatings. In all specimens, fatigue cracks occurred at the roots of the threads as seen in Figure 5. Typical fatigue fracture surface of the tested specimens coated with Zn_Cr^{+3} are given in Figure 5. The failure pattern was very similar for the samples coated with Zinc-flake. A representative SEM image from the fracture surface of the samples can be seen in Figure 6. Considering the geometry of the fatigue zone and instantaneous fracture zone, it was inferred that the applied nominal stress during fatigue testing was low enough for fatigue cracks to initiate and propagate. In addition, based on the morphology of the fatigue zone and instantaneous fracture zone, it was observed that the thread roots acted as stress concentration leading to the fracture surface as given in Figure 5 and Figure 6. Considering the fatigue zone, no clear fatigue striations were observed. For the instantaneous fracture zone, "woody" like morphology, i.e. elongated dimple rupture, was seen.

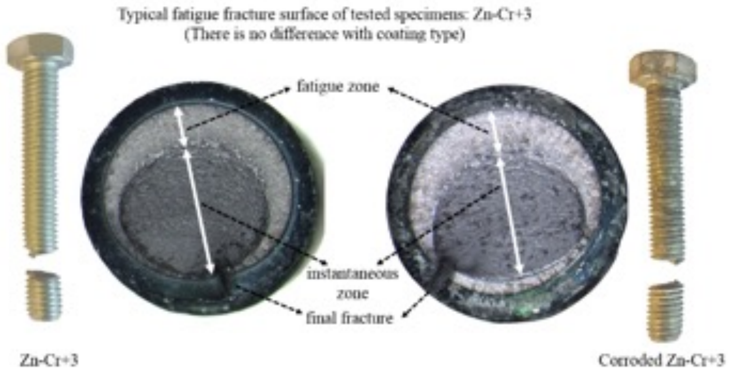

Fig. 5. Fatigue fracture surface of the tested specimen; Zn-Cr^{+3} vs corroded Zn-Cr^{+3}.

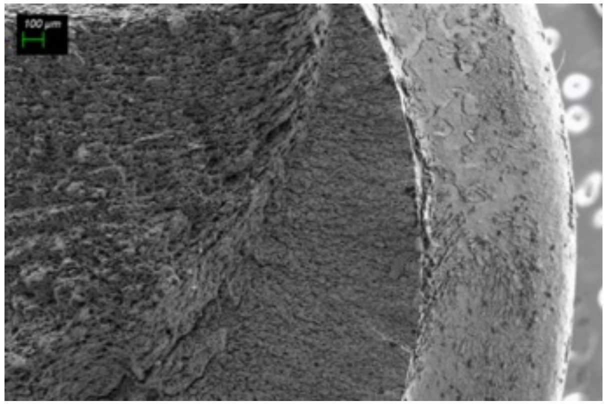

Fig. 6. SEM image of fracture surface of the tested specimen.

In Figure 7(a), fatigue life of Zn-Cr^{+3} coated bolts tested at force amplitudes of 5.36, 3.50 and 2.50 kN were presented. Significant fatigue life reduction was observed after salt spray tests. For force amplitudes of 5.36 kN and 3.50 kN, percent reductions in fatigue life were 23% and 28%, respectively. However, when force amplitude was 2.50 kN, the decrease in fatigue life was 45%. Considering the S-N curves for the Zn-Cr^{+3} bolts before and after salt spray test, fatigue performance was adversely affected from corrosion (Figure 7(b)). Zn-Cr^{+3} coated bolts exhibits 1.30 to 1.82 times higher fatigue resistance than 144 hours salt spray tested Zn-Cr^{+3} coated bolts.

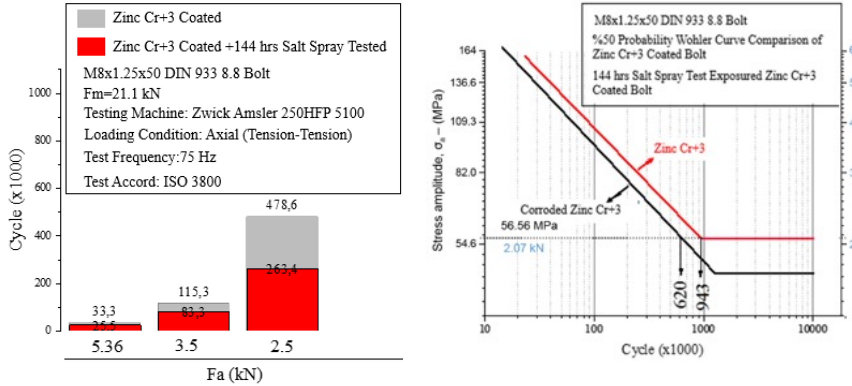

(a) (b)

Fig. 7. (a) Fatigue tests results and (b) Wöhler curves of Zn-Cr^{+3} coated bolts before and after salt spray tests.

In Figure 8(a), fatigue life of Zinc flake coated bolts tested at force amplitudes of 5.36, 3.50, 2.50 and 2.35 kN were introduced. As for Zn-Cr^{+3}, remarkable fatigue life degradation was find after salt spray tests. For force amplitudes of 5.36 and 3.50 kN, decrease in fatigue life was found as 23%. When force amplitude was decreased to 2.50 and 2.35 kN, decrease in fatigue life was 9% and 16%, respectively. Considering the S-N curves for the Zinc flake bolts before and after salt spray test, fatigue performance was adversely affected from corrosion (Figure 8(b)). Zinc flake coated bolts exhibits 1.09 to 1.29 times higher fatigue resistance than 600 hours salt spray tested Zinc flake coated bolts.

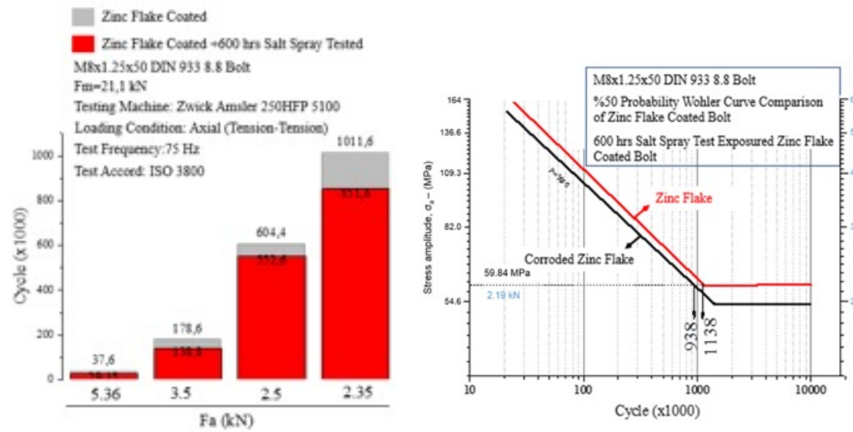

(a) (b)

Fig. 8. (a) Fatigue tests results and (b) Wöhler curves of Zinc flake coated bolts before and after salt spray tests.

Considering fatigue life of coated bolts before and after salt spray tests, Zinc flake coated bolts showed higher number of cycles compared to Zn_Cr^{+3} (Figure 9) though salt spray testing was conducted for 144 and 600 hours for Zn_Cr^{+3} and zinc flake, respectively. The difference was more significant as the force amplitude of fatigue tests were increased; i.e. Zinc flake bolts showed 1.1, 1.7 and 2.1 times higher fatigue performance for the force amplitude of 5.36, 3.50 and 2.50 kN, respectively.

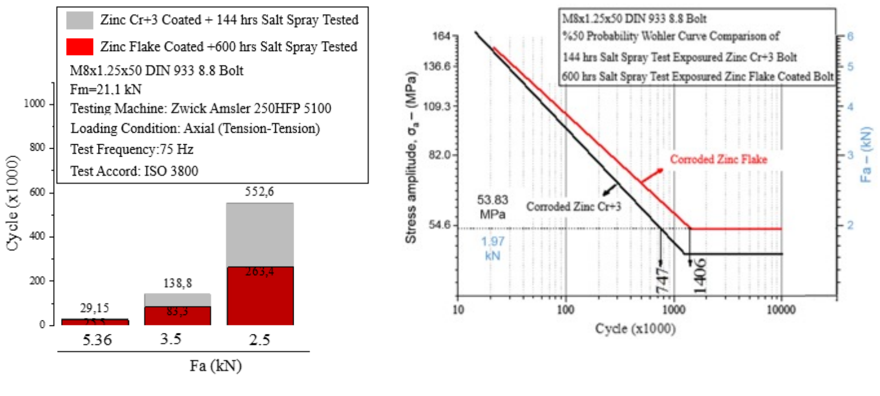

(a) **(b)**

Fig. 9. Comparison of (a) Fatigue tests results and (b) Wöhler curves of Zinc flake and Zn_Cr^{+3} coated bolts after salt spray tests.

Fatigue life of corroded Zinc flake coated bolts were compared to plain Zn_Cr^{+3} coated bolts in Figure 10. As depicted in the figure, fatigue life of both bolts were found to be similar. Main reason of that can be attributed to the difference in coating process of Zn_Cr^{+3} and zinc flake. Zn_Cr^{+3} coating is based on electrolytic bonding between the coating and the substrate. However, zinc flake coating is non-electrolytically applied. Since, zinc plating is an electrolytic proses, surface roughness is higher compared to zinc flake coating. As discussed in the literature [14-17] depending on the conditions, surface roughness can act as a stress concentrator and lead to premature crack initiation leading fractures due to fatigue. Therefore, fatigue performance was higher for zinc flake coating having better surface finish compared to Zn_Cr^{+3} plating.

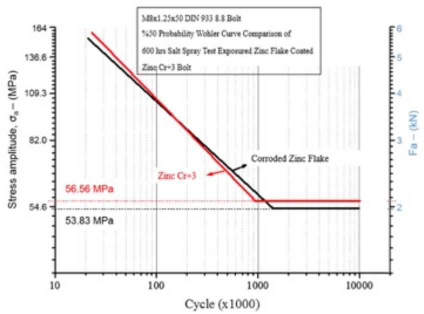

Fig. 10. Fatigue life comparison of Zinc flake bolts after corrosion test and Zn_Cr^{+3} coated bolts.

4. Conclusions

In this study, fatigue behavior of Zn_Cr^{+3} and zinc flake coated bolts was investigated experimentally by considering corrosion effects. Based on the results, following conclusions can be drawn:

• Zinc flake coated bolts showed higher fatigue resistance compared to Zn_Cr^{+3} coated bolts. This phenomenon can be explained by effect of porous morphology of thread roots of Zn_Cr^{+3} coated bolts. This porous morphology can act as a trigger for crack initiation leading to lower fatigue resistance. Another factor contributing to fatigue performance difference can be incorporated with the higher coating thickness of zinc flake leading to higher radius on thread root and decrease in stress concentration at possible crack tips.

• As a result of comparison of Wöhler curves of corroded bolts, corrosion lowers the fatigue resistance of both coating type. However, negative effect of corrosion on fatigue life of Zn_Cr^{+3} coated bolts was higher than Zinc flake coated bolts.

• 600 hours salt spray tested Zinc flake coated bolts and non-salt spray tested Zn_Cr^{+3} coated bolts exhibit similar fatigue resistance. Therefore, it can be concluded that zinc flake coated bolts have significantly higher resistance to corrosion fatigue compared to Zn_Cr^{+3} coated bolts.

5. References

[1] F. C. Campbell, "Elements of Metallurgy and Engineering Alloys", Publisher: ASM International, 2008.

[2] A. Hudgins and B. James, "Fatigue of threaded fasteners," Adv. Mater. Process., vol. 172, no. 8, pp. 18–22, 2014.

[3] P. Zampieri, A. Curtarello, C. Pellegrino, and E. Maiorana, "Fatigue strength of corroded bolted connection," Frat. ed Integrita Strutt., vol. 12, no. 43, pp. 90–96, 2018, doi: 10.3221/IGF-ESIS.43.06.

[4] L. Mordfin, "Some Problems of Fatigue of Bolts and Bolted Joints in Aircraft Applications", U.S. Dep. Commer. Natl. Bur. Stand., 1962.

[5] S. Ifergane, N. Eliaz, N. Stern, E. Kogan, G. Shemesh, H. Sheinkopf and D. Eliezer, "The effect of manufacturing processes on the fatique lifetime of aeronautical bolts," Eng. Fail. Anal., vol. 8, no. 3, pp. 227-235, 2001, doi: 10.1016/S1350-6307(00)00013-3.

[6] A. L. Marcelo, A. Y. Uehara, R. M. Utiyama, and A. I. Ferreira, "Fatigue properties of high strength bolts," Procedia Eng., vol. 10, pp. 1297–1302, 2011, doi: 10.1016/j.proeng.2011.04.216.

[7] S. Mushtaq, N. A. Sheikh, "Experimental evaluation of the effect of thread angle on the fatigue life of bolts," Int. J. Fatigue, vol. 7, no. 1, pp. 12–19, doi: 10.1016/j.ijfatigue.2004.06.011.

[8] G. H. Majzoobi, G. H. Farrahi, and N. Habibi, "Experimental evaluation of the effect of thread pitch on fatigue life of bolts," Int. J. Fatigue, vol. 27, no. 2, pp. 189–196, 2005, doi: 10.1016/j.ijfatigue.2004.06.011.

[9] S. Griza, M. E. G. da Silva, S. V. dos Santos, E. Pizzio, and T. R. Strohaecker, "The effect of bolt length in the fatigue strength of M24×3 bolt studs," Eng. Fail. Anal., vol. 34, pp. 397–406, Dec. 2013, doi: 10.1016/j.engfailanal.2013.09.010.

[10] J. W. Hobbs, R. L. Burguete, P. F. Heyes and E. A. Patterson, "The effect of eccentric loading on the fatigue performance of high-tensile bolts," Int. J. Fatigue, vol. 22, no. 6, pp. 531–538, Jul. 2000, doi: 10.1016/S0142-1123(00)00004-9.

[11] L. Solazzi, R. Scalmana, M. Gelfi, and G. M. L. Vecchia, "Effect of different corrosion levels on the mechanical behavior and failure of threaded elements," J. Fail. Anal. Prev., vol. 12, no. 5, pp. 541–549, 2012, doi: 10.1007/s11668-012-9593-x.

[12] H. L. Wang, J. G. Xia, and S. F. Qin, "High-strength bolt corrosion fatigue life estimate model and its application," Dalian Haishi Daxue Xuebao/Journal Dalian Marit. Univ., vol. 40, no. 3, 2014.

[13] U. İnce, B. Güler, N. E. Kılınçdemir and M. Güden, "The effect of coating type on bolt fatigue life" 2. International Iron&Steel Symposium, Karabük, 2015.

[14] N. Sanaei and A. Fatemi, "Analysis of the effect of surface roughness on fatigue performance of powder bed fusion additive manufactured metals," Theor. Appl. Fract. Mech., vol. 108, no. March, p. 102638, 2020, doi: 10.1016/j.tafmec.2020.102638.

[15] B. Vayssette, N. Saintier, C. Brugger, and M. El May, "Surface roughness effect of SLM and EBM Ti-6Al-4V on multiaxial high cycle fatigue," Theor. Appl. Fract. Mech., vol. 108, no. March, p. 102581, 2020, doi: 10.1016/j.tafmec.2020.102581.

[16] V. Martín, J. Vázquez, C. Navarro, and J. Domínguez, "Effect of shot peening residual stresses and surface roughness on fretting fatigue strength of Al 7075-T651," Tribol. Int., vol. 142, no. October 2019, 2020, doi: 10.1016/j.triboint.2019.106004.

[17] A. du Plessis and S. Beretta, "Killer notches: The effect of as-built surface roughness on fatigue failure in AlSi10Mg produced by laser powder bed fusion," Addit. Manuf., vol. 35, no. March, p. 101424, 2020, doi: 10.1016/j.addma.2020.101424.

ABNORMAL BURR FORMATION IN COLD FORGING

Cenk KILIÇASLAN

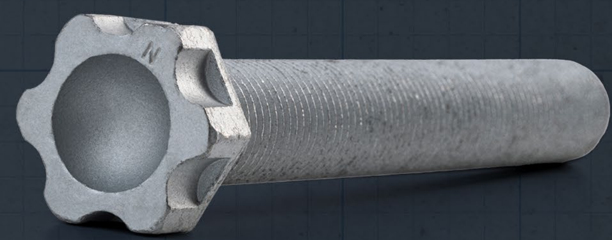

Forge Magazine, June 7, 2021

ABNORMAL BURR FORMATION IN COLD BOLT FORGING

Cenk Kılıçaslan*

* Norm Cıvata San. ve Tic. A.Ş., Türkiye.

Cold forging is a proven and efficient serial production method for bolt manufacturing. Despite the many advantages of cold forging, the method requires high forging forces due to the low material formability. This leads to the generation of high contact pressures between workpieces and dies. This operational challenge may lead to serious problems in the effectiveness of the final product.

From a Small Issue to a Huge Problem

Although significant failure modes in fasteners are generally related to secondary operations like heat treatment or coating, some problems may arise from improper forging. These can be lap or shear-band formation, which causes sudden cracking in the fastener during assembly. There is another type of failure that can occur during the forging operation: burr formation. This type of failure is rare and mainly related to differences in dimensional tolerances in die segments or die components. These spaces may be filled with flowing material during forging, which leads to the formation of burrs on the semi-finished product and possibly sudden die failures.

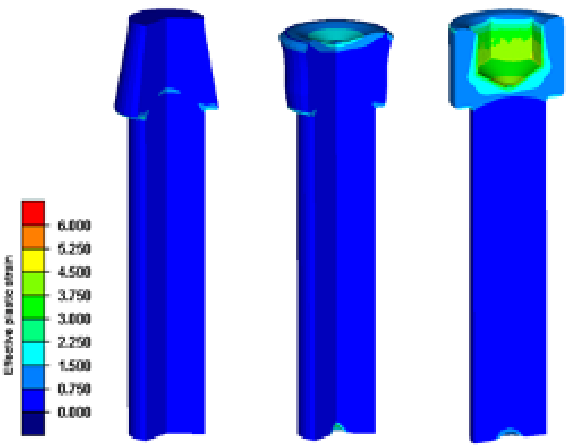

Fig. 1. Numerical representation of forging steps of a bolt having internal socket.

Bolts are tightened either externally (hex-headed bolts) or internally (Allen bolts). In the second case, Allen bolts have internal sockets for tightening. Internal sockets are formed during the heading operation by pushing a punch in the shape of a socket through the forged semi-product (Figure 1).

In serial-production conditions, flaws in socket formation may take different forms, such as cone-shape formation, socket bulging and burr formation. These failures can, in turn, lead to serious assembly problems in use, such as the fracture of the tightening apparatus and even complete failure of the tightening operation. An example of burr formation in Allen heads in M20, DIN 912 bolts can be seen in Figures 2a and 2b. As seen in the figures, a layer of the head surfaces can rupture, and burrs occurred in the hex-form socket. This leads to serious tightening problems at end-user operations.

(a) **(b)**

Fig. 2. a.) Burr formation in Allen bolts; b.) Close-up of burr formation in hex-socket of M20 DIN 912 Bolt.

Proper Modeling and Process Review

Understanding the core of a problem relies on a complete failure evaluation. In today's digital environment, the first thing to do is conduct numerical modeling. Here, forging models were prepared in the Simufact Forming software platform to analyze the basics of the process.

In numerical modeling of metal forming operations, it is crucial to use proper FEA model parameters like material model, friction model, mesh distribution and element type. Besides, understanding of mechanics of the operation is also very important to use proper models in simulations. As stated in ref. [1], contact pressure plays a significant role on metal forming operations in terms of conditions of friction. Under high contact pressures, friction between tool and work-piece vanishes and material sticking occurs. Material sticking is also triggered by increasing temperature during forming operations.

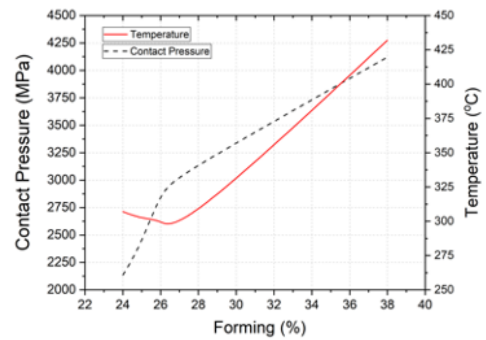

Fig. 3. Variation of contact pressure and forming temperature during forging.

Figure 3 helps us understand this. It is a graph of contact pressure plotted against temperature variation during forging. Contact pressure between punch and work-piece material increases rapidly in the beginning of the forming and linearly reaches to its maximum value around 4,100 MPa. Similarly, temperature is also seen to be increase during forging operation up to 440 °C which is high for cold operations.

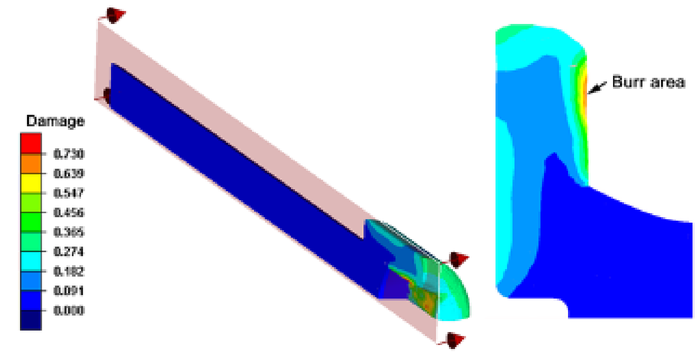

(a)

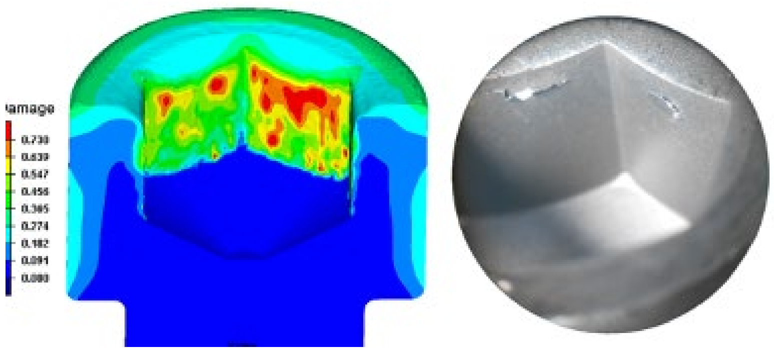

(b)

Fig. 4. Distribution of damage in socket area.

As depicted in reference 2, traditional friction models like Coulomb cannot represent the friction realistically under high forming pressures. Therefore, friction model in the numerical simulation was changed from Coloumb to shear model which relates frictional stress to shear strength of the material via friction constant, m. In shear model, sticking starts when friction stress reaches materials shear strength. In accordance with these findings, the shear model should be used to simulate friction on this model.

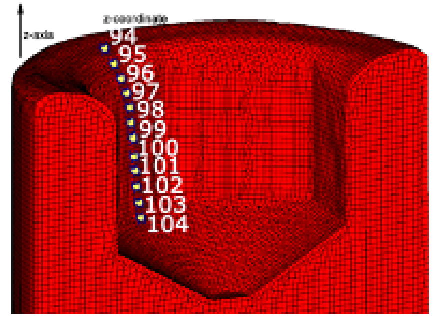

Fig. 5. Data collection on socket region.

Damage distribution, (damage is calculated using Cockroft-Latham model which is based on first principle stress and effective plastic strain), on the product after forging is shown in Figure 4a and 4b with the comparison of burr formed in the socket. Our simulation predicted the exact location of the burr formation. However, it is still not clear that this damage value can generate a failure in the socket. To gain deeper insight, data were collected along the z-coordinate of the bolt in the socket section (Figure 5).

Failure evolution in forming operations is generally related to variations of damage, stress triaxiality and temperature. These variables were analyzed at the end of the forging operation (Figure 6a and 6b). In the burr region, both

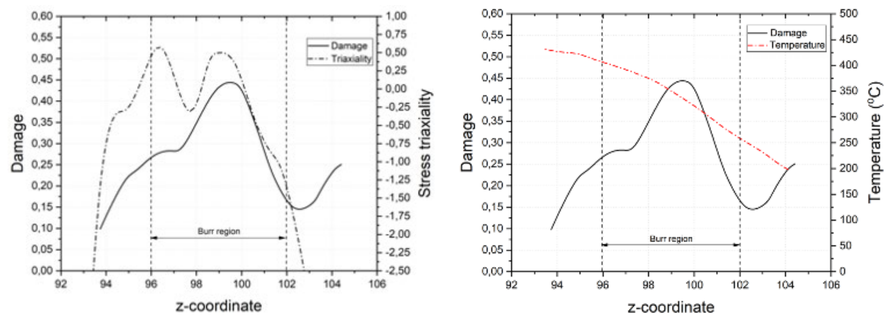

(a) **(b)**

Fig. 6. Variation of damage, stress triaxiality and temperature in the socket region.

damage and stress triaxiality values reach maximum, while forging temperature decreases almost linearly. However, maximum values of damage and stress triaxiality are not high enough to trigger any failure evolution.

Tool and Punch Wear

These findings imply that burr formation in the socket region is not completely related to the forging operation itself. Although damage and stress triaxiality values reach their maximum at the burr area, they are not so high as to form a surface tear or fracture.

Accordingly, a different mechanism may be the cause of this problem: wear. In cold-forging operations, punches are mainly coated with TiN, TiAlN or AlCrN to slow tool wear, eliminate material sticking and dissipate forming heat away from the tool surface. The thickness of coatings varies between 3 and 5 μm, [3] and coating thickness decreases during the forming operation on each forging pass. Therefore, the condition of the coating on the tool and punches is of critical importance.

Figure 7 shows the surface of the punches after 2,000, 8,000 and 10,000 forging cycles. As depicted in Fig. 7a, the forming surface of the punch is not deformed after 2,000 forging passes. The surface looks golden in color, and it

(a) **(b)** **(c)**

Fig. 7. Surface conditions of TiN coated punches after (a) ~2,000, (b) ~8,000 (arrow shows surface segregation/pitting) and (c) ~10,000 (arrow shows coating removal from surface).

is not textured. However, the forming surface of the punch experienced surface pitting (Fig. 7b). This may lead to accumulation of the workpiece material in these micro-channels during forming, which eventually leads to surface tearing and burrs. Moreover, the coating of the surface totally vanished with the increasing number of forging cycles (Fig. 7c). This leads to material sticking on the tool surface, and it may lead to surface tearing on the socket (Fig. 2b).

Conclusions

A complete failure analysis was conducted to determine the core reason for burr formation in hex-bolt sockets. The numerical study clearly showed that mechanical variables are related to our understanding of the forming mechanism during the heading operation to form the socket section. Although solid data taken from the numerical model may yield some conclusions, these findings cannot fully explain the phenomenon.

Some traditional observations and analysis of the product and processes helped solve the problem. Burr formation in the Allen-bolt socket was found to be causally related to punch wear and surface segregation/pitting. This shows the importance of process control. In a fast operation like cold forging, instant control of dies and punches becomes crucial to eliminate future problems in forged material.

Briefly put, control of the forging forces and control of die surfaces are critical for proper production.

References

[1] P. M. Dixit and U. S. Dixit, Modeling of Metal Forming and Machining Processes by Finite Element and Soft Computing Methods: Springer, 2008.

[2] T. Altan, G. Ngaile, and G. Shen, Cold and Hot Forging Fundamentals and Applications: ASM International, 2005.

[3] S. Zhang and W. Zhu, "TiN coating of tool steels: a review," Journal of Materials Processing Technology, vol. 39, pp. 165-177, 1993.

NORM CIVATA’DAN OTOMOTİV SEKTÖRÜ İÇİN AĞIRLIĞI AZALTILMIŞ İNOVATİF ÜRÜNLER

Özlem TOKER

TAYSAD Dergisi, Kasım-Aralık 2021, Sayı 123, Yıl: 23

NORM CIVATA'DAN OTOMOTİV SEKTÖRÜ İÇİN AĞIRLIĞI AZALTILMIŞ İNOVATİF ÜRÜNLER

Son yıllarda sürdürülebilir bir dünya ve üretim anlayışının yaygınlaştırılmasına yönelik çalışmalar hem ulusal hem de global ölçekte hızla artmaktadır. 2050 yılı itibarıyla karbon nötr Avrupa hedefine ulaşmak için sürdürülebilir üretim anlayışının benimsenmesi ve kalıcı hale getirilmesine yönelik faaliyetler gerçekleştirilmektedir. Otomotiv sektörü özelinde düşünüldüğünde, artan karbon emisyonunun neden olduğu iklim değişiklikleri ve petrol kaynaklarının hızla tükenmesi gibi konuların gündeme gelmesi ile birlikte ağırlık azaltma çalışmaları hız ve önem kazanmıştır. Bunun yanı sıra çevreye duyarlı olduğu ifade edilen elektrikli ve hibrit araçlar özelinde de menzil artışı sağlamak amacıyla ağırlık azaltma çalışmalarına yönelik faaliyetler sürdürülmektedir. Sonuç olarak, otomotiv sektöründe hem güncel hem de yakın gelecek trendleri göz önünde bulundurulduğunda ağırlık azaltma çalışmalarının önemi yadsınamaz bir gerçektir.

Bağlantı elemanları, araç üretiminde emniyetli bağlantıların vazgeçilmez unsuru olarak kullanılan makine elemanlarıdır. Araç tipine bağlı olmakla birlikte bir araçta yaklaşık 3000 - 8000 arasında bağlantı elemanı kullanılmaktadır. Bağlantı elemanı olarak standartlarla tanımlanmış cıvata, somun kullanımıyla beraber araç özelinde müşteri ihtiyaçlarına özel tasarlanan ve üretilen farklı bileşenler de bulunmaktadır. Bağlantı elemanlarının bir araçtaki kullanım yoğunluğu göz önüne alındığında, araç ağırlığının hafifletilmesi amacıyla gerçekleştirilen çalışmaların bağlantı elemanları özelinde yapılması oldukça gerekli ve beklentilerin karşılanması açısından da önemli bir konudur.

Norm Cıvata, çevresel ve ekonomik nedenlerin yanı sıra araç performansını arttırmak amacıyla otomotiv sektörü başta olmak üzere ağırlık azaltma çalışmalarına destek olmakta ve sektörün ihtiyacına yönelik yenilikçi çözümler sunmak için çalışmalar yapmaktadır. Bu kapsamda gerçekleştirilen Ar-Ge faaliyetleri sonucunda, mekanik performanstan ödün vermeden tasarım ve metriğe bağlı olarak bağlantı elemanlarının ağırlığında önemli ölçüde azalmaların sağlandığı inovatif tasarımlar geliştirilmektedir. Bugüne kadar gerçekleştirilen ağırlık azaltma çalışmaları sonucu ortaya çıkan inovatif tasarımlara yönelik yurt içi ve yurt dışında toplam 9 adet patent başvurusu ve 1'i uluslararası olmak üzere 6 adet endüstriyel tasarım başvurusu gerçekleştirilmiştir.
Otomotiv sektöründe de yaygın olarak kullanılan altı köşe başlı cıvatalar üzerinde gerçekleştirdikleri ağırlık azaltma çalışmalarına yönelik Ar-Ge faaliyetleri neticesinde Hexlight® markası altında farklı formlarda inovatif ürünler ortaya çıkarılmıştır. Standartlarda belirtilen mekanik özellikleri karşılayan ve montaj koşullarında herhangi bir değişiklik yapılmadan kullanılabilen Hexlight® ürünlerinde ciddi bir ağırlık azaltma sağlanmıştır.

Norm Cıvata, otomotiv sektörü başta olmak üzere birçok sektörde önemi giderek artan ağırlık azaltma konusunda özgün ve yenilikçi çözümler sunmak hedefiyle çalışmalarına devam etmektedir. Bu kapsamda, teknolojik gelişmeler ve sektörel ihtiyaçlar yakından takip edilmekte ve konuyla ilgili araştırma ve geliştirme çalışmaları her geçen gün artan bir ivme ile sürdürülmektedir.

FLOW CURVE PREDICTION OF COLD FORGING STEEL BY ARTIFICIAL NEURAL NETWORK MODEL

Fatih KOCATÜRK
M. Burak TOPARLI
Barış TANRIKULU
Sezgin YURTDAŞ
Doğuş ZEREN
Cenk KILIÇASLAN

24th International Conference on Material Forming (ESAFORM 2021)

FLOW CURVE PREDICTION OF COLD FORGING STEEL BY ARTIFICIAL NEURAL NETWORK MODEL

Fatih Kocatürk[a,b,*], M. Burak Toparlı[a], Barış Tanrıkulu[a,c], Sezgin Yurtdaş[a,d], Doğuş Zeren[a], Cenk Kılıçaslan[a]

[a]R&D Center, Norm Cıvata San. ve Tic. A.Ş., AOSB, İzmir, Türkiye
[b]Graduate School, Applied Mathematics and Statistics, İzmir University of Economics, İzmir, Türkiye
[c]The Graduate School of Natural and Applied Sciences, Dokuz Eylül University, İzmir, Türkiye
[d]Mechanical Engineering Department, Katip Çelebi University, İzmır, Türkiye
*Corresponding author: Fatih Kocatürk. E-mail address: fatih.kocaturk@norm-fasteners.com.tr

Abstract

A limited number of material models or flow curves are available in commercial finite element softwares at varying temperature and strain rate ranges for plasticity analysis. To obtain more realistic finite element results, flow curves at wide temperature and strain rate ranges are required. For this purpose, a material model for a medium carbon alloy steel material which is used for fastener production was prepared. Firstly, flow curves of the material were obtained at 4 temperatures (20, 100, 200, 400 °C) and 3 strain rates (1, 10, 50 s^{-1}). Then, experimental data was used to construct an artificial neural networks model (ANN) for the material. 75% of the experimental data was used to train the model and the rest was employed for validation and verification. ANN model used in flow curve prediction was developed using the scikit-learn library on Python. Temperature, strain rate and strain were employed as input parameters and flow stress as output parameter in ANN model. In order to increase the accuracy of the ANN model, the number of hidden layers and the number of neurons were also optimized by mean squared error approach. As a result of studies, an ANN-based material model that can be used for wide range of temperature and strain rate values were developed based on the experimental data.

Keywords: Flow Curve Prediction, Artificial Neural Network, Python, Medium Carbon Alloy Steel

1. Introduction

Numerical simulation softwares are actively used in many areas of the industry today. Boundary conditions and material properties must be defined as accurately as possible in order to coincide the results of simulation studies with actual production conditions. In this context, this study was carried out to expand the material models with the help of Artificial Neural Network (ANN) in order to increase the analysis capability of the Simufact.forming software, which is actively used for bolt forming and tool analysis. Since there is a limited number of material data in the Simufact. forming software, the software creates a value outside the data range by interpolating during the analysis phase. In order to prevent interpolating and to obtain more accurate analysis results, ANN models were used to reproduce the existing material data and were integrated into the simulation software. The artificial neural network models can be adapted to solve an optimization problem by appropriately selecting synaptic connections. In the study conducted by Dhingra and Rao (1992) [1], neural network models were designed to solve four design optimization problems and the model results were presented to show the computational power of these networks. Optimum solutions obtained by using neural networks are well adapted to the solutions obtained using gradient-based search techniques. Garrett et al. (1993) [2] presented the application of neural network technology to several engineering problems (problems requiring adaptive control, problems requiring a mapping or classification of distributed noisy data, problems requiring the simultaneous solution of many different constraints for multi-objective functions). The implemented applications have demonstrated the potential of neural networks to solve certain types of engineering problems. In master thesis of Denizer (2008) [3], ANN was used to draw the constitutive laws of tungsten fibre reinforced bulk metallic glass matrix composites. The purpose of the inverse analysis performed through ANN was to optimize the values of Voce and power law parameters and a total of seven parameters including the freezing temperature. First, a feed forward ANN was created that tried to match the FEA predictions run multiple times by random selection of seven parameters, then inverse ANN models were created to optimize the values of the seven parameters. Finally, optimized parameters were entered into forward ANN and compared with experimental data. The ANN approach was proposed by Toros and Öztürk (2011) [4] to determine the material flow curves of strain-hardened 5083-H111 and 5754-O Al-Mg alloys between room temperature and 300 °C and 0.0016-0.16 s^{-1} strain rate range. Tensile tests were conducted to determine the material response at various temperatures and strain rates, and the ANN model was developed to estimate the flow curves of materials using experimental data. A three-layer feed forward network is trained with the BFGS (Broyden, Fletcher, Goldfarb, and Shanno) algorithm. The results revealed that the values predicted by the ANN model were in good agreement with the experimental data. Various applications of soft computing (SC) tools in metal forming processes were reviewed by Pattanaik (2013) [5]. In this context, they studied ANN, fuzzy logic, genetic algorithms and the hybridization of these methods to show the ability of SC tools and techniques to effectively address various metal forming problems and related issues. They observed that the basic applications of the mentioned SC tools can be classified into the areas of design, optimization and forming processes prediction. Metal forming processes using SC tools were: Design of dies and preforms, rolling force/torque estimation, optimum force calculation, springback prediction and many more applications during forging, rolling, bending, extrusion and different sheet metal works. Mehtedi et al. (2019) [6] used the ANN model to estimate the flow curves of ZAM100 magnesium alloy sheets under hot forging conditions and obtained predictions with low error rates. A computer-aided tool in order to estimate the physical and mechanical properties used in the determination of metallic materials was developed by Merayo et al. (2020) [7]. The developed system is based on the use of the ANN model, supported by the collection of large data on the properties of thousands of materials. After training the ANN model, the system was able to make predictions about the material density and Young's modulus with an average confidence of 99% and more than 98%, respectively. A semi-autonomous vision-based method for detecting loose bolts in critical joints was proposed by Huynh et al. (2019) [8]. The method was using the idea of estimating the rotation angle of bolts from connection images by integrating deep learning technology with image processing techniques. For this case, a regional convolutional neural network based deep learning algorithm was developed to automatically detect and crop the reasonable bolts in the connection image, and the results showed that the perspective angle should not exceed 40 degrees for the accuracy of detection results. Zhang et al. (2020) [9] aimed to validate the use of machine vision and deep learning for structural health monitoring, focusing on the practice of detecting a specific bolt loosening. In this direction, a data set containing 300 images was collected first and then a faster region-based convolutional neural network was trained and validated. Test results showed that bolt damage detection was at an average sensitivity rate of 0.9503.

Obtaining flow curves of materials at different temperature, strain rate and plastic strain values is costly due to existing test systems. Studies in the literature where material flow curves are predicted with ANN models verify the ability of neural networks to predict material flow curves. The aim of this study is to establish an ANN model with reference to the material flow curves obtained by experimental methods and to reproduce the material flow curves for different temperature and strain rate values with the established model. Material flow curves for all temperature and strain rate ranges were obtained by utilising the constructed ANN model. Therefore, the errors are avoided resulting from interpolation or extrapolation that the simulation program uses for missing material data.

2. Experimental Studies and Artificial Neural Network Model

2.1 Material

In order to determine the flow curves of a medium carbon alloy steel raw material used in bolt production by cold forging method, cylindrical compression testing specimens having 8 mm diameter and 12 mm length measures were prepared in accordance with ASTM E9 standard [10]. Compression tests were carried out on the prepared cylindrical samples in ZWICK universal tensile/compression test device. The deformation rate was determined as 5 mm/min. corresponding to the quasi-static strain rate. Machine compression tables were lubricated with MoS_2 based lubricant before each compression test. In this way, the friction condition (barrelling) affecting the material flow behaviour is minimized. Strain values were measured with load cell during compression test. In Fig. 1, the flow stress-plastic strain graphs for strain rate $1s_{-1}$ and for different temperatures were given for a medium carbon alloy steel material. The flow stress-plastic strain graphs for 100 °C and three strain rates were given in Fig. 2. As can be seen in Fig. 1 and Fig. 2, true stress values depending on the plastic strain increased as the temperature decreased and the strain rate value increased. The flow curves were obtained as a result of compression tests performed at four different temperatures (20, 100, 200 and 400 °C) and three different strain rates (1, 10, 50 s_{-1}). Three tests were conducted for each temperature and strain rate values. By using data processing method, average flow curves for each temperature were found and final stress-strain curves of the materials were obtained. Within the scope of this study, an artificial neural network model was created for the material model, which is the most preferred in numerical simulation studies in cold forging industry. The flow curve data obtained by the experimental method were used in training and validation of the ANN model.

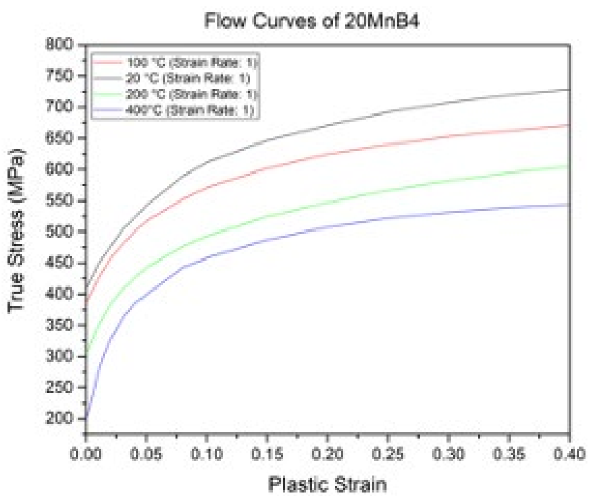

Fig. 1. Experimental flow curves for a medium carbon alloy steel material at different temperatures for strain rate 1 s^{-1}.

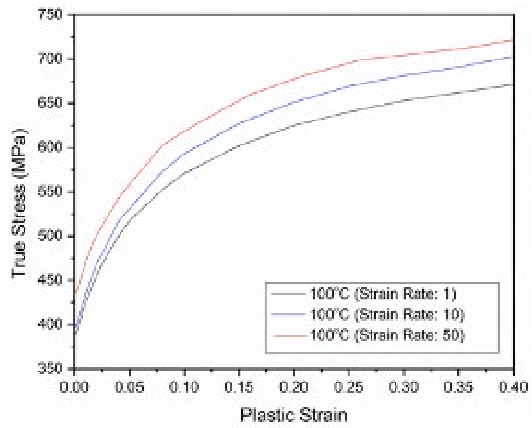

Fig. 2. Experimental flow curves for a medium carbon alloy steel material at different strain rates for 100 °C.

2.2 ANN Model

ANN model uses a parallel distributed computing paradigm as an alternative to sequential command-based computing. ANN is inspired by the structure of real neural networks in the human brain, and the knowledge gained from neuroscience is used to develop reliable, noise and error tolerant computing architectures that can make generalizations (Haykin (1999)[11]). ANN was defined as any computing architecture consisting of simple neural processors connected to each other massively parallel in Lau (1992) [12]. This definition shows that simple neural processors called neurons are central to the implementation of artificial neural networks. Neural network terminology architecture refers to the arrangement of neurons in layers and the pattern of synaptic connections between layers and between neurons. In a layered network, there is an input layer consisting of source nodes, an output layer of computation nodes, and one or more hidden neuron layers between input and output layers. There are two main classes of neural network architecture depending on the type of connection between neurons: i) Feed forward neural networks, ii) Recurrent neural networks. In feed forward neural networks, the signal flows in one direction between layers and there is no connection between neurons in the same layer. In recurrent neural networks there is at least one feedback loop that results in a dynamic system and can contain a unit delay operator where both types of connections are allowed.

A multilayer feed forward network or multilayer perceptron commonly mentioned in the literature consists of an input layer, one or more hidden layers, and an output layer. The training of a multilayer perceptron is performed in a controlled manner using the back propagation algorithm. At the beginning of the training process, random values are assigned to the synaptic weights of the network. The network is then presented with a sample of training at each iteration. The training sample consists of an input and a corresponding output. Training samples are obtained from experimental or simulation data. The network processes the input and generates an output, then it compares the output with the target. The difference between target and output determines the error. Then the synaptic weights of the network are changed by the learning algorithm in proportion to the error. The aim of the training process is to repeatedly reduce the error below a predetermined value. This requires the presentation of many training samples that make up a training set. A complete training set offering is called an epoch. This mode of supervised learning is called error correction learning. Back propagation algorithm (BPA) is based on error correction learning rule (McClelland et al. (1986)[13]). BPA consists of two stages: In the first stage, the input is presented and propagated through the network to calculate the output value for each unit (neuron). This output value gives an error signal for each output unit when compared to the targets. The second stage involves a backward transition over the network where the error signal is transmitted to each unit in the network and appropriate weight changes are made. Weight changes are made according to the steepest gradient descent method. Local slopes are calculated based on the location of a neuron in the network.

In order to predict flow curves of a medium carbon alloy steel material, the ANN model was created on Python programming language by using scikit-learn library which is an open access machine learning library running on Python. Multilayer Perceptron package in the scikit-learn library was used in order to construct ANN model. In order to construct the ANN, first of all, the input and output parameters must be determined. Taking into account the experimentally obtained material data given in Fig. 1, temperature, strain rate and plastic strain were determined as input parameters, and flow stress as output parameter. The values of input parameters were given in Table 1. The model to be established with the specified input variables was designed to give the true stress or flow stress values for each combination of input values. The schema of constructed ANN model was given in Fig. 3.

After obtaining the input data, the parameters affecting the performance of ANN model were determined and optimized for the best accuracy level of predictions. The parameters most affecting the prediction performance of the ANN model, which learns with the multilayer feed forward and back-propagation algorithm, are the activation function,

Table 1. Input parameters and values used in the artificial neural network model.

Input parameters	Values
Temperature (°C)	20,100, 200,400
Strain rate (s-1)	1,10,50
Plastic strain	0-1

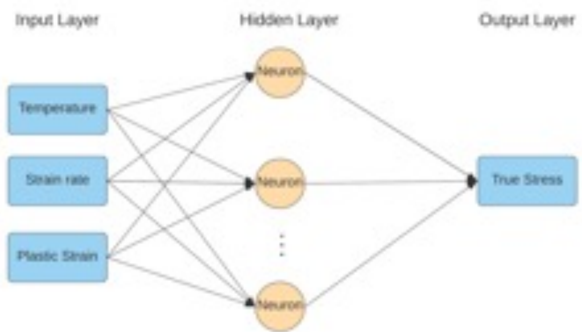

Fig. 3. The schema of constructed ANN model.

solver algorithm, hidden layer size and the randomness value, respectively. Considering the number of input and output parameters, it was decided to construct the model with a single hidden layer. By increasing the number of hidden layers, deep learning structure is adopted and this model is generally used in cases where input and output parameters are more and their relationships are more complex. For this reason, the number of hidden layers was determined as one in this study. Since the output parameter is the true stress (σ_{true}), which is a continuous variable, the hyperbolic tangent function, f (x) = tanh(x), was determined as the activation function used for transition between hidden layers. Since the experimental data set is relatively small (300 rows), the BFGS algorithm, which is known to give better results in small data sets and is one of the quasi-Newton methods, was used as the solver algorithm. When a random value is required in software development, the random number generation library in the system is used. The random number generation function needs an initial (seed) value to start working. A different random number list is produced according to the entered initial value. This initial value is generally zero by default. By changing the initial value of the random number generation function, the algorithm result can be improved by using different random numbers within the algorithm, and obtaining the same result is guaranteed every time the algorithm is run. In the ANN model, it is important to find the random initial value that the ANN model gives the best result, since the weight values used in transitions between neurons are randomly assigned at first and random value assignments are used in the solver. For this purpose, the randomness value was examined together with the number of neurons. An optimization study was carried out for the randomness value. The randomness value was tested for all integers in the range [0,100] and the best value was found that gives the lowest mean squared error (MSE). As a result of the study, the lowest MSE was obtained for the randomness value of 53. After determining the general structure of the model, the number of hidden layers and the solver algorithm, the process of obtaining the number of neurons to be defined for the hidden layer was started. At this stage, it was decided to use 75% of the experimentally obtained data for training the model and the remaining 25% for the validation of the model. Using the determined training data set, the process of determining the number of neurons to be used in the hidden layer was conducted. The number of neurons is one of the most important parameters to be determined for the ANN model. The number of neurons in the hidden layer can cause problems such as underfitting and overfitting. When the number of neurons is low, the model created does not fully reflect the data and may cause erroneous results. In case of high number of neurons, overfitting problem arises and the model is more affected by parameter changes. Therefore, a comprehensive study has been carried out for the number of neurons. MSE measure was also used in order to obtain the number of neurons. The change in the MSE parameter was recorded by increasing the number of neurons one by one starting from 2 neurons. The smallest number of neurons for which the MSE value is fixed was determined as the optimum number of neurons. As a result of the study conducted for the number of neurons, the graph given in Fig. 4 was obtained and the optimum number of neurons was determined as 9. Finally, the parameters and their values used in the Multilayer Perceptron module were presented in Table 2.

Table 2. The parameters and their values used in the Multilayer Perceptron module.

Parameters	Values
# input parameters (Temperature, plastic strain, strain rate)	3
# output parameters (True stress)	1
# hidden layers	1
# neurons	9
Activation function	tanh
Solver	lbfgs
Randomness	53
# epochs	1000

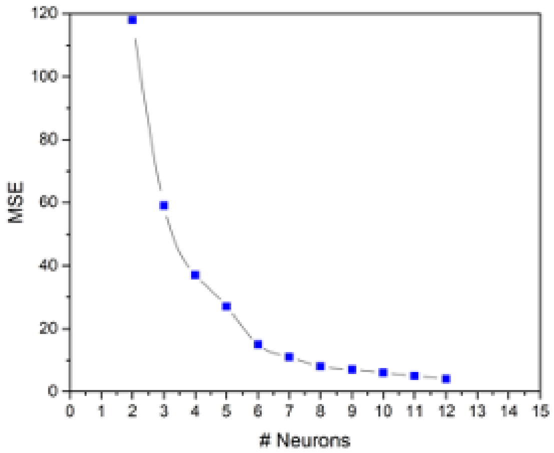

Fig. 4. MSE plot obtained to find the optimum number of neurons.

3. Flow Curve Prediction by Using Artificial Neural Network Model

In order to measure the performance of the developed ANN model, determination coefficient R^2 and root mean square error (RMSE) measurements were used. The RMSE value for the estimated ANN model results is calculated according to Equation (1).

$$RMSE = \sqrt{\frac{(y_{exp}-y_{pre})^2}{N}} \tag{1}$$

where N is the total number of observations, y_{exp} is experimental result, and y_{pre} is predicted value. In order to verify the generalization capability of the developed ANN model, 25% of the data obtained by the experimental compression tests (flow curve data for 100 °C) is reserved. By using the ANN model trained with the remaining 75% of the experimental data (flow curve data for 20, 200, 400 °C), the material model predictions at 100 °C were obtained for different strain rate values. Comparison charts of predicted and target (real) data for strain rate 1, 10 and 50 values are given in Fig. 5,6,7, respectively. As seen in the figures, R^2 values are very high and the proposed ANN model predicted true stress values very close to the real data. Considering these graphs, it was observed that the difference between the predicted and actual true stress values is at most 14 MPa. As a result, it was concluded that the proposed ANN model reflected the input parameters very well and made promising predictions in very short CPU time as 8.10 seconds.

True stress values for strain rate of 1 s^{-1} at 100 °C was good agreement with the predicted values. The obtained true stress predictions had RMSE=3.53 and R^2=0.9996 which confirm the generalization capability of ANN model.

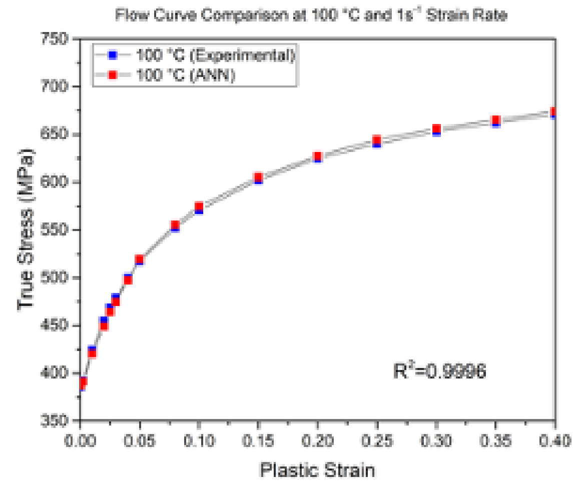

Fig. 5. Comparison of ANN predictions for the validation data set, strain rate: 1 s^{-1}.

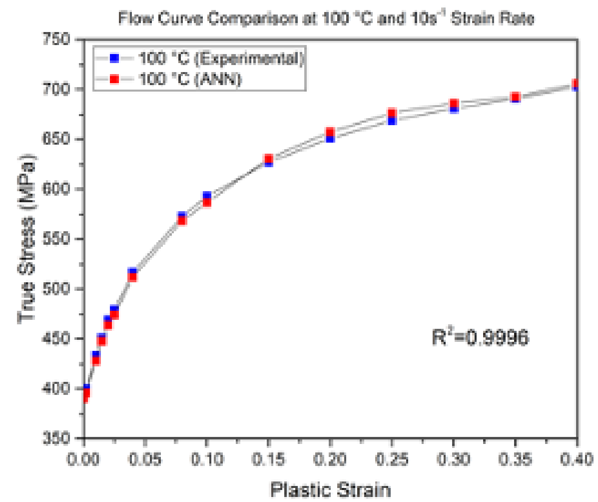

Fig. 6. Comparison of ANN predictions for the validation data set, strain rate: 10 s^{-1}.

True stress values for strain rate of 10 s^{-1} at 100 °C was also good agreement with the predicted values. The obtained true stress predictions had RMSE=4.77 and R2=0.9996 which also confirm the generalization capability of ANN model.

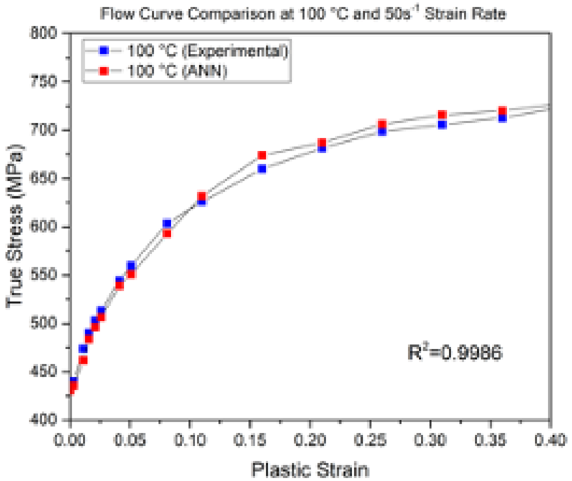

Fig. 7. Comparison of ANN predictions for the validation data set, strain rate: 50 s^{-1}.

4. Conclusion

A limited number of material models are preloaded on Simufact.forming software, so it finds values by interpolating or extrapolating for material property ranges that are not defined during analysis. Interpolating or extrapolating material properties causes the analysis results to be erroneous. For this reason, material models for the raw materials are obtained by experimental method and integrated into the finite element software. Although obtaining the material model with experimental methods and integrating it into the software improves the analysis results, it is very costly to create a material model experimentally for each temperature and strain rate value. Therefore, flow curves of a medium carbon alloy steel material, which is frequently used in bolt production by cold forming method, were experimentally obtained by compression tests within the scope of this study. Afterwards, ANN model was created to predict the flow curves of the material and the results were compared with the experimental data. Prediction results obtained with the ANN model were able to predict the material data allocated for verification at a high accuracy rate. As a result, it was concluded that the proposed ANN model reflected the input parameters very well and made promising predictions.

References

[1] Dhingra, A. K., and Rao, S. S. A Neural Network Based Approach To Mechanical Design Optimization. Engineering Optimization, 1992, 20(3), 187-203. DOI 10.1080/03052159208941280.

[2] JR, J. H. Garrett, Case, M. P., Hall, J. W., Yerramareddy, S., Herman, A., Sun, R., Ranjithan, S., and Westervelt, J. Engineering Applications of Neural Networks. Journal of Intelligent Manufacturing, 1993, 4, 1-21.

[3] Denizer, B. Artificial Neural Network Analysis of the Mechanical Properaties of Tungsten Fiber / Bulk Metallic Glass Matrix Composites via Neutron Diffraction and Finite Element Modelling. MS thesis, 2008, Iowa State University.

[4] Toros, S., and Ozturk, F. Flow Curve Prediction of Al-Mg Alloys under Warm Forming Conditions at Various Strain Rates by ANN. Applied Soft Computing, 2011, 11(2), 1891-1898. DOI 10.1016/j.asoc.2010.06.004.

[5] Pattanaik, L. N. Applications of Soft Computing Tools in Metal Forming: A State-of-Art Review. Journal of Machining & Forming Technologies, 2013, 5(1/2), 1-15.

[6] Mehtedi, M. El, Forcellese, A., Greco, L., Pieralisi, M., and Simoncini, M. Flow Curve Prediction of ZAM100 Magnesium Alloy Sheets Using Artificial Neural Network-Based Models. Procedia CIRP, 2019, 79, 661-666. DOI 10.1016/j.procir.2019.02.050.

[7] Merayo, D., Rodriguez-Prieto, A., and Camacho, A. M. Prediction of Physical and Mechanical Properties for Metallic Materials Selection Using Big Data and Artificial Neural Networks. IEEE Access, 2020, 8, 13444-13456. DOI 10.1109/ACCESS.2020.2965769.

[8] Huynh, T.-C., Park, J.-H., Jung, H.-J., and Kim, J.-T. Quasi-Autonomous Bolt-Loosening Detection Method Using Vision-Based Deep Learning and Image Processing. Automation in Construction, 2019, 105(May), 102844. DOI 10.1016/j.autcon.2019.102844.

[9] Zhang, Y., Sun, X., Loh, K. J., Su, W., Xue, Z., and Zhao, X. Autonomous Bolt Loosening Detection Using Deep Learning. Structural Health Monitoring, 2020, 19(1), 105-122. DOI 10.1177/1475921719837509.

[10] ASTM E9-19. Standard Test Methods of Compression Testing of Metallic Materials at Room Temperature. ASTM International, 2019, West Conshohocken, PA.

[11] Haykin, S. Neural Networks; a Comprehensive Foundation. Prentice-Hall, 1999, Upper Saddle River.

[12] Lau, C. Neural Networks, Theoretical Foundations and Analysis. IEEE Press, 1992, New York, NY.

[13] McClelland, J. L., Rumelhart, D. E., and PDP Research Group. Parallel Distributed Processing. MIT Press, 1986, Cambridge, MA.

EFFECT OF WC-CO GRADE ON HEADING DIE PERFORMANCE IN COLD FORGING

M. Burak TOPARLI
İlhan Burak ÖZHAN

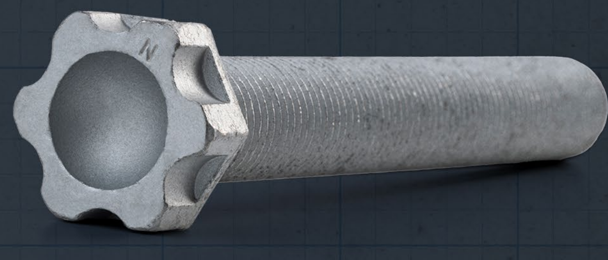

International Conference on Structural Integrity 2021

EFFECT OF WC-CO GRADE ON HEADING DIE PERFORMANCE IN COLD FORGING

M. Burak Toparlı[1,2], İlhan Burak Özhan[1]

[1]Nedu Bağlantı Elemanları San. ve Tic. A.Ş., AOSB, Çiğli, İzmir, Türkiye, burak.toparli@norm-fasteners.com.tr
[2]Norm Cıvata San. ve Tic. A.Ş., AOSB, Çiğli, İzmir, Türkiye

WC-Co hard metals **Cold forging** **Failure analysis**

Abstract

In this study, heading dies used for production of fasteners with external 6-lobe head form were investigated. In cold forging, forming dies are generally produced from WC-Co hard metals and tool steels. Inserts made of WC-Co hard metals are shrink-fitted with rings made of tool steels to have prestressing. Depending on operation, the choice of WC-Co grade is very crucial and has significant effect on die performance. Based on Co content and WC grain size, mechanical properties such as hardness and transverse rupture strength of WC-Co materials are greatly changing. In this study, according to initial die design and material selection, fasteners were produced and heading die performance was monitored. During production, it was observed that internal socket dimensions of heading dies were enlarged after about 90,000 product and dies were replaced to ensure that produced fasteners were in tolerance limits. After production, failure analysis was performed to used heading dies. It was revealed that main failure mechanism was abrasive wear leading to enlargement in the internal socket form. There was no visible cracking or damage on used dies. In order to improve performance against abrasive wear, WC-Co grade with lower Co content and smaller WC grain size was employed. New heading dies were used in production to investigate the effect of material change. It was revealed that new heading dies were cracked after about 563,000 products. Failure analysis of revised heading dies showed that both abrasive wear and fatigue cracking were contributed to failure. Therefore, it was concluded that use of WC-Co inserts with lower Co content and smaller WC grain size improved the wear resistance leading to improved performance.

INVESTIGATION OF DELAYING COLD HEADING CRACK FORMATION WITH SHOT PEENING PROCESS

Cenk KILIÇASLAN
M. Burak TOPARLI
Sezgin YURTDAŞ
Doğuş ZEREN
Barış TANRIKULU

IMMC'2021 International Metallurgy & Materials Congress, 10-12 June 2021, Digital Platform

INVESTIGATION OF DELAYING COLD HEADING CRACK FORMATION WITH SHOT PEENING PROCESS

Cenk Kılıçaslan[1,*], M. Burak Toparlı[1], Sezgin Yurtdaş[1], Doğuş Zeren[1], Barış Tanrıkulu[1]

[1]Norm Cıvata San. ve Tic. A.Ş., A.O.S.B., Izmir, Türkiye

Abstract

In this study, steel coil samples were subjected to shot peening process to delay crack initiation during cold heading. By this way, it was aimed to forge products having high head diameter / shaft diameter ratio. After shot peening of steel samples, compression experiments were conducted to samples having two different geometries as tapered and flanged. It was seen after shot peening, surface roughness and hardness values were increased after shot peening. However, compression test results revealed that expected improvement in crack initiation retardation to increase forgeability limit was not achieved after shot peening due to heavily deformed steel surface.

Keywords: Shot peening, cold forging, forgeability, compression test

1. Introduction

Shot peening is one of the mechanical surface treatment methods used especially in aviation. Metal or ceramic spheres accelerated with compressed air are directed to the surface of the material to be processed. As a result of plastic deformation in the area close to the surface, compressive residual stresses occur and hardness increases. In this way, crack initiation and propagation can be delayed and fatigue life of the material can be increased significantly [1,2].

2. Materials and Methods

In this study, two different compression test geometry made of 41Cr4 were employed (Fig 1). Characterization tests including surface roughness and hardness were carried out. Compression tests were conducted in order to determine crack initiation limit, which is very important parameter in terms of metal forming via cold forging. Compression tests up to 350 kN were done to obtain the maximum load at which crack initiation was not observed. The limiting study was carried out on samples with and without shot peening treatment. Two of the post-compression test sample images after shot peening with surface cracks can be seen in Fig. 2.

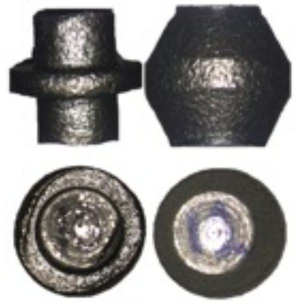

Fig. 1. Shot peened samples.

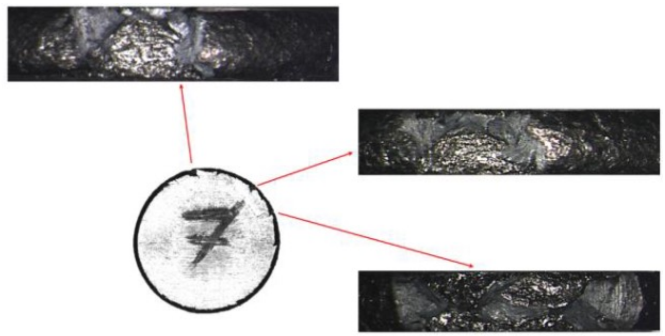

Fig. 2. Surface cracks and their locations of two different shot peened samples subjected to compression tests.

3. Results and Conclusions

In the characterization tests performed after the shot peening, a 25% hardness increase was obtained on the material surfaces. However, the surface morphology deteriorated and the surface roughness values (Ra and Rz) increased by up to 7.5 times. As a result of the compression tests, it was determined that this process does not have a positive effect on the forging of the products with high target head diameter / shaft diameter ratio after the shot peening.

Acknowledgment

The authors would like to acknowledge Deniz Civan Özuğurlu for his contribution.

References

[1] M.B. Toparli, Experimental Techniques, 44 (2020), 37-47.

[2] B. Karahan and U. İnce, Derin, 5 (2015), 74-90.

EFFECT OF COATING ON SURFACE INTEGRITY OF TOOLS AND END PRODUCTS AFTER PIERCING OPERATION

Fuat Can AĞARER
Hatice SANDALLI
M. Burak TOPARLI

24th International Conference on Material Forming (ESAFORM 2021)

EFFECT OF COATING ON SURFACE INTEGRITY OF TOOLS AND END PRODUCTS AFTER PIERCING OPERATION

Fuat Can Ağarer[1], Hatice Sandallı[1,*], M. Burak Toparlı[2]

[1]Norm Somun San. ve Tic. A.Ş., A.O.S.B., Izmir, Türkiye
[2]Nedu Bağlantı Elemanları San. ve Tic. A.Ş., A.O.S.B., Izmir, Türkiye

Abstract

Cold forging is an extensively used metal forming technique in many industries due to advantages over other methods including casting and machining. Having said that, tools used in cold forging may experience extreme tribological conditions such as high contact pressure and temperature. These conditions may lead to premature tool wear and tool failure. In addition, surface quality of end products is very dependent on the surface integrity of tools used in cold forging. With the aim of extending tool service life and enhancing end product quality, different surface treatment techniques can be applied on cold forging tools. In this study, TiN coating was applied on piercing punch and its wear performance was observed in the production line. In addition, surface quality of end parts produced by these tools were investigated. It was found that, tools coated with TiN and uncoated reached the limiting punch diameter after 70.000 and 5.000 parts, respectively. It was also revealed that surface integrity of end product is very dependent on surface conditions of cold forging tools.

Keywords: TiN coating, PVD, wear, cold forging

1. Introduction

Cold forging is one of the metal forming methods preferred thanks to superior surface quality of the end products, improved mechanical properties and suitability for mass production. Owing to its advantages over other metal forming methods, it is extensively used in various engineering applications such as bolt and nut production.

In cold forging, the contact pressure between work-piece and forging tool can reach up to 3000 N/mm^2, relative velocities can reach about 500 mm/s and die temperature may raise up to 600 [1]. Due to these extreme tribological conditions, forging tools experience wear phenomenon. Tool wear is one of the important type of failure in manufacturing, as it affects both work-piece quality and production efficiency.

In industrial applications, hard thin film coating technologies such as PVD (Physical Vapor Deposition) and CVD (Chemical Vapor Deposition) are employed in coating of forging tools in order to extend their lifetime, to reduce wear and to increase the efficiency of production.

2. Materials and Methods

In this study, effect of TiN coating via PVD on wear of a piercing punch was investigated. A comparison was made

between the lifetime of TiN coated and uncoated samples. The wear on piercing punches was monitored by checking diameter with caliper at regular intervals during production and by visual inspections. In addition, surface quality of end products was also investigated with the same intervals.

3. Results and Conclusions

Within the scope of this study, it was revealed that, diameters of punches were decreased due to wear, as expected. After a critical diameter, so-called limiting punch diameter, tear marks were observed during piercing operation, leading to burr in tapping operation. It was found that, TiN coated and uncoated tools reached the limiting punch diameter after 70.000 and 5.000 parts, respectively. Therefore, it was revealed that surface integrity of end products was very dependent on tool wear in terms surface profile and dimensional requirements. The results of this study exposed the importance of hard thin film coating in cold forging processes particularly for piercing operations in terms of tool life and surface integrity of end products.

References

[1] P. Groche, C. Müller and A. Jahn, Tribology Letters, 53 (2014), 599-605.

LOOSENING BEHAVIOUR OF CONICAL WASHER USAGE IN BOLTED JOINTS UNDER VIBRATION

Birtan GÜLER
Sezgin YURTDAŞ
Sarper DOĞAN

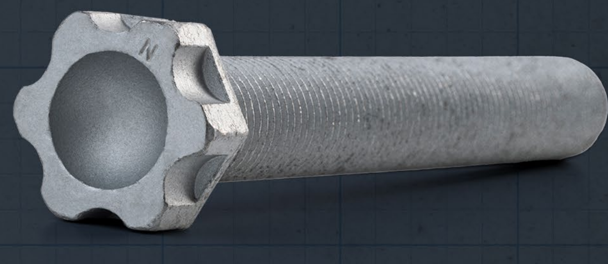

10th International Automotive Technologies Congress, OTEKON 2020
6-7 September 2021, Virtual Congress

LOOSENING BEHAVIOUR OF CONICAL WASHER USAGE IN BOLTED JOINTS UNDER VIBRATION

Birtan Güler[1], Sezgin Yurtdaş[2], Sarper Doğan[2]

[1] TOFAŞ Türk Otomobil Fabrikası A.Ş., Bursa, Türkiye
[2] Norm Cıvata San. ve Tic. A.Ş., A.O.S.B., İzmir, Türkiye
Corresponding Author: Birtan Güler, birtan.guler@tofas.com.tr

Abstract

Bolted joints are widely used joining type in the automotive industry. It is common to use conical (belleville) washers to prevent the self-loosening phenomenon that can occur in time for bolted joints. Despite the extensive use of conical washers, there is no study regarding their loosening resistance under vibration conditions depending on some joint parameter changes. In this study, loosening behavior under transversal vibration of the conical washer usage in bolted joints investigated experimentally according to clamping length and clamping force.

Within the scope of the loosening tests, to observe clamp length effect, tests were performed with two levels which are 25 mm and 75 mm. In order to examine the effect of clamp force, which is great importance in terms of loosening, the tests were conducted to correspond to 50% and 75% of the "proof load" value according to the ISO 898-1 standard. M8x1.25x8.8 quality bolts were used during the tests.

Testing set was created as 23 full factorials with 6 replicates in the Minitab program and the effect of each parameter was examined with regression curves. The findings show that the clamping length and clamping force directly affect the performance of the conical washer.

Keywords: Fastener, conical washer, clamping length, loosening, regression

Özet

Cıvatalı bağlantılar otomotiv sanayinde sıklıkla kullanılan bir birleştirme çeşitidir. Bağlantılarda zamanla oluşabilen gevşeme fenomenini önlemek için konik(belleville) rondela kullanımı yaygındır. Konik cıvataların yaygın kullanımına ragmen, titreşim altında göstermiş oldukları gevşeme dirençlerinin parametrelere bağlı olarak değişimini içeren bir çalışma bulunmamaktadır. Bu çalışma ile cıvatalı bağlantılarda konik rondela kullanımının, yatay titreşim altında gösterdiği gevşeme davranışları bağlantı kilitleme boyu ve kilitleme yüküne bağlı olarak deneysel olarak incelenmiştir.

Gevşeme testleri kapsamında kilitleme boyunun etkisini görebilmek adına testler 25 ve 75 mm kilitleme boyu değerlerinde gerçekleştirilir iken, gevşeme açısından büyük öneme sahip kilitleme yükünün etkisinin de incelenebilmesi adına testler ISO 898-1 standardında mevcut olan "proof load" değerlerinin %50 ve %75' ine tekabül edecek şekilde seçilmiştir. Testler esnasında M8x1.25x8.8 kalite cıvatalar kullanılmıştır.

Deney seti, 2^3 tam faktöriyel 6 tekrarlı olarak oluşturulmuş, test sonuçları Minitab programında analiz edilerek, regresyon eğrileri ile her bir parametrenin etkisi incelenmiştir Elde edilen bulgular kilitleme boyunun ve kilitleme yükünün konik rondelanın performansına doğrudan etki ettiğini göstermektedir.

Anahtar kelimeler: Bağlantı elemanı, konik rondela, kilitleme boyu, gevşeme, regresyon

1. Introduction

Bolted joints are commonly used one of the joining methods in the automotive industry. The reason of that joints which are created with bolts and nuts, are relatively low cost compared to their durable, ductile benefits with respect to other joining methods, and at the same time, maintenance costs are low because they can be easily assembled and disassembled. Bolted joints are exposed to high external loads such as fatigue or misuse loads which that can be triggered to the self-loosening phenomenon. To prevent this self-loosening phenomenon, bolts must be fastened required clamp load considering external loads and other boundary conditions. According to DIN 25201-2 standard, clamping length – bolt diameter ratio shall be 3..5 are recommended to provide more flexibility to the joint. In the literature, there are some experimental studies about clamping length – bolt diameter ratio. By determining the clamping length - bolt diameter ratio as 1 to 4, the resistance of the joints against sliding was investigated by applying a fixed shear force in the transversal direction under 2 different torques and clamping lengths. It was observed that the clamping length - bolt diameter ratio and clamping length did not have a significant effect on loosening. (Denkert continued, 2019)

Junker (1969), showed that transversal loads acting on bolted joints play a more critical role in self-loosening than axial loads which performed in Junker vibration test device. (Sanclemente and Hess, 2007) conducted a study to examine the loosening mechanism parametrically and the effects of clamp load and pitch on loosening resistance. The study shows that clamp load and pitch has a direct impact on loosening behaviors of fasteners. In another study, Nishimura et. al. (2007) directly focused on loosening prediction. Findings revealed that loosening was caused by the formation of micro slips in the thread area due to the lateral force. (Dravid continued, 2014) investigated that the vibration behavior of the usage of plain and spring washers under 3 different torque values in the experimental setup which they created themselves. As a result of experimental tests, it has been shown that the spring washer behaves worse performance than the plain washer, and the resistance of the joint to loosening increases when the applied torque increases. (Yokohama continued, 2008) created a virtual M10 dimensioned 3D joint model and performed virtual tests on the model to show conical washer effect on loosening. The clamping force adjusted as 10 kN and 20 kN for both 3D models and were subjected to vibration with transversal load and the loosening angle of the nut and the preload loss on the bolt were investigated. These two levels of clamping load application simulate the situation in which the washer is fully flattened and not. The conical washer used model under 10 kN clamping force behaves worse condition than without washer usage. It has been found that the use of conical washers under 20 kN clamping load has no advantage over usage of non-washer. (Izumi continued, 2009) showed that the loosening performance of the usage of double nuts and spring washers in bolted joints under vibration was examined on the 3D virtual analysis model, and it was revealed that the application of double nuts is an effective method of preventing vibration, but the spring washer does not have a positive effect on preventing vibration. (Bhattacharya continued, 2008) compared the vibration resistance of various locking fasteners. It was also used 4 different types of washers in these tests. These were plain washers, spring washers, bottom and top knurled washers. The vibration resistance of chemically locked solutions is better than all types of washers, the nylok nut comes after chemical locking fasteners.

2. Material and Method

2.1. Test Sample Dimensions

Within the scope of the experimental tests carried out, M8x1.25x80 size 8.8 quality bolts according to ISO 15071 standard and M8x1.25 8 quality to comply with DIN 934 standard nuts were used in. The drawing of the bolts and nuts used during the tests is given in Figure 1. The drawing of the conical washers which is the main scope of the study, to comply with DIN 6796 is given in Figure 2. All bolts, nuts and washers used within the scope of the tests are coated with Delta Protect KL100 VH301 GZ coating and the friction coefficient range determined between 0.10-0.16.

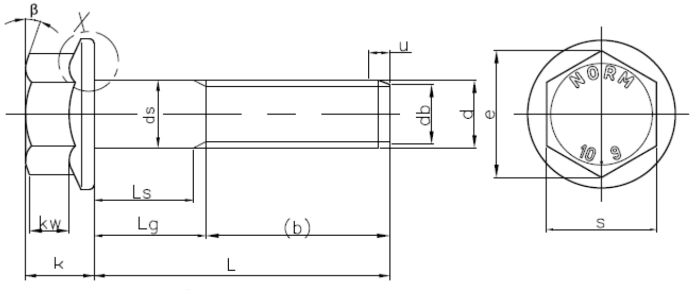

Fig. 1. Drawings of ISO 15071 bolt used in the junker vibration tests.

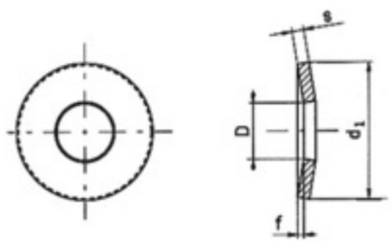

Fig. 2. Drawings of the conical washer used in vibration tests.

According to the DIN 6796 standard, the dimensions of the conical washer is shown in Table 1.

Table 1. Showing DIN 6796 Dimensions for Conical Washer

Size	D	s	d1	f
M8	8.4	1.5	22	0.65

2.2. Experimental Set-Up

The experiment set was prepared in order to observe the effect of the conical washer performance on clamping length and clamping force parameters which are given in Table 1. 8 different experimental sets were determined with 6 replicates. A total of 48 Junker vibration tests were carried out. The tests were conducted in the Junker test device under 0.9 mm horizontal displacement, which is shown schematically in Figure 3. Each fastener was used only once, so tests were carried out directly in the range of the friction coefficient value of the coating.

Table 2. 2^3 Full factorial experiment set-up.

Experimental Setting	Clamping Force Level	Clamping Length (mm)	Conical Washer Usage
Set1	Proof load*0,75: 16 kN	75	No
Set2	Proof load*0,75: 16 kN	75	Yes
Set3	Proof load*0,75: 16 kN	25	No
Set4	Proof load*0,75: 16 kN	25	Yes
Set5	Proof load*0,50: 11 kN	75	No
Set6	Proof load*0,50: 11 kN	75	Yes
Set7	Proof load*0,50: 11 kN	25	No
Set8	Proof load*0,50: 11 kN	25	Yes

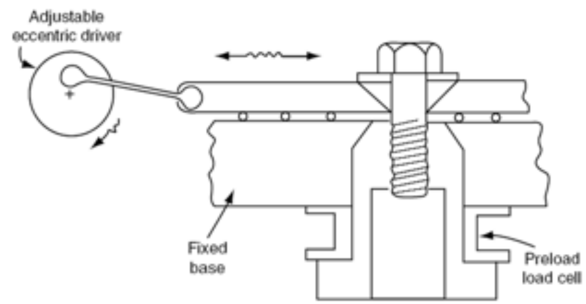

Fig. 3. The Junker vibration test device (Bickford, 2008).

3. Experimental Test Results

Experimental studies were performed with reference to the DIN 65151 standard created by Junker's work. As a result of the Junker tests, clamping force – cycle graphics were created with the average values of 6 experiments performed for each set of experiments. Clamping force – cycle graphics which obtained as a result of the experiments are given in Figure 4. The loosening rates were found from the clamp load - cycle graphics by the linear curve fitting method. Clamping length is one of the most important factors affecting bolted joint loosening. According to the findings obtained, as a result of the vibration tests performed with a clamping length of 75 mm, the loosening behavior of the joint was found to be more resistant as expected compared to the tests performed with a clamping length of 25 mm. Within the tests which performed at 75 mm clamping length, similar results were obtained for both clamping force values. Accordingly, the effect of the conical washer was clearly seen in the tests with a clamping length of 75 mm. Similarly, in the tests performed with bolts with a clamping length of 25 mm, it was observed that the conical washer had no positive effect with both clamping force levels.

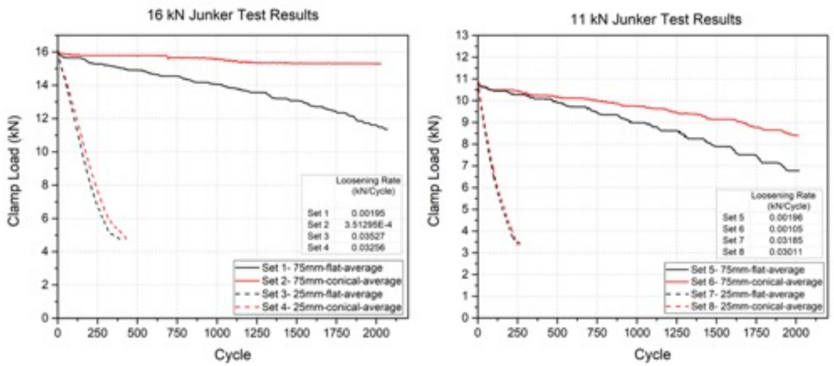

(a) **(b)**

Fig. 4. Junker vibration test results of 16 kN (a) and 11 kN (b).

4. Regression Analysis

A full factorial DOE was created using the Minitab program in order to examine the suitability of the loosening rate data obtained from the vibration tests and the effects of the parameters on the output relaxation rate were compared with regression analysis. The data used in the regression analysis includes 48 loosening rate values obtained as a result of physical tests and the average values are shared in Table 3.

Table 3. DOE experimental set.

Experimental Setting	Clamping Force Level(N)	Clamping Lenght(mm)	Conical Washer Usage	Loosening Rate Average (kN/cycle)
Set1	16000	75	No	0,00195
Set2	16000	75	Yes	0,000351
Set3	16000	25	No	0,03527
Set4	16000	25	Yes	0,03256
Set5	11000	75	No	0,00196
Set6	11000	75	Yes	0,00105
Set7	11000	25	No	0,03185
Set8	11000	25	Yes	0,03011

The aim of the regression analysis is to create a multivariate equation that will express the loosening rate, which is the output, for the input parameters which are determined as the clamping length, clamping force and the usage of conical washer in this study. The regression formula resulting from this analysis is shared with Equation 1.

Loosening Rate = 0,04413 - 0,000626 Clamp Length + 0,000012 Clamp Force - 0,000785 Conical Washer Usage (1)

As a result of the regression analysis, the adjusted R-sq value was found to be 96.31%, this value means that the input parameters explain the output parameter at the rate of 96.31%. Adjusted R-squared is more important than R-squared. Meaningless independent variables eliminated and when we add a new variable, if the value increases, it is decided to add that variable to the equation. The model which is established as a result of the analysis is meaningful, there is 1 outlier in number of 48 experiments. Outlier value has no effect on the results, as a result of the analysis of conformity to normal distribution, the P-value value was found less than 0.005.

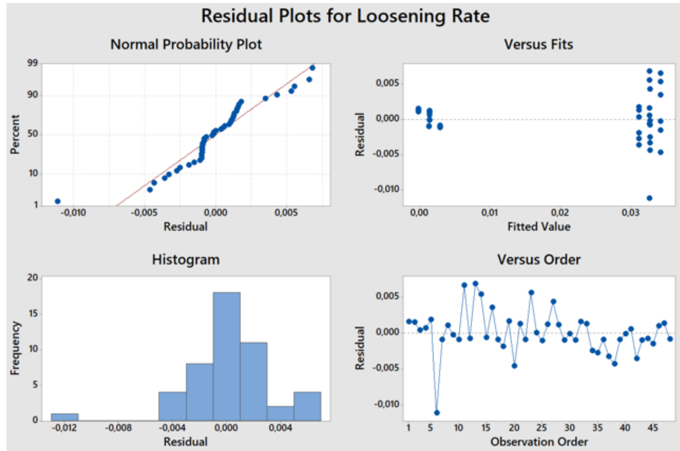

Fig. 5. Residual analysis of loosening rate.

According to the pareto graphic which is shown in Figure 6, the effect of the clamping length on loosening in the joints is much higher than the clamping force and the usage of a conical washer. Although the effect of clamping load and conical washer is close to each other, its effect on loosening has not been observed exactly due to the dominant effect of clamping length.

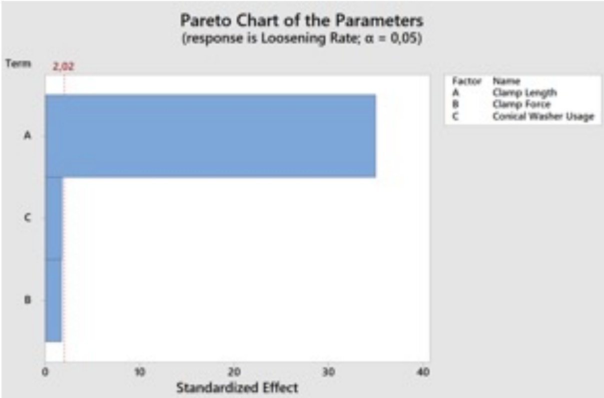

Fig. 6. Pareto chart of parameter effects.

With the created regression equation, the loosening rate can be calculated with different input parameters, or it can be predicted under which conditions this loosening rate will be seen by targeting the loosening rate. If we explain with an example, when the relaxation rate is taken 0.02 kN / cycle as the target, this value is formed for a clamping length of 47.6993 mm, under 16000 N clamping force and no usage of washers. As shown in Figure 7, the fact that the value of "d" which means desirability, comes out to 1 shows that the estimate is quite valid.

Fig. 7. Prediction of 0,02 kN/cycle loosening rate conditions.

5. Conclusions

Based on the vibration test results, conclusions which are listed below can be drawn from the experimental data in this study:

1. Clamping length has a major effect on the loosening of bolted joints. Due to this superiority, the influence of the other parameters which are the conical washer usage and the clamping length can not be fully observed.

2. In low loosening rate conditions, the conical washer positive effect on loosening can be seen more clearly. However, in high loosening rate which is heavily triggered by the shorter clamping length relatively no positive effect has observed in respect to non-usage of the conical washer.

3. More research is required to develop a deeper understanding of the relationships between conical washer effect and bolted joint loosening phenomenon. Experimental tests are needed to be increased with lower transvertial amplitude and clamping length must be taken as a constant.

References

[1] Izumi, S., Yokoyama, T., Kimura, M., and Sakai, S., (2009) "Loosening-resistance evaluation of double-nut tightening method and spring washer by three-dimensional finite element analysis", Engineering Failure Analysis 16, pp.1510–1519.

[2] Bickford, J.H., (2008) "An introduction to the design and behavior of bolted joints", 4th edition, Boca Raton: CRC Press.

[3] Bhattacharya A, Sen A, and Das S., (2010) "An investigation on the anti-loosening characteristics of threaded fasteners under vibratory conditions" Journal of Mechanism and Machine Theory 45, pp.1215-1225.

[4] Junker G., (1969) "New criteria for self-Loosening of fasteners under vibration". Transactions of the Society of Automotive Engineers, 78, pp.314-335.

[5] J.A. Sanclemente and D.P. Hess., (2007) "Parametric study of threaded fastener loosening due to cyclic transverse loads." Engineering Failure Analysis, 14, pp. 239-249.

[6] N.Nishimura, T. Hattori, M. Yamashita.,(2007) "Self Loosening Behavior of Metal Thread Joints under Transverse Cyclic Loading." Key Engineering Materials Vols. 340-341, pp 1467-1472.

[7] Dravid, S., Tripathi, K., and Chouksey, M., (2014) "Role of washers in controlling loosening of full threaded bolted joints" Procedia Technology 14, pp.543-552.

[8] Denkert, C., Kalkowsky, F., Flügge, W., (2019) "Experimental studies on the clamp length diameter ratio in highly stressed bolted joints" 24ème Congrès Français de Mécanique.

[9] Yokoyama, T., Oishi, K., Izumi, S., and Sakai, S., (2008) "Evaluation of loosening resistance performance of conical spring washer by three-dimensional finite element analysis" Journal of Solid Mechanics and Materials Engineering, Vol. 2, No. 1.

GELİŞTİRİLMİŞ DAYANIMA SAHİP BİR BAĞLANTI ELEMANI TASARIMI

Sezgin YURTDAŞ
Barış TANRIKULU
Özlem TOKER
Cenk KILIÇASLAN
Umut İNCE

Manisa Celal Bayar Üniversitesi
III. Ulusal Üniversite Sanayi İşbirliği, Arge ve İnovasyon Kongresi, 29 Aralık 2020

GELİŞTİRİLMİŞ DAYANIMA SAHİP BİR BAĞLANTI ELEMANI TASARIMI

Sezgin Yurtdaş[1], Barış Tanrıkulu[1], Özlem Toker[1], Cenk Kılıçaslan[1], Umut İnce[1]
[1]Norm Cıvata Ar-Ge Merkezi, İzmir, Türkiye
Email: sezgin.yurtdas@normcivata.com

Özet

Ağırlık azaltma çalışmaları otomotiv sektöründe son yılların en popüler çalışma konularından bir tanesidir. Özellikle elektrikli ve hibrit araçların kullanımında menzil mesafelerinin artırılması, CO_2 emisyon değerlerinin düşürülmesi ve daha düşük yakıt tüketiminin sağlanabilmesi amacıyla makine elemanlarında hafifletme çalışmaları önem kazanmış durumdadır. Çalışma kapsamında incelenen DIN EN ISO 7380-2 bağlantı elemanı, karbon çeliği ve alaşımlı çeliklerden üretilen bağlantı elemanlarının mekanik özelliklerinin verildiği ISO 898-1 şartnamesinde tam dayanıma sahip olmayan bağlantı elemanı olarak ifade edilmektedir. İlgili şartnameye göre DIN EN ISO 7380-2 ürününün çekme dayanımı standart ürünlerin %80'ini sağlamaktadır. Yapılan çalışma ile DIN EN ISO 7380-2 grubunda yer alan M12x1,75x40 ürününün kafa geometrisinde tasarım revizesi sayesinde ürün gramajında bir değişime yol açmadan tam dayanıma sahip bağlantı elemanı mekanik özellik değerlerini göstermesi hedeflenmiştir. Revize edilen tasarımın 3 boyutlu modelleme çalışmaları Catia, soğuk şekillendirme malzeme akış analizleri ise Simufact Forming yazılımları ile gerçekleştirilmiştir. Numune üretimi tamamlanan revize bağlantı elemanı formu için çekme ve tork testleri gerçekleştirilmiş ve ISO 898-1'de istenen mekanik değerlerde tam dayanımı sağladığı tespit edilmiştir.

Anahtar Kelimeler: Soğuk dövme, bağlantı elemanı, ağırlık azaltma, CO_2 emisyonu, çekme dayanımı.

Giriş

Bağlantı elemanları uygulama alanlarına göre farklı standartlar altında derlenmiş olup metal endüstrisinde en yaygın kullanılan emniyet elemanlarından birisi olarak ifade edilmektedir. Artan küresel rekabet ortamı nedeniyle bağlantı elemanı üreticilerinden üstün mekanik dayanım ve ağırlık azaltma konularında ürün beklentisi oluşmaktadır. Nüfusun artışı ve teknolojinin ilerlemesiyle birlikte son yıllarda araçların yoğun olarak kullanılması ve araçlardan salınan CO_2 oranının giderek artış göstermesi, sera gazlarının atmosferdeki yoğunluğunda artışa neden olmaktadır. Küresel iklim değişikliğinin de önemli sebeplerinden birisi olarak gösterilen sera gazlarının atmosferde birikmesi gün geçtikçe daha tehlikeli boyutlara ulaşmaktadır (Osakada, 2007). 2009 yılından itibaren Avrupa Birliği tarafından yayınlanan yönetmeliklerle, karbon emisyonunun büyük ölçüde kaynaklandığı kara yolu taşımacılığında araçlar için zorunlu emisyon hedefleri konulmaktadır. 2030 itibariyle sera gazı emisyonunda ara hedef olarak en az %55'lik bir azalma ve 2050 yılı itibariyle de iklim-nötr Avrupa'nın gerçekleştirilmesi hedeflenmektedir (Avrupa Birliği Komisyonu ve Konseyi, 2009). Karbon emisyonuna neden olan yakıt tüketiminin azaltılması amacıyla otomotiv sektöründe ağırlık azaltma çalışmaları son yıllarda oldukça önem kazanmış olup yakıt fiyatları da yakıt kullanımını açıkça etkileyen önemli bir araç haline gelmiştir (Basso ve Oum, 2007). Ham petrol fiyatlarındaki yerel ve global artış, müşteri eğilimlerini önemli ölçüde etkileyerek otomotiv üreticilerini daha hafif ve dolayısıyla yakıt tüketimi açısından daha ekonomik araç üretimine yönlendirmiştir (Schipper, 2014). Bir binek araçta yaklaşık 3500 ile 7000 arasında bağlantı elemanı kullanıldığı göz önünde bulundurulduğunda bağlantı elemanlarında yapılan ağırlık azaltma çalışmaları aracın ağırlığında kayda değer bir azalmaya yol açabilmektedir. Yapılan çalışmada bağlantı elemanlarında ağırlık azaltmanın 3 yöntem ile gerçekleştirilebileceği belirtilmiştir. Bunlardan birincisi, bağlantı elemanının üretiminde kullanılan çelik gibi yüksek yoğunluklu malzemelerin yerine alüminyum alaşımları gibi yoğunluğu daha düşük malzemelerin kullanılmasıdır. Ancak bu durumda, üretim maliyetinde artış, farklı malzeme kullanımından dolayı ortaya çıkabilecek galvanik korozyon riski ve malzemenin üretim aşamasında kalıplara yapışması/tutunması gibi problemlerle karşılaşılabilmektedir. İkinci yöntem, bağlantı elemanları geometrisinin mekanik özelliklerinden ve servis performansından ödün vermeden modifiye edilerek hafifletilmesidir. Üçüncü ve son yöntem olarak da bağlantı elemanının montaj yönteminin değiştirilmesiyle bağlantı elemanı başına elde edilecek ağırlık kazanımı sayesinde iş parçasının nihai ağırlığında hafifleme sağlanabilmesidir (Toparli vd., 2018). Otomotiv sektöründe ağırlık azaltma yapılanmaları güvenlik ve sürüş konforu için ayrıca kritik bir öneme sahiptir (Lange vd., 1992). Ağırlık azaltma çalışmaları, mekanik tasarım, malzeme bilimi, imalat bilimi ve optimizasyon yöntemleri gibi farklı mühendislik ve bilim disiplinlerini içermektedir (Groenbaeck ve Hinsel, 2000).

Bağlantı elemanlarının geometrisinde yapılan modifikasyonlarla ağırlık azaltma üzerine çok sayıda tasarım çalışması yapılmış olsa da bu çalışmaların yaygın olarak altı köşe başlı bağlantı elemanlarına yönelik uygulandığı görülmektedir. Yapılan çalışmada, DIN EN ISO 7380-2 standardına uygun M12x1,75x40 ürünün kafa geometrisi revize edilerek bağlantı elemanının toplam ağırlığında bir değişime yol açmadan ISO 898-1'e göre istenilen tam mekanik dayanım değerlerini sağlaması hedeflenmiştir. Bu sayede montaj noktalarında azaltılmış dayanım nedeniyle meydana gelebilecek kırılma problemlerinin minimize edilmesi ve bağlantı elemanı gramajında bir artışa yol açmadan tam dayanıma sahip cıvata formunun elde edilmesi mümkün hale gelebilecektir.

Tasarım ve Nümerik Çalışmalar

Tasarım

Çalışma kapsamında incelenen M12x1,75x40 ürün formu DIN EN ISO 7380-2 grubu içerisinde yer almaktadır. İlgili ürün grubu, karbon çeliği ve alaşımlı çeliklerden üretilen bağlantı elemanlarının mekanik özelliklerinin verildiği ISO 898-1 şartnamesinde tam dayanıma sahip olmayan bağlantı elemanı olarak ifade edilmektedir. Belirtilen şartnameye göre ilgili ürün grubunun sağlaması gereken çekme dayanım değeri, standart tam dayanıma sahip ürünlerinin %80'ine karşılık gelmektedir (Tablo 1). Dolayısıyla gerçekleştirilecek çalışmalarda ilgili ürün formunun gramajında herhangi bir artışa yol açmadan tam dayanım mekanik değerlerini sağlaması üzerine yoğunlaşılmıştır. Bu kapsamda üzerinde çalışılan DIN EN ISO 7380-2 ürün grubunda yer alan M12x1,75x40 ürün formuna ait teknik resim Şekil 1'de verilmiştir. Çalışması yapılan ürün formu hâlihazırda orta karbonlu bir çelik malzemesinden soğuk dövme yöntemi ile 4 istasyonlu bir soğuk şekillendirme presinde üretilmektedir.

Tablo 1. Dayanımı azaltılmış bağlantı elemanları için minimum çekme yükü (N).

Metrik	Kalite sınıfı	
	8.8[a]	10.9[a]
	Dayanımı azaltılmış ürün formu için minimum çekme yükü (N)	
M10	37.100	48.200
M12	53.900	70.200
M16	100.000	130.000
[a]ISO 898-1'e göre %80 çekme yükü		

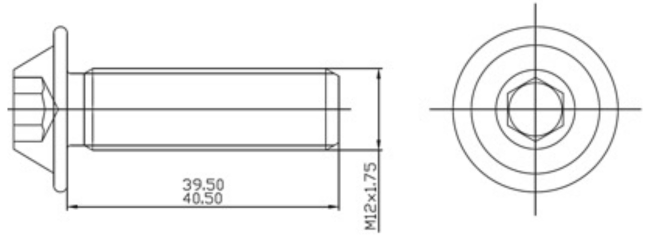

Şekil. 1. M12x1,75x40 (DIN ISO EN 7380-2).

Tam dayanıma sahip olmayan bağlantı elemanı tasarımında kritik bölge ürünün kafa geometrisi olduğu için belirlenen üründe kafa formunu oluşturan parametreler üzerinde alternatif tasarım çalışmaları gerçekleştirilmiştir. Bu doğrultuda Şekil 2'de verilen parametrelerin bağlantı elemanı dayanımı üzerine etkisi incelenmiş olup belirlenen alternatif geometriler özel matematiksel modeller ile kontrol edilerek dayanım performansları tespit edilmiştir. Yapılan nümerik çalışmanın ardından belirlenen revize kafa formuna ve mevcut tasarıma ait katı modellere Şekil 3'de yer verilmiştir.

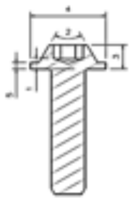

Tasarım parametreleri

Numara	Tanım
1	w ölçüsü
2	konik açısı
3	kafa kalınlığı
4	flanş çapı
5	flanş kalınlığı

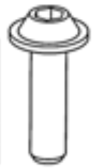

Şekil. 2. Ürün tasarımında incelenen tasarım parametreleri.

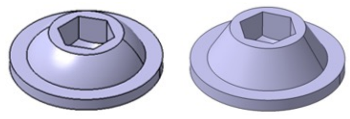

(a) **(b)**

Şekil. 3. Bağlantı elemanı kafa formu;
(a) DIN EN ISO 7380-2 (b) revize tasarım.

Nümerik Çalışmalar

Tam dayanım performansı sağlayacak final kafa geometrisinin tespit edilmesinin ardından nümerik simülasyon çalışmaları gerçekleştirilerek final formun soğuk şekillendirilebilirliği üzerinde çalışılmıştır. Bu doğrultuda Catia yazılımından faydalanılarak nihai bağlantı elemanı formu modellenmiş ve hacim eşitliği prensibi gözetilerek istasyon tasarımı oluşturulmuştur. Belirlenen ara istasyon modelleri kullanılarak kalıp modelleri elde edilmiş ve soğuk dövme analizlerinin gerçekleştirileceği Simufact.forming yazılımına entegre edilmiştir. Simülasyon çalışmalarından alınan final ürün formu Şekil 4'de verilmiştir. İlgili ürün formları incelendiğinde simülasyonlarda herhangi bir akış kusurunun meydana gelmediği ve istenilen tolerans değerlerinde nihai ürün formunun elde edilebildiği belirlenmiştir.

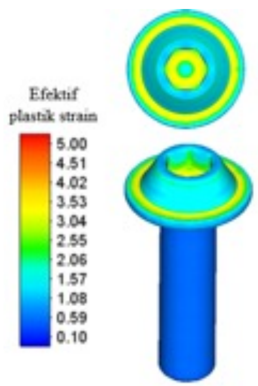

Şekil. 4. Simülasyondan alınan final ürün formu.

Sonuçlar

Nümerik çalışmalarda final ürün formunun tamamen soğuk şekillendirme ile dövülebilirliği tespit edildikten sonra soğuk dövme kalıplarının imalat aşamasına geçilmiş olup gerekli kalıp formlarının sağlanmasının ardından üretim hattı denemeleri gerçekleştirilmiştir. Üretim denemeleri simülasyonlarda tespit edilen dövme yükleri göz önünde bulundurularak 4 istasyonlu JBF19B4S presinde gerçekleştirilmiştir. Yapılan ara istasyon ayarları neticesinde final ürün formu istenilen tolerans değerleri içerisinde dövülebilmiştir. Belirlenen istasyon tasarımı ve kalıp performansını sınamak üzere 1000 adetlik numune üretimi gerçekleştirilmiş olup herhangi olumsuz bir durum meydana gelmemiştir.

Soğuk şekillendirme prosesinin nümerik çalışmalara paralel olarak sorunsuz bir şekilde tamamlanmasının ardından elde edilen yarı mamuller sırasıyla ısıl işlem ve kaplama proseslerine tabi tutularak nihai ürün formu elde edilmiştir. Isıl işlem prosesi sonucunda ürün formunun 10.9 kalite sınıfına erişmesi ve bu kapsamda istenilen mekanik değerleri yerine getirmesi sağlanmıştır. Bu aşamanın ardından ürüne lamelli bir kaplama çeşidi olan Delta Protect KL 100 VH 301 GZ uygulanarak hem korozyon direnci kazanması hem de sürtünme katsayısının daha dar bir tolerans aralığında meydana gelmesi sağlanmıştır. Şekil 5'de tüm ara prosesleri tamamlanmış ve mekanik testlere hazır hale getirilmiş final ürün formuna yer verilmiştir.

Şekil. 5. Revize M12x1,75x40 final formu.

İlgili ürün formu için tüm ara prosesler tamamlandıktan sonra rastgele belirlenen 3 adet numune için çekme ve tork testleri gerçekleştirilmiştir. Testlerde elde edilen mekanik veriler cıvatanın tam dayanıma sahip olduğunu doğrulamaktadır. Şekil 6'da çekme testi grafiği verilmiş olup cıvatanın kritik noktalardaki değerleri de Tablo 2'de ifade edilmiştir. Numunelere gerçekleştirilen tork testleri sonucunda elde edilen total, kafa altı ve diş sürtünme değerleri ise Tablo 3'de ayrıntılı olarak paylaşılmıştır.

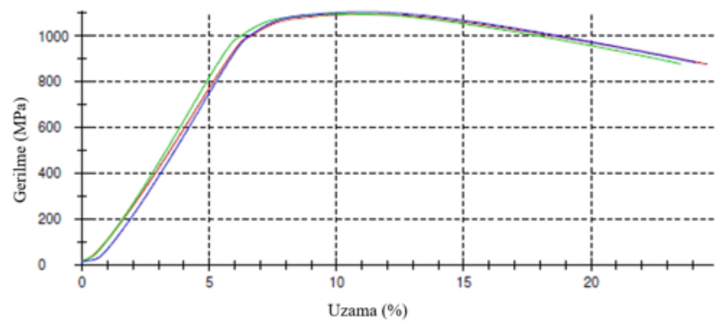

Şekil. 6. Çekme testinde gerilme-uzaman ilişkisi.

Tablo 2. Çekme testi sonuçları.

No	S0 (mm^2)	$R_{p0,2}$ (MPa)	R_m (MPa)	F_m (kN)	Kopma uzaması (%)
Test 1	84,3	991	1095	92,32	18,9
Test 2	84,3	995	1097	92,48	18,2
Test 3	84,3	1004	1104	93,04	18,3

Tablo 3. Tork-kilitleme yükü- sürtünme katsayısı test sonuçları.

No	F (kN)	T_{tot} (Nm)	T_{kafa} (Nm)	$T_{diş}$ (Nm)	μ_{kafa}	$\mu_{diş}$	μ_{tot}
Test 1	52,53	119,71	67,68	52,03	0,13	0,11	0,12
Test 2	52,54	121,66	68,06	53,60	0,13	0,12	0,12
Test 3	52,52	122,99	70,22	52,78	0,13	0,12	0,13

Sonuçlar

Yapılan çalışmada DIN EN ISO 7380-2 ürün grubunun kafa geometrisinde tasarım revizesi yapılarak ISO 898-1 şartnamesine göre gerekli çekme dayanım değerleri elde edilmiş ve nihai ürün formu tam dayanıma dönüştürülmüştür. ISO 898-1 şartnamesine göre M12 10.9 kalite sınıfına sahip ürünün tam dayanım mekanik özelliklerini sağlayabilmesi için çekme testinde minimum 87,7 kN değere sahip olması gerekmekte iken bu değer revize ürün formunda minimum 92,3 kN olarak tespit edilmiştir. Belirlenen final kafa formu ile ürünün gramajında bir değişime yol açmadan mekanik özelliklerinde iyileşme sağlanmış ve yeni nesil bir bağlantı elemanı elde edilmiştir.

Teşekkür: Yazarlar çalışmalarda göstermiş oldukları katkılardan dolayı Norm Cıvata üretim ekibine teşekkür etmektedirler.

Referanslar

1. Basso, L.J., Oum, T.H., (2007). Automobile fuel demand: a critical assessment of empirical methodologies. Transport Reviews 27 (4), 449–484.

2. EU Parliament and Council (2009). Regulation (EC) No 443/2009: Setting emission performance standards for new passenger cars as part of the community's integrated approach to reduce CO2 emissions from light-duty vehicles, https://ec.europa.eu/clima/policies/transport/vehicles/regulation_en.

3. Groenbaeck, J., Hinsel, C., (2000). Improved fatigue life and accuracy of precision forging dies by advanced tripwound prestressing system, SME Clinic on Precision Forging Technology, Columbius, Ohio, USA.

4. Lange, K., Cser, L., Geiger, M., Kals, J.A.G. (1992). Tool life and tool quality in bulk metal forming. CIRP Annals 41 2, 667-675. Osakada, K. (2007). Cold forging in Japan, Presentation at the 40th International Cold Forging Group, Plenary Meeting, Padova, Italy, September.

5. Schipper L., (2011). Automobile use, fuel economy and CO2 emissions in industrialized countries: Encouraging trends through 2008?, Transport Policy, 18, 2, pp. 358-372.

6. Toparli, M.B., Kılınçdemir, N.E., Yurtdaş, S., Tanrıkulu, B., İnce, U. (2018). Weight reduction of fasteners in automotive industry, Int. Automot. Technol. Congr. (9).

EFFECT OF STAGE DESIGN ON FAILURE OF M16x47 ECCENTRIC FASTENERS USED IN AUTOMOTIVE INDUSTRY

Sezgin YURTDAŞ
M. Burak TOPARLI
Sarper DOĞAN
Doğuş ZEREN
Umut İNCE

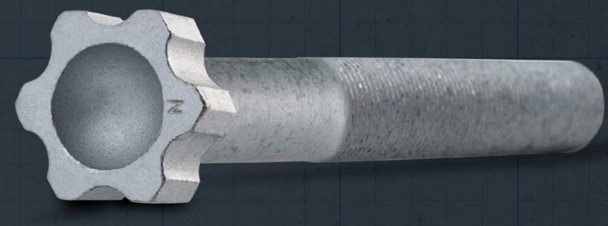

4. International Conference on Materials Science, Mechanical and Automotive Engineerings and Technology (IMSMATEC'21) May 28-30 2021

EFFECT OF STAGE DESIGN ON FAILURE OF M16X47 ECCENTRIC FASTENERS USED IN AUTOMOTIVE INDUSTRY

Sezgin Yurtdaş[a,*], M. Burak Toparli[a], Sarper Doğan[a], Doğuş Zeren[a] and Umut İnce[a]
[a]Norm Cıvata R&D Center, İzmir, Türkiye
*sezgin.yurtdas@norm-fasteners.com.tr

Abstract

Considering technological developments in the automotive industry, there has been an increase in the use of fasteners with complex and extra-ordinary forms. When examined in terms of design, functional and aesthetic requirements are evolving with the requirements driven by the recent trends. In this study, the head damage occurring in the fatigue tests of the special M16x47 fasteners with eccentric form in terms of head and shaft axis's were investigated. Within the scope of this study, stage and tool designs were made according to the final product geometry of the fastener. Material flow analysis was performed in the Simufact.Forming software. In addition, Cockroft-Latham damage parameter was investigated in the finite element analyses. As a result of cold forming simulations, it was determined that the critical Cockroft-Latham damage value was found as very close to the critical level in the transition region from head to shaft region for the initial design. Fatigue tests were also conducted and it was revealed that cracks were occurring at the regions where Cockroft-Latham damage was found to be as critical. Based on finite element modelling and experimental studies, stage design of the fastener was revised and the work piece diameter was increased by 24.8%. Based on new work piece diameter, stage and tool designs were updated. According to revised designs, finite element material flow analyses were repeated. The critical Cockroft-Latham damage value obtained from finite element simulations was reduced to 0.55 indicating that the new stage design leading to head-crack-free fasteners. After revised simulation studies in terms of material flow, further die analyses were carried out by using finite element modelling. According to revised die analyses, stress levels were obtained well-below the static failure limits for the cold forging dies. Based on the new stage and tool design, production of 5,000 fasteners were completed. After production, heat treatment process was carried out in order to obtain 9.8 grade. To obtain the friction coefficient in between a certain tolerances and to increase the corrosion resistance, fasteners were subjected to zinc flake coating. After the completion of all required production stages, fatigue tests were carried out within the scope of verification studies. In this context, tests were carried out by using Zwick/Roell high frequency tester. Fatigue tests done with 60 samples showed that the fatigue damage was obtained at the thread region, as expected for full-strength fasteners. In addition, there was no damage at the head to shaft transition region at the tested final fasteners. As a result of the work conducted in this study, the problem of head fracture occurring in low cycle fatigue tests were eliminated as a result of revised design verified by finite element modelling and experimental studies.

Keywords: Eccentric Fasteners, Cold Forging, Cockroft Latham, Fatigue

EPDM RONDELA KULLANIMININ MONTAJ KOŞULLARINA VE CIVATA ÇÖZÜLME HIZINA OLAN ETKİSİNİN İNCELENMESİ

M. Burak TOPARLI
Sezgin YURTDAŞ

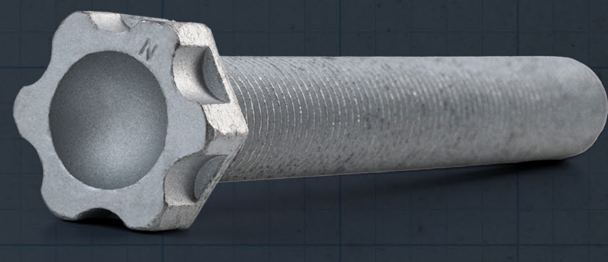

6th International Conference on Material Science and Technology in Cappadocia (IMSTEC'21),
November 26-27-28, 2021, Cappadocia /Türkiye

EPDM RONDELA KULLANIMININ MONTAJ KOŞULLARINA VE CIVATA ÇÖZÜLME HIZINA OLAN ETKİSİNİN İNCELENMESİ

M. Burak Toparli[a], Sezgin Yurtdaş[a]
[a]Norm Cıvata San. ve Tic. A.Ş., İAOSB, Çiğli, İzmir, Türkiye
E-mail: burak.toparli@normcivata.com

Özet

Bu çalışmada, montaj koşullarında özelikle sızdırmazlık ihtiyacı nedeniyle yaygın bir kullanımı olan kauçuk rondelanın uygulanan tork değeri sonrası elde edilen kilitleme yüküne ve titreşim altında çözülme davranışına olan etkisi incelenmiştir. Çalışma kapsamında 60 Shore A sertlik değerine sahip EPDM rondela kullanılmıştır. M8x1,25 cıvata ile yapılan tork kilitleme yükü testleri sırasında EPDM rondelada plastik deformasyon görülmüştür. Bu nedenle çalışma kapsamında uygulanacak nihai tork değerini belirlemek için ön testler gerçekleştirilmiştir. Belirlenen nihai tork değeri ile yapılan testlerde bağlantı elemanı kilitleme yükünde %25'e varan oranlarda kayıp yaşandığı tespit edilmiştir. EPDM rondela kullanımının çözülme hızına olan etkisini incelemek için junker titreşim test cihazında tek yönlü (yatay) titreşim testleri uygulanmıştır. Elde edilen sonuçları karşılaştırabilmek için rondelasız ve düz çelik rondela kullanımının dâhil edildiği ilave titreşim testleri gerçekleştirilmiştir. Elde edilen çözülme hızları karşılaştırıldığında en hızlı çözülmenin EPDM rondela kullanımı sonucunda olduğu belirlenmiştir. Kauçuk rondela kullanılarak yapılan titreşim testlerinde düz çelik rondela kullanımına kıyasla yaklaşık 1,5 kat, rondela kullanılmadan yapılan testlere kıyasla da 3,8 kat mertebesinde daha hızlı çözüldüğü görülmüştür. Yapılan tork-kilitleme yükü ve çözülme hızını karakterize etmek için kullanılan titreşim testleri sonucunda, EPDM rondelanın viskoelastik malzeme özelliği göstermesi nedeniyle montaj koşullarında tork kaybı ve çözülme hızında artış tespit edilmiştir. Sonuç olarak EPDM ve/veya benzer özellik gösteren malzemeden yapılmış rondelalı bağlantı elemanı kullanımının gerekli olduğu montaj koşullarında malzemenin viskoelastik özelliğinin göz önünde bulundurulması gerektiği ortaya çıkarılmıştır.

Anahtar Kelimeler: EPDM rondela, tork-kitleme yükü, junker titreşim test cihazı, bağlantı elemanı çözülme hızı

BAĞLANTI ELEMANI KAFA ALTINDA YER ALAN ÖZEL KANAL FORMUNUN DÜZ OVALAMA YÖNTEMİ İLE ÜRETİMİNİN İNCELENMESİ

M. Burak TOPARLI
Umut İNCE
Sezgin YURTDAŞ

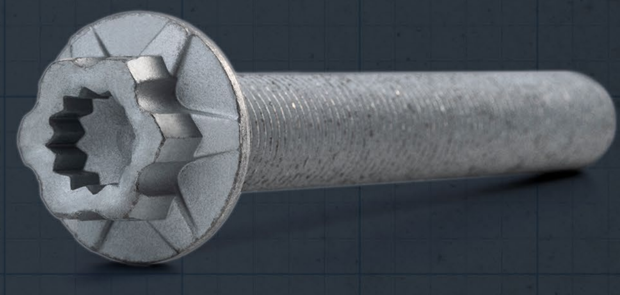

6th International Conference on Material Science and Technology in Cappadocia (IMSTEC'21),
November 26-27-28, 2021, Cappadocia /Türkiye

BAĞLANTI ELEMANI KAFA ALTINDA YER ALAN ÖZEL KANAL FORMUNUN DÜZ OVALAMA YÖNTEMİ İLE ÜRETİMİNİN İNCELENMESİ

M.Burak Toparlı[a], Umut İnce[a], Sezgin Yurtdaş[a]

[a]Norm Cıvata San. ve Tic. A.Ş., İAOSB, Çiğli, İzmir, Türkiye
E-mail: burak.toparli@normcivata.com

Özet

Gelişen mühendislik gereksinimleri doğrultusunda farklı performans beklentisine sahip makine elemanlarının bir arada kullanılmaya başlanmasından dolayı birden fazla fonksiyona sahip özel bağlantı elemanlarına olan ihtiyaç artmaktadır. Bu doğrultuda, iki veya daha fazla bileşenin birbirine geçici süreyle bağlanmasının yanı sıra kullanım alanına göre standart ürünlerde olmayan formların olduğu bağlantı elemanlarının kullanımı yaygınlaşmaktadır. Bu tür farklı özelliklerin bağlantı elamanına kazandırılması için standart üretim yöntemlerinin yanı sıra ikincil işlem operasyonlarına da ihtiyaç duyulmaktadır. Belirtilen işlemin gerçekleştirilmesi için talaşlı imalat veya ilave makine ihtiyacı nedeniyle ekstra maliyetler ortaya çıkmaktadır. Bu çalışmada, bağlantı elemanlarının kafa altında yer alan özel kanal formlarının talaşlı imalat ya da ekstra yatırım gerektiren silindirik ovalama makinaları yerine diş çekme operasyonlarında kullanılan düz taraklar ile üretimi incelenmiştir. Böylece, ilave maliyet artışı olmadan ürün formunda yer alan kanal geometrisinin hali hazırda bağlantı elemanlarına diş çekme operasyonunda kullanılan düz ovalama tarakları ile elde edilmesi hedeflenmiştir. Kafa altında yer alan kanal formunun düz ovalama makinalarında üretilebilmesi için özel ovalama tarak tasarımları oluşturularak bağlantı elemanının malzeme akışı ve ovalama çapının belirlenmesine yönelik tasarım ve simülasyon çalışmaları gerçekleştirilmiştir. Çalışma kapsamında belirlenen soğuk şekillendirme istasyon tasarımı doğrultusunda dövme işlemleri takip edilerek final ürün geometrisi elde edilmiştir. Bu prosesin ardından ovalama aşamasına geçiş yapılarak kafa altındaki kanal formunun oluşumu tecrübe edilmiştir. Ürünün kafa altı kanal formunda belirlenen kritik ölçüler kontrol edilerek tasarım ve simülasyon çalışmalarının doğrulaması yapılmıştır. 1000 adetlik numune üretimi sürecinde elde edilen kanal geometrisine ait tüm ölçüler kontrol edilmiş ve tanımlı tüm değerlerin ilgili toleranslar arasında olduğu tespit edilmiştir. Bu çalışma sonucunda istenilen final ürün geometrisi, talaşlı imalat veya ekstra makina yatırımı gerektiren silindirik ovalama makinesi kullanılmadan düz ovalama tarakları ile elde edilmiştir.

Anahtar Kelimeler: Bağlantı elemanı, soğuk dövme, kanal form, ovalama

FLANŞLI SOMUN KALIBI ÜRETİMİNDE RADYUS FORMLU VE KARBÜR ALAŞIMLI BAKIR ELEKTROTUN KULLANIMI

Bülent ÖZDEN
Gökay YALDIZ
Nurşen ŞAKLAKOĞLU
M. Burak TOPARLI
Erdem ÖZYURT
Gökhan BAĞBOZAN
Murat ÇETİNKAYA

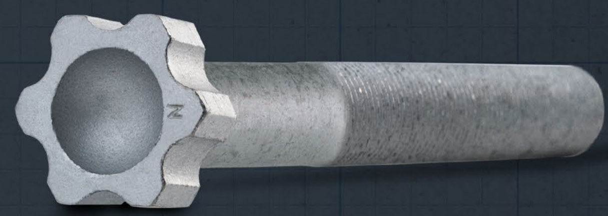

6th International Conference on Material Science and Technology in Cappadocia (IMSTEC'21), November 26-27-28, 2021, Cappadocia /Türkiye

FLANŞLI SOMUN KALIBI ÜRETİMİNDE RADYUS FORMLU VE KARBÜR ALAŞIMLI BAKIR ELEKTROTUN KULLANIMI

B.Özden[1,2*], G.Yaldız[1], N.Şaklakoğlu[1,2], M.B.Toparlı[1,3], E.Özyurt[1], G.Bağbozan[1], M.Çetinkaya[1]

[1] Norm Kalıp San. ve Tic. A.Ş., İAOSB, Çiğli, İzmir, Türkiye
[2] Makine Mühendisliği, Manisa Celal Bayar Üniversitesi, Manisa, Türkiye
[3] Norm Cıvata San. ve Tic. A.Ş., İAOSB, Çiğli, İzmir, Türkiye
E-mail: bulent.ozden@nedukalip.com

Özet

Bu çalışmada, soğuk dövme yöntemi ile dişi bağlantı elemanı olan flanşlı somunların üretiminde kullanılan bir somun kalıbı ele alınmıştır. Yüksek adetlerde üretim yapması beklenen flanşlı somun kalıplarında erken çevrim adetlerinde hasarlar tespit edilmiştir. Düşük ömürlerde hasara uğrayan kalıplar incelenerek hasarın neden meydana geldiğine dair kök neden analizleri yapılmıştır. Hasarlı kalıplar incelendiğinde seçilen malzemelerde bir uygunsuzluk görülmemiştir. Kritik ölçüler kontrol edildiğinde ise kalıbın flanş formunun olduğu yerden anahtar ağzına geçiş kısmındaki radyusun istenilen ölçüde ve formda olmadığı görülmüştür. Bu bölgedeki form bozukluğunun malzeme akışını olumsuz yönde etkilediği ve buradaki yüksek aşınma oranlarından dolayı kalıpların erken çevrimlerde tırnak atarak hasara uğradığı tespit edilmiştir. Kalıplarda ömür artışı sağlamak adına öncelikle mevcut radyus işlemede tercih edilen spiral taşla manuel olarak işleme metodunun alternatifleri üzerine durulmuştur. Yapılan çalışmalar neticesinde kalıbın taban formunun yanı sıra anahtar ağzı bölgesindeki radyusu ve flanşı da beraber tek seferde işleyecek bir bakır elektrot tasarımı geliştirilmiştir. Geliştirilen karbür alaşımlı ve radyus formlu bakır eletkrot ile dalma erozyon yöntemi kullanılarak revize somun kalıpları üretilmiştir. İlk denemelerde erken çevrimde kırılmalara neden olan radyusların, geleneksel işleme metodu ile üretilenlere göre revize yönetm ile istenilen formda ve yüzey pürüzlülüğünde elde edildiği görülmüştür. Yeni geliştirilen bakır elektrot ile üretilen somun kalıplarının çalışma adetleri soğuk şekillendirme operasyonlarında takip edilmiş ve kalıp ömürlerinde yaklaşık 6 katlık bir iyileşme sağlanmıştır. Bu sayede, flanşlı somun kalıpları üretiminde özellikle radyus formların önemi ortaya çıkarılmış ve üretim yöntemi değişikliği sayesinde kalıp performansında ciddi iyileşme olabileceği kanıtlanmıştır.

Anahtar Kelimeler: Soğuk şekillendirme, somun kalıbı, bakır elektrot, hasar analizi, dalma erozyon

ÖZEL KAFA FORMUNA SAHİP M10x74 ÜRÜNÜN MALZEME AKIŞ ANALİZLERİNİN GERÇEKLEŞTİRİLMESİ VE MARKA ZIMBASINDA MEYDANA GELEN HASAR PROBLEMİNİN İNCELENMESİ

Sezgin YURTDAŞ
M. Burak TOPARLI
Umut İNCE
Özlem TOKER
Tolga AYDIN

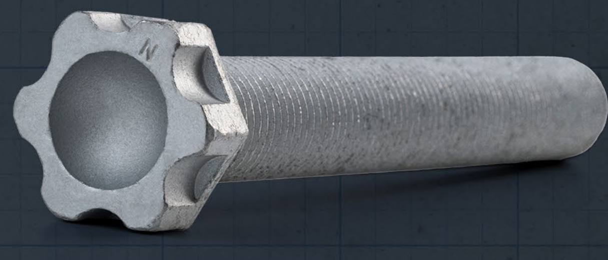

Manisa Celal Bayar University
IV. National University Industry Cooperation, R&D and Innovation Congress,
15-16 December 2021

ÖZEL KAFA FORMUNA SAHİP M10x74 ÜRÜNÜN MALZEME AKIŞ ANALİZLERİNİN GERÇEKLEŞTİRİLMESİ VE MARKA ZIMBASINDA MEYDANA GELEN HASAR PROBLEMİNİN İNCELENMESİ

Sezgin Yurtdaş[1], M. Burak Toparlı[1], Umut İnce[1], Özlem Toker[1], Tolga Aydın[1,*]
[1]Norm Cıvata Ar-Ge Merkezi, İzmir, Türkiye
*Email: tolga.aydin@normcivata.com

Özet

Yapılan çalışmada özel torx formuna ve düşük kafa yüksekliğine sahip M10x74 bağlantı elemanının soğuk dövme operasyonlarında meydana gelen şekillenme kusuru ve kafa dövme işleminde yaşanan zımba hasarı sayısal simülasyonlar aracılığıyla incelenmiştir. Gerçekleştirilen malzeme akış analizleri sonucunda üretim hattında karşılaşılan şekillenme bozuklukları tespit edilmiş ve bu süreçte zımba formunda meydana gelen kritik gerilmeler belirlenmiştir. Mevcut durumun nümerik platformda doğrulanmasının ardından alternatif istasyon ve kalıp tasarımları ile malzeme akışında istenilen form sağlanarak zımba formuna etkiyen gerilme yığılması minimize edilmiştir. Soğuk şekillendirme süreçlerine ait malzeme akış ve elastik kalıp analizleri Simufact Forming yazılımı ile gerçekleştirilmiştir. Belirlenen revize zımba tasarımında yüzey alanı %34 mertebesinde artırılarak etki eden gerilme düşürülmüştür. Ayrıca zımba geometrisinin bası yönünde zorlanıma maruz kaldığı ve bu nedenle bası yönünde daha yüksek yorulma ömrüne sahip toz metalurjisi ile üretilen bir takım çeliği malzemesinden üretilmesi gerektiği tespit edilmiştir.

Anahtar Kelimeler: Bağlantı elemanı, zımba, hasar, yorulma.

Giriş

Mühendislik alanında meydana gelen gelişmeler makine elemanlarının daha fonksiyonel olması konusunda zorlamaktadır. Otomotiv sektöründe özgün tasarımların değerinin artmasıyla beraber daha karmaşık formlara olan yönelimde de artış meydana gelmektedir. Otomotiv alanında yaşanan bu gelişmeler bağlantı elemanları sektöründe de çok daha karmaşık forma sahip, dar toleranslı ürünlerin üretim talebini beraberinde getirmektedir. Bu kapsamda ürün dayanımını ve işlevselliğini artırmaya yönelik çalışmalar gerçekleştirilmektedir. Literatürde kritik soket derinliklerini belirlemeye yönelik çeşitli çalışmalar gerçekleştirilerek matematiksel bir ifade ortaya çıkarılmıştır [1]. Bunun yanı sıra bağlantı elemanı kafa formunda özel bir tasarımla çeki dayanımı %20 seviyesinde artırılmıştır [2]. Literatürde özel bağlantı elemanlarının geliştirilmesine yönelik farklı çalışmalar yer almakta olup bu çalışma ile özel kafa formuna sahip bir ürün formunun (Şekil 1) soğuk şekillendirme sürecinde yaşanan malzeme akış ve zımba hasarının giderilmesine yönelik bir çalışma gerçekleştirilmiştir.

Mevcut istasyon tasarımına göre kalıp formları modellenerek malzeme akış analizleri gerçekleştirilmiş ve dövme işlemleri yürütülmüştür. Üretim hattında tespit edilen papatyalanma durumu nümerik analizlerde de tespit edilerek üretim hattı koşulları simülasyonda yakalanmıştır (Şekil 2). Kafada oluşan batma problemi nedeniyle anahtar ağzı köşelerine akan malzemenin flanşta bu duruma sebep olduğu tespit edilmiştir.

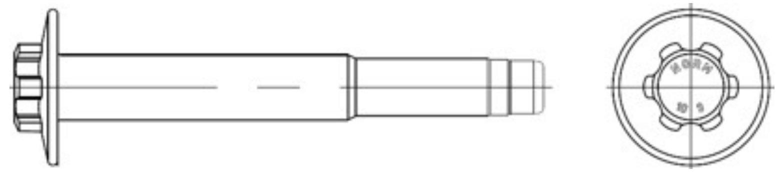

Şekil. 1. Ürün teknik resmi.

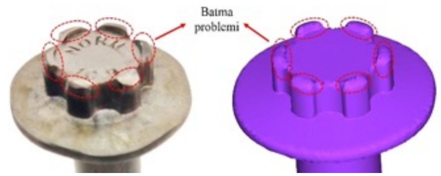

(a) **(b)**

Şekil. 2. Kafa formunda meydana gelen batma; (a) üretim, (b) simülasyon.

Sonuçlar

Üretim hattında sonuç alabilmek için 4. istasyon vurucu kalıbı revize edilerek malzeme akışının daha homojen ve kontrollü bir şekilde olması hedeflenmiştir. Bu aksiyon flanştaki papatyalanma oluşumunu azaltmakla beraber batma problemi giderilememiş ve ilgili şekillenme kusuru devam etmiştir (Şekil 3). Mevcut kalıp ve zımba tasarımlarına göre üretim ve simülasyon ortamında tespit edilen problemin çözümüne yönelik zımba geometrisinde tekrar bir revizyona gidilerek yüzey alanı mevcut duruma göre kıyasla %34 seviyesinde artırılmıştır (Şekil 4). Bu sayede dövme sürecinde zımba formuna etki eden gerilme değerlerinin düşürülmesi hedeflenmiştir.

(a) **(b)**

Şekil. 3. Vurucu kalıp yüzeyinin papatyalanmaya etkisi; (a) mevcut tasarım, (b) kaba pürüz verilmesi.

(a) **(b)**

Şekil. 4. Marka zımba geometrisi; (a) mevcut, (b) revize.

Şekillenme simülasyonu sonucunda batma problemi ortadan kaldırılmış olup elde edilen form Şekil 5'de verilmiştir. Marka zımba geometrisinin revize edilmesiyle yüzey alanında elde edilen artıştan dolayı birim alana etki eden gerilme düşürülmüştür. Şekil 6'da dövme işlemi sonunda zımba formunda meydana gelen asal gerilme oluşumlarına yer verilmiştir.

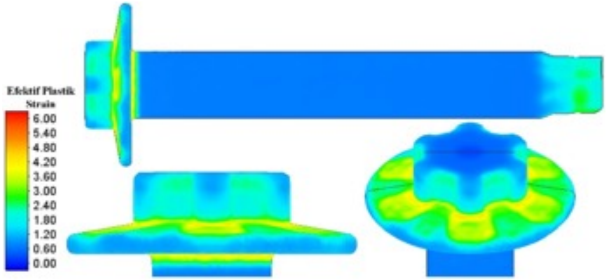

Şekil. 5. Marka zımbasının revize edilmesi sonucu simülasyondan alınan yarı mamul ürün formu.

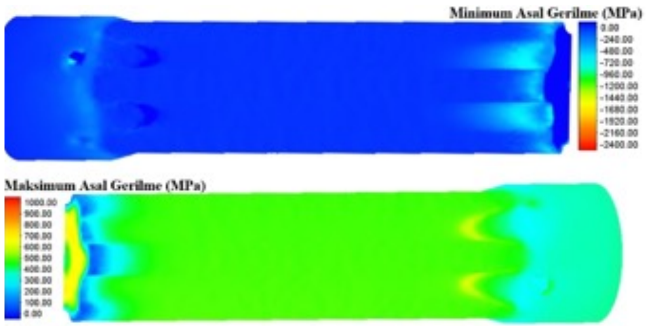

Şekil. 6. Dövme sonunda zımba formunda oluşan minimum asal gerilme değerleri.

Yapılan çalışmada Şekil 1'de teknik resmi verilen M10x74 özel torx formlu bağlantı elemanının numune üretiminde yaşanan problemler ele alınarak marka zımbasının düşük çevrimlerde kırılması ve kafa geometrisindeki batma nedeniyle flanş formundaki papatyalanma oluşumu incelenmiştir. Yapılan tasarım ve analizler sonucunda marka zımba malzemesi ve geometrisi revize edilerek yüzey alanı %34 seviyesinde artırılmış olup bu sayede zımba formuna etki eden gerilme değerleri düşürülmüştür. Gerçekleştirilecek deneme üretimleriyle revize marka zımba geometrisiyle kafadaki batmanın giderilmesi ve bu sayede flanştaki papatyalanmanın minimize edilmesi öngörülmektedir.

Referanslar

[1] Tanrıkulu, B., Toparli, M.Burak., Kilincdemir, E., Yurtdas, S., Ince, U. (2019). Determination of the Critical Socket Depths of 10.9 and 8.8 Grade M8 Bolts with Hexagonal Socket Form, Engineering Failure Analysis.

[2] Yurtdas, S., Tanrıkulu, B., Toker, O., Kilicaslan, C., Ince, U. (2020). Geliştirilmiş Dayanıma Sahip Bir Bağlantı Tasarımı, III. Ulusal Üniversite Sanayi İşbirliği, ArGe ve İnovasyon Kongresi.

DESIGN STUDIES FOR SCRAP-FREE PRODUCTION OF WEIGHT-REDUCED HEXAGONAL SPECIAL BOLT

Doğuş ZEREN
Sezgin YURTDAŞ
M. Burak TOPARLI

Manisa Celal Bayar University
IV. National University Industry Cooperation, R&D and Innovation Congress,
15-16 December 2021

DESIGN STUDIES FOR SCRAP-FREE PRODUCTION OF WEIGHT-REDUCED HEXAGONAL SPECIAL BOLT

Doğuş Zeren[1], Sezgin Yurtdaş[1], M. Burak Toparlı[1]
[1]Norm Cıvata San. ve Tic. A.Ş., R&D Center, İzmir, Türkiye
Email: dogus.zeren@norm-fasteners.com.tr

Abstract

In this study, various stage designs and numerical simulations were carried out to examine the production of the hexagonal flanged weight-reduced M8x91 special bolt without any further operation. Numerical simulations of the metal forming operations were prepared on Simufact Forming finite element software. Owing to alternative simulation trials, most suitable design was determined for the sake of weight reduction with no additional operation. Production trials were conducted with the stage design determined as a result of the simulation studies. Through the numerical analyses and production trials, it was verified that the proposed new design leads to significant weight reduction with no further operation after cold forging.

Keywords: Cold forging, fastener, bolt, weight-reduction, sustainable production

Introduction

In recent years, there has been an increase in demand of special weight-reduced bolts. Due to complex geometry, secondary operations including cutting become necessity in most cases, leading to inefficiency by producing scrap. In order to prevent loss of raw materials by scraping, studies have been initiated to improve designcapabilities with cut-free production [1,2]. Within the scope of this study, different stage designs were examined for the production of weight-reduced M8x91 special bolt without any further cutting operation. The design studies was made by employing Simufact Forming finite element package program.

While working with different stage designs, there were various issues so that secondary operations were required. Particularly, final flange geometry was challenging to obtain without any further cutting operation. Owing to stage design efforts coupled with numerical simulations conducted by using Simufact Forming, a stage design was revealed for both satisfying the dimensional requirements and eliminating cutting operation leading to production inefficiency by scrap production. The final stage design was tested in actual production floor and it was verified that final stage design can be used for the investigated special bolt.

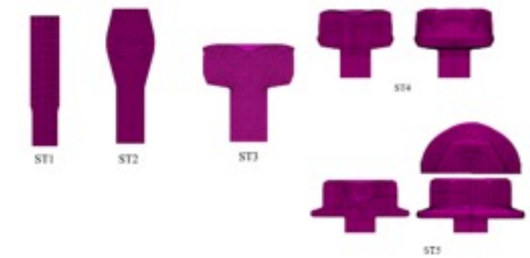

Figure 1. Proposed stage design.

Figure 2. Production based on proposed stage design.

Conclusions

As a result of design and numerical simulation efforts, a stage design was offered for the M8x91 weight-reduced hexagonal special bolt. The final stage design was verified at the production floor for the sake of scrap-free production. Hence, more efficient and sustainable production route was proposed for the investigated weight-reduced special bolt.

References

[1] Light-weightForgingofSteelAlloyFasteners,Dr.CenkKılıçaslan,SezginYurtdaşNiyaziEmrahKılınçdemirUmutİnce, International Conference "New Developments in Forging Technology, 2017.

[2] Otomotiv Sanayinde Kullanılan Bağlantı Elemanlarında Ağırlık Azaltma, M. Burak Toparli, N. Emrah Kılınçdemir, Sezgin Yurtdaş, Barış Tanrıkulu, Umut İnce, 8.Otomotiv Teknolojileri Kongresi, 2016.

www.normfasteners.com